5-2003

The Rate of Fluid Absorption in Porous Media

Ran Wei Rioux

THE RATE OF FLUID ABSORPTION IN POROUS MEDIA

By

Ran Wei Rioux

B.S., Beijing University of Chemical Technology, 1995

A THESIS

Submitted in Partial Fulfillment of the

Requirements for the Degree of

Master of Science

(in Chemical Engineering)

The Graduate School

The University of Maine

May, 2003

Advisory Committee:

Douglas W. Bousfield, Professor of Chemical Engineering, Advisor

Yang Xiang, Research Engineer in Chemical Engineering

Adriaan van Heiningen, Ober Chair and Professor of Chemical Engineering

THE RATE OF FLUID ABSORPTION IN POROUS MEDIA

By Ran W. Rioux

Thesis Advisor: Dr. Douglas W. Bousfield

An Abstract of the Thesis Presented
in Partial Fulfillment of the Requirements for the
Degree of Master of Science
(in Chemical Engineering)
May, 2003

Fluid flow in porous media is an important process for many applications such as oil recovery, packed bed absorption columns and filtration. Short time fluid uptake is important for processes such as textile sizing, paper coating and printing. But more work is needed to characterize the parameters that determine the absorption rate.

This work is focused on short time absorption rate on uncoated and coated paper. Absorption rate is measured with a Bristow Wheel device for seven different uncoated papers and eleven coated papers. Gloss dynamics of freshly printed samples and tack dynamics are measured with two novel devices. Various absorption models are compared to the experimental results.

For absorption into paper, the absorption rate is found to be related to fluid-substrate contact angle and fluid properties. The combined influence of fluid viscosity, surface

tension and contact angle on absorption rate is not well described by the Lucas-Washburn equation.

For coated paper, the absorption rate depends on the base paper absorption rate, the coating pore size, coating binder level and fluid-coating contact angle. The coatings on high absorbance base paper have a higher absorption rate than coatings on low absorbance base paper. Small pore size of coating and low fluid-coating contact angle increase penetration rate. Low binder level in coating increases absorption rate. The absorption rate is proportional to the value of $(\gamma\cos(\theta)/\mu)^{0.5}$ as predicted by the Lucas-Washburn equation.

Both the micro-tack and dynamic gloss tests depend on absorption rate. A good relationship between the absorption rate and tack peak time is obtained. The dynamic gloss heel time correlates to absorption rate.

The proposed model for absorption into paper works well, but the Lucas-Washburn expression over predicts the results. For coated samples, a model is proposed that predicts the results for inks and ethylene glycol, but the Darcy coefficient needs to be obtained from an absorption experiment. The Lucas-Washburn equation does not apply for coated paper absorption prediction.

ACKNOWLEDGEMENTS

First, I would like to thank my advisor, Doctor Douglas Bousfield, for his instruction and help in my degree program. I would also like to thank HP for their financial and technical support.

Thanks to my committee members, Doctor Yang Xiang and Doctor Adriaan van Heiningen for using their valuable time and knowledge to assist me.

I would like to thank all the graduate students and the staff of the Chemical Engineering Department for being very helpful to my program, especially Basant, Amol, Emily and Yingfeng.

At last, I would like to thank my husband Bob Rioux, for his support and encouragement.

TABLE OF CONTENTS

LIST OF TABLES

LIST OF FIGURES

NOMENCLATURE

A	Area of the medium
B	Length of the opening of the liquid container
E	Coating thickness
F	Force to separate two surfaces with fluid in between
h	Gap between the two surfaces
K	Darcy coefficient
k_1	Coefficient in Carmon-Kozeny equation, with a value of 4.1
K_a	Absorption coefficient
K_r	Roughness coefficient
L	Depth that the fluid penetrates into the medium
L_t	Approximate length of the track left on the substrate
L	Thickness of the sample
L_c	Thickness of the coating layer
L_s	Thickness of the substrate
N	Actual number of openings at the surface of the coating
N_p	Number of pores per unit area
P_e	External pressure at the entrance of the capillary tube
Q	Volumetric fluid flow rate
R	Pore radius

R_s	Radius of the upper surface
R_c	Dominate pore radius of the coating layer
R_p	Dominate pore radius of the paper layer
R_u	Roughness of the coated sample
S_o	Specific particle areas per particle volume
t	Penetrating time
TLV_c	Absorbed fluid volume by the coating layer part
TLV_w	Water absorption volume
TLV_{w-p}	Water absorbed by the paper
V	Liquid volume transferred to the liquid container
V	Rotation velocity of the wheel
V_b	Intrusion volume of mercury in per unit weight of the base paper
V_p	Volume of fluid absorbed by the capillaries per unit area
V_s	Solid volume of the coating
V_t	Total intrusion volume of mercury per unit weight of the whole sample
V_v	Void volume of the coating
U	Velocity of the upper surface
W	Width of the opening of the ink container and
W_c	Base weight of the coating
W_d	Dry paper weight
W_o	Oil-saturated paper weight
W_p	Base weight of the base paper

x	Distance traveled by the fluid

Greek symbols

ε	Void fraction in the coating layer
ε_c	Void volume fraction of the coating layer
ΔP	Capillary pressure
ΔP_a	Pressure of air exerted on the sample
ΔP_c	Capillary pressure of coating layer
ΔP_p	base paper capillary pressure
ΔP_t	Total pressure exerted the medium
$\Delta P_{w\text{-}c}$	Capillary pressure in the coating layer
$\Delta P_{w\text{-}p}$	Capillary pressure in by the base paper layer
γ	Fluid surface tension
γ_f	Surface tension of the fluid,
γ_w	Surface tension of water.
θ	Contact angle
θ_c	Contact angle between fluid and coating
θ_f	Contact angle between the fluid and the base paper
θ_p	Contact angle between fluid and base paper
$\theta_{w\text{-}p}$	Contact angle between water and the base paper
$\theta_{w\text{-}c}$	Contact angle between water and the coating layer

μ	Viscosity of the fluid
μ_a	Viscosity of air
μ_f	Viscosity of the fluid
μ_w	Viscosity of water
ρ_c	Density of the coating
ρ_o	Density of the silicon oil
τ	Tortuosity factor
υ	Speed of the fluid passing through the medium
υ_a	Velocity that air passes through the sample in the Sheffield air permeability apparatus
ϕ_f	Volume fraction of solid in the filtercake
ϕ_s	Volume fraction of solid in ink

CHAPTER 1: INTRODUCTION

The fluid flow in porous media is important in a number of processes such as oil recovery, packed bed absorption columns and filtration, paper treatment, and printing.

In the paper industry, during paper coating and sizing, fluid penetration into paper influences the process speed as well as the treatment effects.

In the printing industry, a better understanding of the mechanism of fluid permeation into paper or other porous media will be helpful in printing adjustment, print quality control including print clarity and print gloss, and preparation of substrates to be printed.

A better understanding of permeation mechanism is not only of direct commercial value, but also it is closely related to environmental issues. These include the relative environmental impacts of using water or solvent based inks. Water based gravure inks are more beneficial to the environment, but the final print quality does not match that of solvent based inks. The print quality of water based inks may be related to absorption process.

1.1 Theory:

Fluid penetration into a porous media is a process of capillary-driven flow. When idealizing porous media as many vertical parallel cylindrical pores randomly distributed in the media as shown in Figure 1.1, the capillary pressure that drives fluid forward in the pore is expressed by the Young-Laplace equation as:

$$\Delta P = \frac{2 \cdot \gamma \cdot \cos\theta}{R} \tag{1.1}$$

Where ΔP is capillary pressure, γ is fluid surface tension, R is pore radius and θ is contact angle established between the fluid and the inner wall of the pore as shown in Figure 1.1.

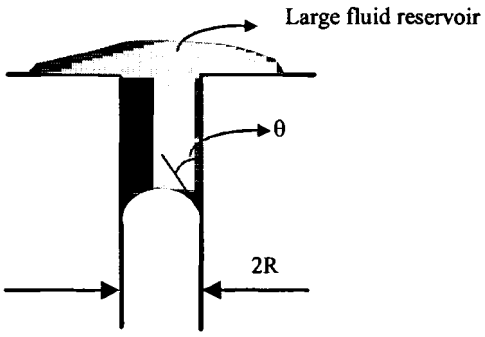

Figure 1.1: Capillary driven flow in a single pore

Darcy's law defines laminar flow of homogeneous fluids in homogeneous porous media:

$$\frac{Q}{A} = \upsilon = \frac{K \cdot \Delta P_t}{\mu \cdot L} \tag{1.2}$$

Where Q is the volume flow through the medium, A is the area of the medium, υ is the rate of the fluid passing through the medium, K is the Darcy coefficient, ΔP_t is the total pressure exerted on the medium, L is the depth that the fluid penetrates into the medium and μ is fluid viscosity.

Flow inside the cylinder is given by Hagen-Poiseuille Law:

$$Q = \frac{\pi \cdot R^4 \cdot \Delta P}{8 \cdot \mu \cdot L} \tag{1.3}$$

Where Q is the volumetric fluid flow rate in the capillary, L is related to flow rate as:

$$Q = \pi R^2 \cdot \frac{dL}{dt} \tag{1.4}$$

where t is penetrating time.

Combining Equation (1.1) - (1.4), and integrating gives the Lucas-Washburn equation:

$$L = \sqrt{\frac{R \cdot \gamma \cdot \cos\theta \cdot t}{2 \cdot \mu}} \tag{1.5}$$

If the number pores per unit area N_p is known, the void fraction ε is:

$$\varepsilon = N_p \cdot \pi R^2 \tag{1.6}$$

The total liquid volume (TLV) absorbed per unit area is

$$TLV = N_p \cdot \pi R^2 \cdot L = \varepsilon \sqrt{\frac{R \cdot \gamma \cdot \cos\theta \cdot t}{2 \cdot \mu}} \tag{1.7}$$

This is the Lucas-Washburn equation expressed in terms of void fraction.

While the Lucas-Washburn equation is used by many researchers to describe the fluid permeation in paper, others question its use. Tollenaar (1967), Ruoff et al. (1959,1960), and Marmur (1988) argued that the Washburn equation applies to non-polar liquids in cylindrical capillaries, and does not always apply to penetration of aqueous inks into tortuous porous coating/paper. Salminen (1988) also mentioned that some factors are missed in the Washburn equation such as:

1. Time and velocity dependence of dynamic capillary pressure.
2. Counter pressure of air.
3. Expansion of fiber network
4. Fiber sorption.

Lepoutre (1978) added a tortuosity factor τ into the Lucas-Washburn equation as:

$$\tau = \frac{L}{E} \tag{1.8}$$

Where E is the coating thickness.

So the porosity ε can be expressed as:

$$\varepsilon = \frac{N\pi R^2 L}{E} = N\pi R^2 \tau \tag{1.9}$$

Where N is the actual number of openings at the surface of the coating.

Combining Equation (1.7) – (1.9), the fluid volume V absorbed by N such capillaries of the coating is:

$$V = \frac{\varepsilon}{\tau}\sqrt{\frac{R \cdot \gamma \cdot \cos\theta \cdot t}{2 \cdot \mu}} \tag{1.10}$$

Xiang & Bousfield (2000) , Aspler et al. (1994), Donigian et al. (1997) and Desjumaux et al. (1998) found that smaller pores set ink faster than larger pores, which contradicted the Lucas-Washburn equation. To explain this contradiction, Xiang & Bousfield postulated the formation of a filtercake during the setting of the ink film. Their model is expressed as:

$$V_p = \varepsilon\sqrt{\frac{Rt\gamma\cos\theta}{2\mu\left[1 + \frac{\varepsilon\phi_s R^2}{8K\phi_f(1-\phi_s)}\right]}} \tag{1.11}$$

Where V_p is the volume of fluid absorbed by the capillaries per unit area, ε is the void fraction in the coating layer, ϕ_s is the volume fraction of solid in ink, ϕ_f is the volume fraction of solid in the filtercake and K is the Darcy coefficient of the filtercake.

When the resistance of filtercake $\frac{\varepsilon\phi_s R^2}{8K\phi_f(1-\phi_s)}$ is low or the filtercake permeability K→∞, Eq. (1.11) reduces to a form of the Lucas-Washburn equation:

$$V_p = \varepsilon\sqrt{\frac{R\gamma\cos\theta\cdot t}{2\mu}} \tag{1.12}$$

If K is small, Eq. (1.11) can be reduced to :

$$V_p = \sqrt{\frac{4Kt\gamma\phi_f(1-\phi_s)\cos\theta}{\mu\phi_s R}} \tag{1.13}$$

Therefore, when the effect of the filtercake formed by ink pigment on coated paper cannot be neglected, the penetration of the fluid should be faster in smaller pores than in larger pores.

Matthews et al. (1993) used software named Pore-Cor to simulate mercury intrusion and absolute permeability in sandstone. In Pore-Cor, they set up a network of void volumes / pores connected by a network of smaller void channels/throats. Their network comprises a unit cell with 1000 cubic pores in a 10×10×10 matrix as shown in Figure 1.2.

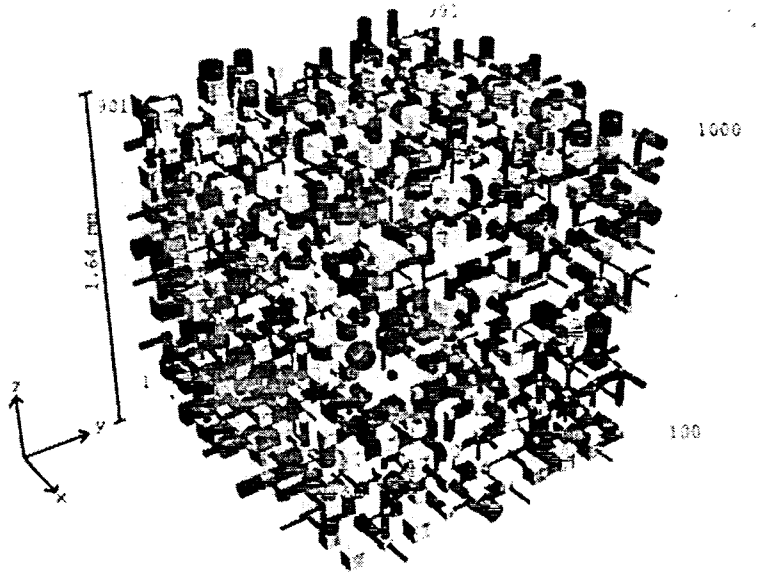

Figure 1.2: The unit cell of the sandstone of Pore-Cor of Matthews et al.

Connected to each pore are up to six cylindrical throats in the positive and negative x, y and z directions. The mean number of throats connected to a particular pore over the whole unit cell is called connectivity. The pore and throat size of the unit cell are correlated according to the known pore distribution of sandstone. The throat size distribution and connectivity are adjusted to give a close fit to the experimental invasion curve. The row spacing of the matrix is optimized so that the porosity of the simulated network equals that of the experimental sample.

Their simulating results have shown that the network reproduces the experimental mercury intrusion curve (shown in Figure 1.3), porosity, connectivity, pore:throat size correlation, tortuosity and gaseous diffusion through a dry sandstone. (Matthews & Spearing 1991, Matthews & Spearing 1992)

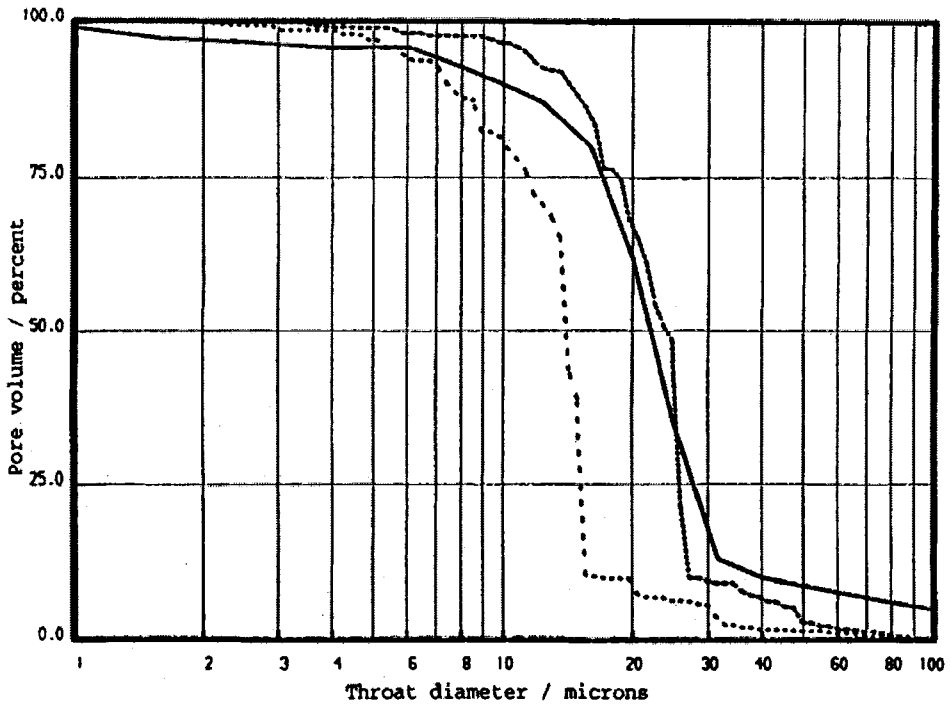

Figure 1.3: Mercury intrusion curves in Pore-Cor modeling of Matthews et al.

—, experimental; ------, optimum distribution; ·····, unskewed distribution.

This Pore-Cor unit cell can be repeated in three directions to form a three-dimensional geometry. In the modeling, no property-independent fitting parameters are invoked. Therefore this model has been applied to many other porous media including medicinal tablets (Ridgway et al. 1997), soil (Peat et al. 2000), mineral blocks (Schoelkopf et al. 2000) and coated paper (Schoelkopf et al. 2000).

Shchoelkopf et al. (2000) modeled a network of liquid permeation in mineral blocks, based on Matthews Pore-Cor unit cell. They used the Bosanquet (1923) equation instead

of the conventional Washburn equation to describe the inertia of an accelerating fluid entering a capillary tube:

$$\frac{d}{dt}\left(\pi r^2 \rho x \frac{dx}{dt}\right) + 8\pi\mu x \frac{dx}{dt} = P_e \pi r^2 + 2\pi r \gamma \cos\theta \tag{1.14}$$

where x is the distance traveled by the fluid, P_e is the external pressure at the entrance of the capillary tube and ρ is fluid density. If there is no applied external pressure P_e, then Eq. 1-11 can be simplified into:

$$x^2 = \frac{2\gamma \cos\theta \cdot t^2}{r\rho} \text{ (at } <<1, P_e=0) \tag{1.15}$$

This equation describes what they referred to as 'inertial flow'. The distance traveled, x, is directly proportional to time, in contrast to the Lucas-Washburn equation for which $x \propto t^{0.5}$. Also in contrast, the distance traveled by inertial flow is independent of viscosity, but inversely related to the radius of the pore and the fluid density. There is a good correlation between their simulations and experiments.

1.2 Factors Affecting Ink Setting Rate:

According to the Lucas-Washburn equation Eq. (1.5), media with larger pores absorb fluid faster. This holds true for many cases. However, some researchers found that penetration rate is indirectly proportional to substrate pore size when the fluid is a suspension. Besides filtercake resistance explanation of Xiang & Bousfield (2000), Schoelkopf et al. (2000) explained that, according to the Bosanquet (1923) equation, for small pores there will be an inertial wetting while there is a retarding force at the entrance

of large pores. The viscous drag only gets established over longer times. Therefore, the absorption into a porous network starts at inertial inhibition for smaller pores and inertial retardation for larger pores. The penetration then follows the Lucas-Washburn equation but still with remaining inertial retardation for the largest pores. Donigian et al.(1997) and Desjumaux et al. (1998) explained that smaller pores result in larger capillary pressure which is the flow driving force.

Lepoutre, (1978) and Xiang & Bousfield (2000) found that absorption rate decreases with increasing latex content. Lepoutre interpreted this as a result of the increasing binder level decreasing the small channels which connect between large pores.

Holman et al. (2002) observed that surface charge influences how fluid is absorbed. The surface of a ceramic particle takes on a charge when in contact with an aqueous solution. It will thus be energetically favorable for charged species in the solution with a charge opposite to that of the surface to adsorb to the surface. In their experiments, the polymer molecules adsorbed to the surface retarded the binder solution passing down through the surface and resulted in a shallower penetration depth.

Hoogeveen et al. (1996) found that a higher energy barrier for adsorption in the system results in slower adsorption, which in turn affects the absorption.

Fluid surface tension is important for fluid-media contact angle and absorption wetting delay. According to Eq. (1.1), capillary pressure is directly proportional to surface tension and the cosine of the fluid-surface contact angle. As high fluid surface tension

leads to high contact angle, the effect of surface tension on fluid penetration is a combined one. By adding surface-tension-lowering surfactant to water, Salminen (1988) found that when the surfactant is well above the critical micelle concentration, the addition of the surfactant increases the fluid transportation significantly. Below the critical micelle concentration the effect of surfactant addition is strongly diminished. Aspler et al. (1987) showed that in liquid absorption, wetting delay decreases with decreasing surface tension.

Eklund & Salminen (1986) reported the pronounced temperature dependence of water penetration in sized paper under no external pressure. In Salminen's experiments, he found that even for hydrophilic paper at no external pressure, the water penetration rate still increased significantly when water temperature increased. He concluded that the temperature increase affected the vapor pressure and the molecular processes ahead of the liquid front. Salminen also found that with the presence of external pressure, this temperature dependence is not that large compared to samples with no external pressure. Because the external pressure increased the external transport momentum, the affect of molecular processes is lessened.

According to Lucas-Washburn equation, the depth of fluid penetration at unit time is indirectly proportional to fluid viscosity. However, in Salminen's experiments, it was found that under no external pressure the affect of fluid viscosity on fluid flow rate is of minor importance.

The pH value is not a major factor in permeation, but several researchers did observe its influence on fluid transport. Price et al. (1953) observed that hydrochloric acid lowers the hydrophobicity of paper by reacting with the sizing agent, thus increases the absorption rate. Bristow's (1968) work showed that adding alkali increases the transport rate. This is because of the chemical interactions between the aqueous liquid phase and the fiber matrix. The change of pH value range may also change the surface charge and change the absorption rate. Holman et al. (2002) found that the surface charge decreases as the pH value of the surroundings increases.

1.3 Summary:

In the past experiments, factors that affect fluid permeation into porous media have been studied. Fluid penetration rate has been found to depend on substrate characteristics, fluid properties, and interaction between fluid and substrate. Contradicting the Lucas-Washburn equation, recent experiments with pigmented ink show that small pore size leads to faster penetration rate. Increasing coating binder level in coating decreases penetration rate. Low surface tension and low contact angle have been found to be advantageous to fast absorption of fluid. Higher fluid temperature helps fluid penetration. Viscosity and pH value may affect the fluid permeation, but their influences are of minor importance.

Models have been set up to predict the fluid permeation into porous media. Based on the Lucas-Washburn equation, the continuous flow in cylindrical capillaries model, some of the models added some other factors that affect the penetration, such as tortuosity and filtercake resistance. Some other models used computers to set up a three dimensional

pore structure to imitate the flow in the porous substrate. One of the successful computer models in recent research is Matthews' Pore-Cor model. This model has been applied to predict penetration in many porous media including medicinal tablets, soil, mineral blocks and coated paper. However, the computer model comes with long calculation times and a need for high-performance computers. Also, the complexity and detailed description of the model prevent the model to be used in general purpose.

While much work has been reported on this topic, a number of questions persist, especially with penetration on coated paper. To establish a simple model to predict low viscosity fluid penetration rate in layers of porous materials, several mathematical models are developed and compared in this work. Several main factors that may affect penetration rate are studied, such as base paper absorbance, coating pore size, contact angle, coating binder level, fluid surface tension and fluid viscosity.

CHAPTER 2: EXPERIMENTAL PROCEDURE

Three main experimental methods are used in this research. A Bristow Absorption Tester is used to test fluid absorption rate on porous substrates. A Micro-Tack Tester is used to test the tack force change of fluid on substrates. A Dynamic Gloss Tester is used to test the gloss change on substrates after being printed. Besides some commercial coating samples, most of the coating samples in the research are produced using a rod coater. Some other experiments such as contact angle, mercury porosity, gloss, and roughness are adopted to characterize the substrates. Except for some coatings that require higher temperatures to form good structures, all experiments are carried out at room temperature.

2.1 Bristow Absorption Tester

A Bristow Absorption Tester is used to test the sample substrate's absorbance in this research. Figure 2.1 is a photo of the Bristow Absorption Tester device. Figure 2.2 is a close-up of the testing process. This apparatus is designed to test liquid absorption in paper or other porous substrates at short contact time, ranging from 0.01 to 2 seconds. The experiment is carried out at constant room temperature and humidity. Samples are put in the constant temperature and humidity room overnight to be conditioned. To do the experiment, the paper strip to be tested is attached to the rim of the wheel whose speed is adjustable. Then 10 μL of ink is added to the liquid container. The liquid

container leaves a track on the sample through a 1 mm width, 15mm length opening. By measuring the area of the track, the liquid quantity transferred per unit area at certain contact time can be attained. This liquid quantity transferred per unit area is called Total Liquid Volume (TLV, cm^3/m^2).

$$TLV = V / (L_t \cdot B) \quad (2.1)$$

Where V is the liquid volume transferred to the liquid container, L_t is the approximate length of the track left on the substrate and B is length of the opening of the liquid container which is 15mm.

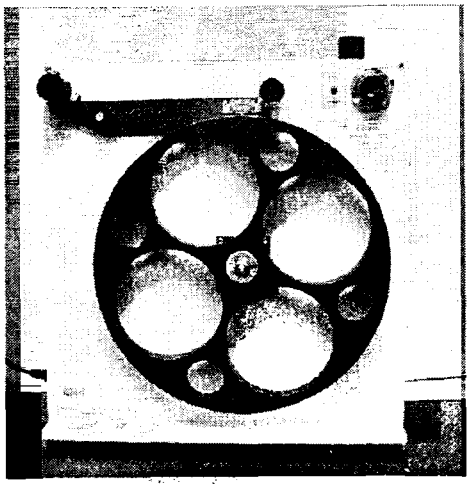

Figure 2.1: Bristow Wheel device.

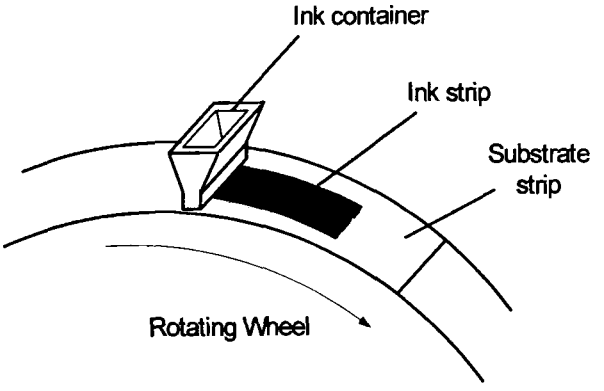

Figure 2.2: Bristow absorption testing process

Contact time is :

$$t = W / v \quad (2.2)$$

Where t is contact time, W is the width of the opening of the ink container (1mm), and v is the rotation velocity of the wheel.

This contact time is the nominal contact time used in Bristow test plot. However, in the Bristow Absorption Tester manual, it is said "The nominal time is based on the assumption that the width of the opening of the liquid container determines the absorption time. It has, however, been shown that the effective absorption time is usually slightly longer and that the width of the edge of the liquid container should also be taken into account in accurate work. This is, however, of small importance when the apparatus is used for comparison of different papers or for quality control." This difference of contact time is shown in Figure2.3:

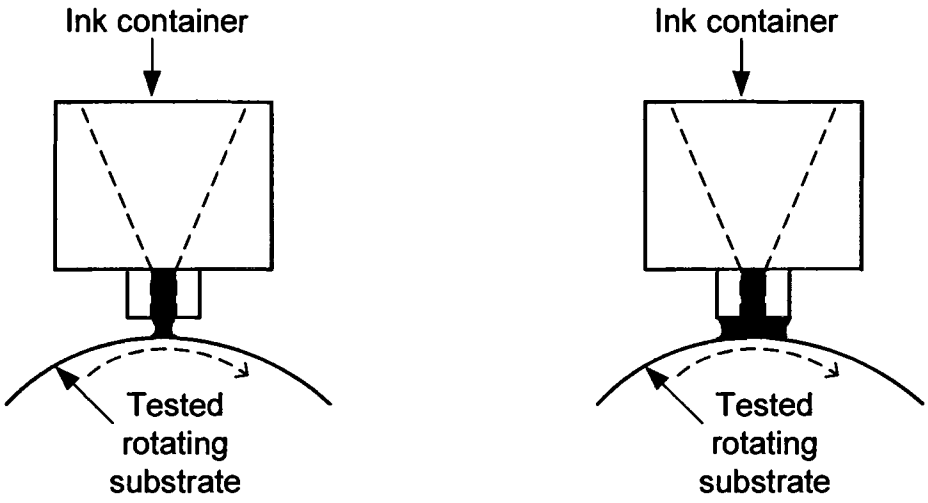

nominal contacting time actual contacting time

Figure 2.3: Comparison of nominal contacting time and actual contacting time in Bristow absorption test.

Since we need our Bristow test data to be compared with our prediction data later, we counted in the edge of ink container and take W as the width of ink container (3mm).

After a series of measurements at different rotation speeds, TLV can be plotted against the square root of contact time. Using contact time at a square root scale should make the studied curves linear. Typical Bristow plots are shown in Figure 2.4. The slope K_a is the absorption coefficient, reflecting the absorption rate. The intercept K_r is the roughness coefficient, characterizing sample surface roughness. The initial horizontal portion of the curve corresponds to a wetting delay, during which only the surface pores are filled and no significant absorption takes place. This wetting delay would not show in plot Figure 2.4 (a) because the absorption rate is not as low as that shown in Figure2.4 (b).

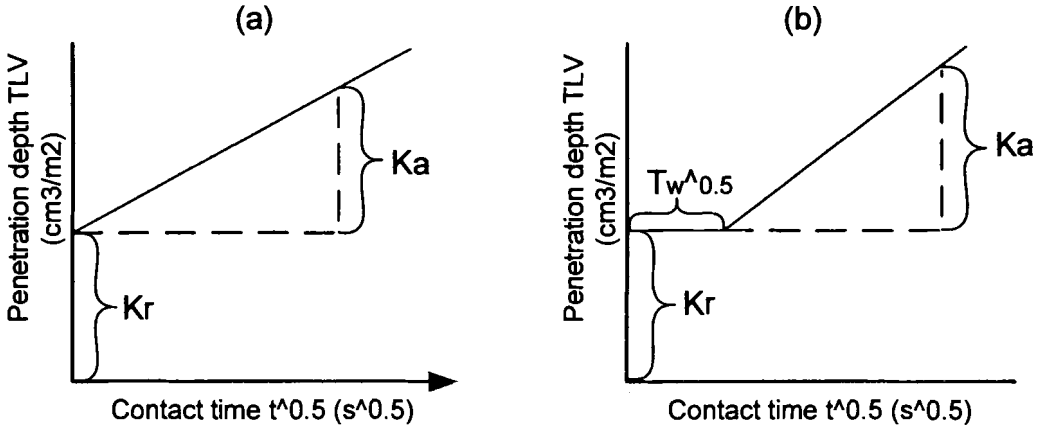

Figure 2.4: Typical Bristow absorption curves

2.2 Micro-tack Tester

Ink tack is one of the major concerns in printing industry. If ink tack does not decay after paper is printed, it will cause overlapped paper to stick together or printed content to be transferred to the backside of other paper when separating the printed papers.

The Micro-tack Tester used in this research was first developed to record the tack force changing process of high viscosity oil based inks on paper substrates (Xiang et al. 1999). In this work, it is modified to test water based inks or low viscosity fluids on paper, which has not been attempted before. The recording curves show similar trends as those produced from oil based inks, except for some very absorbent substrates whose curves are flat because the tack force change ends too soon to be recorded.

Figure 2.5 is schematic of the Micro-tack device. The tested sample is secured to a heavy sample base which keeps the sample still during the test. Since the tack head size is 3.5 mm diameter, an ink drop produced from micro-liter scale syringe is too large. To obtain a small amount of ink, a drop of fresh ink is first placed on a plastic film, and the tack head is moved down to the ink. To produce an even smaller size drop, before moved to the substrate for test, the tack head is made to touch dry plastic film twice. Fewer contacts leave too much ink while more drops the reproducibility. The vertical movement of the tack head is controlled by computer commands. The probe will change direction to go up when it touches the substrate. In this way, the probe will touch the substrates and separate the ink drop in a constant manner. This ensures that the ink drops obtained from this separating method are around the same size. Figure 2.6 shows the process of taking ink.

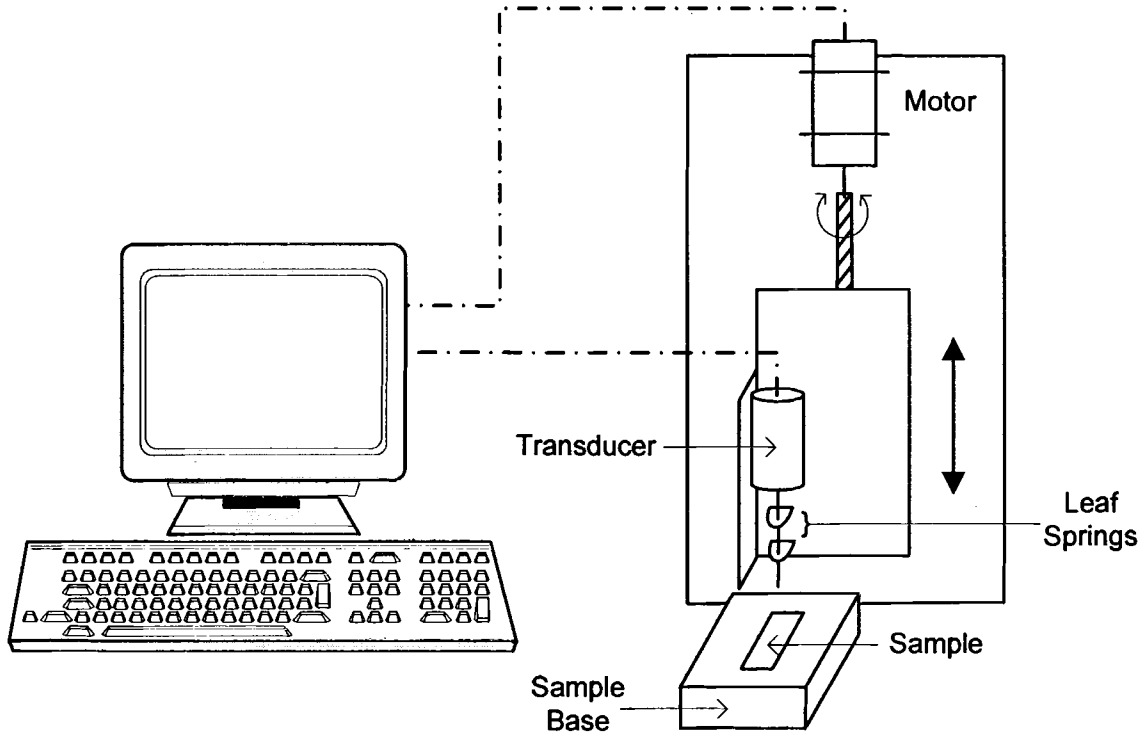

Figure 2.5: Schematic of Micro-tack device

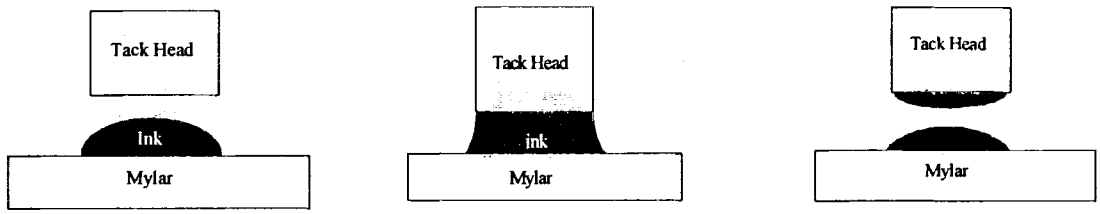

Figure 2.6: Process of taking an ink drop

After the tack head gets an ink drop, the motor drives the tack probe down to touch the sample to be tested. The probe stops going down when the tack probe touches the sample and then starts going up. Now the force generated from extending the ink bridge between

the tack head and the substrate deflects the spring which is sensed by the linear voltage displace transducer. The force reaches its highest point during this extension of the ink bridge and the ink bridge breaks. Under computer command, the probe repeatedly touches the substrate and is pulled away, and the device records force data each time the ink bridge breaks. Each test is repeated 10 times to obtain the average.

In the middle of Figure 2.7 is a typical tack test curve. The numbered figures around it explain what happens at each stage. In the stage 1, the tack force is small since the liquid bridge between the tack head and the substrate is dilute and not much force is needed to separate them. As part of the ink is absorbed by the substrate, the liquid between two surfaces gets thicker and lesser. According to Stefan's Law:

$$F = \frac{3}{2} \cdot \frac{\pi \cdot \mu \cdot U \cdot R_s^4}{h^3} \tag{2.3}$$

Where F is force to separate two surfaces with fluid in between, μ is the viscosity of the fluid, U is the velocity of the upper surface, R_s is the radius of the upper surface, and h is the gap between the two surfaces.

The force increases as the viscosity increases and as gap h decreases. During the process of liquid part of ink absorbed, the ink viscosity increases. The tack force keeps increasing until it reaches the peak at the stage 2 of Figure2.6. At the peak, the probe may start touching "dry" spots. After this point, instead of splitting a filament with diameter 3mm, many small filaments are pulled by the probe. As R decreases, the force decreases as show in stage 3 in Figure2.6. In the stage 4 the ink on the tack area all dry or almost dry, no more major ink bridge can form between tack head and the substrate, so

tack force decreases to or close to zero. From the respect that the test records absorption process, the tack test is another method to test the absorption rate of substrates.

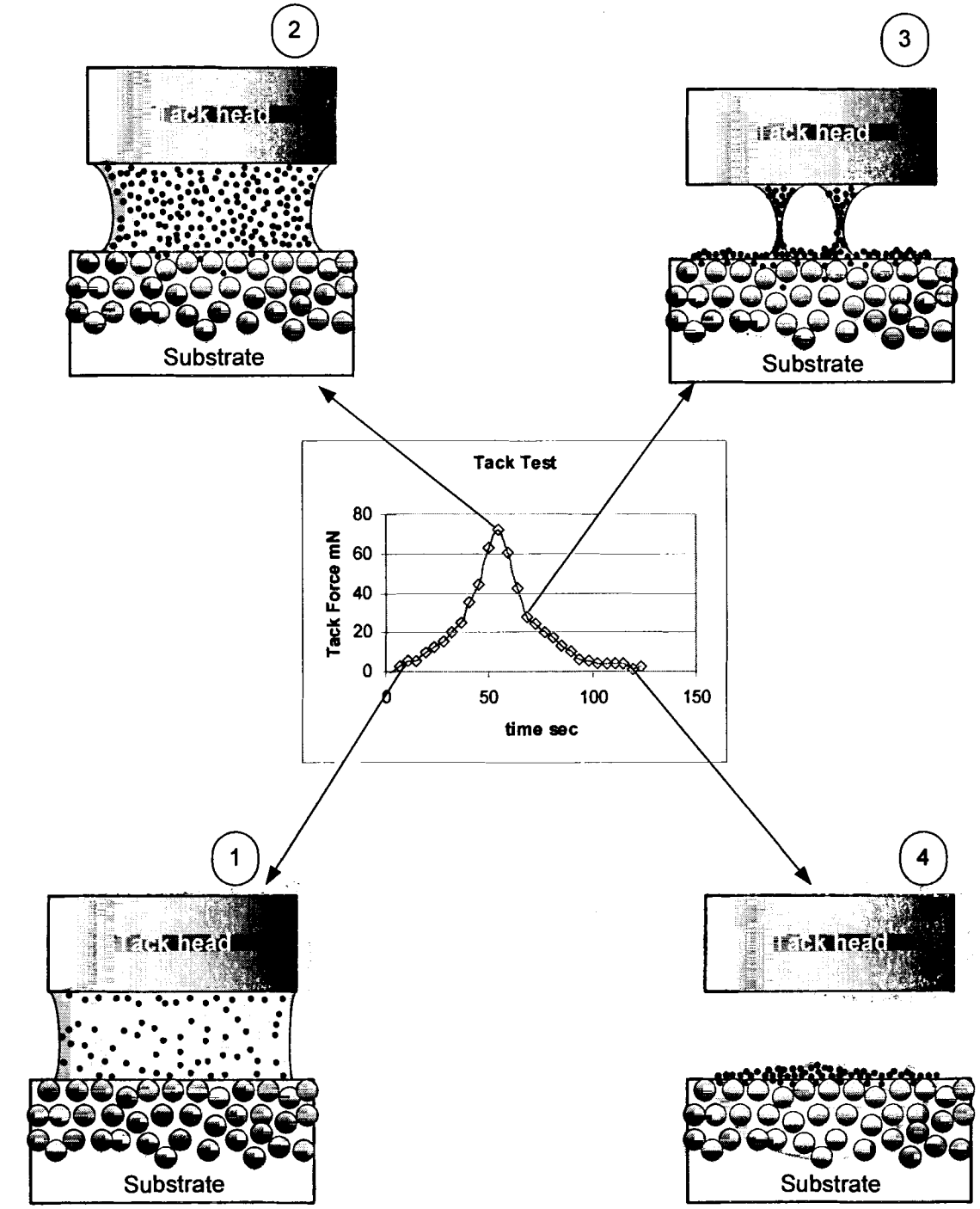

Figure 2.7: Tack test curve and explanation of each stage

2.3 Dynamic Gloss Meter

A typical Dynamic Gloss Tester can test the gloss change of oil based inks on substrates. This Dynamic Gloss Tester is established to test gloss change of inkjet ink on substrates. Figure 2.8 is schematic of the dynamic gloss tester.

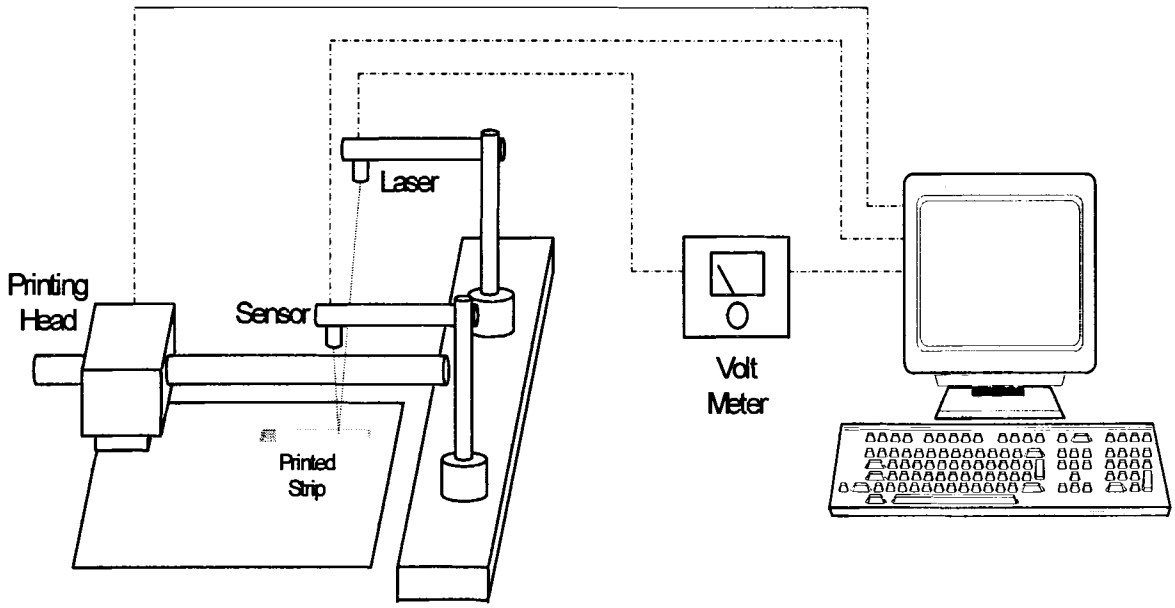

Figure 2.8: Schematic of Dynamic Gloss device

The device is composed of a rearranged inkjet printer (970 Cxi inkjet, Hewlett-Packard), a 680nm, 5mW laser source and a laser detector, a 10 volt capacity voltmeter and a computer connected to all of the above parts. A Visual Basic program is used to acquire data and modified PCL files control the printer during the printing process. Controlled by the computer program, the printer picks up a sample sheet and prints a 10mm×90mm rectangular strip on it. The laser source gives out a laser light at a 20 degree angle onto the sample at the printed area, and the laser detector receives reflected light signals and

transfers them back to computer. In the program we chose, the device records 1000 electrical dynamic gloss signals per second and thus the data series provides detailed gloss change of the printed part of the paper. The standard test time in the experiment is 30 seconds. All the tests are carried out in a dark room to eliminate the chance of light interfering with the result. Each test is repeated six times to get an average curve. Figure 2.9 is a plot of dynamic gloss of dye base ink on $CaCO_3$ coating:

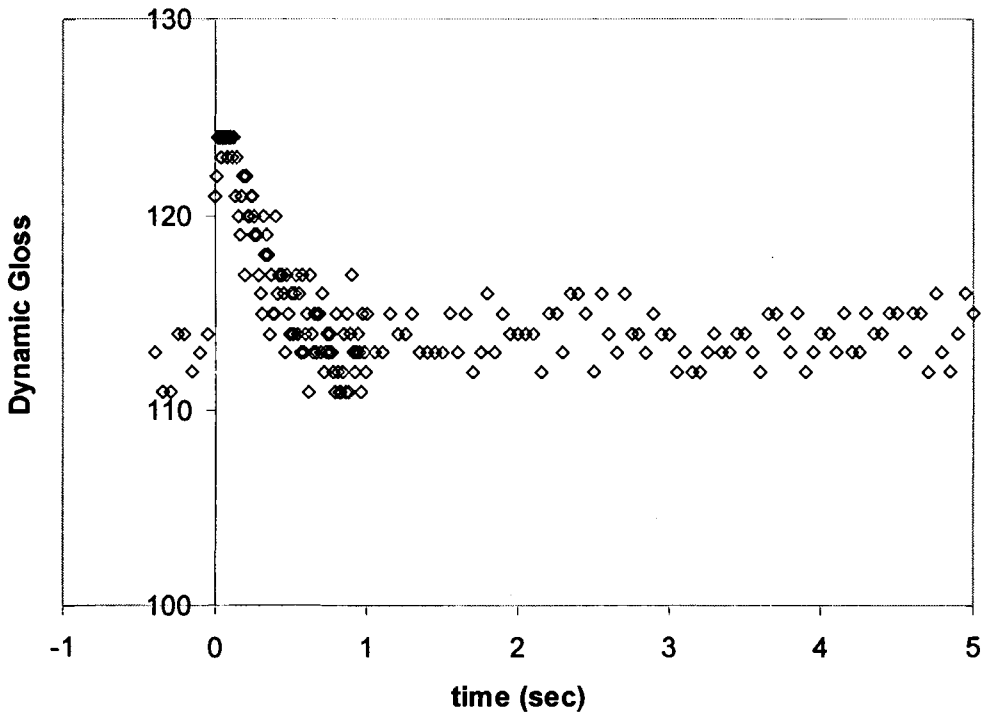

Figure 2.9 Dynamic gloss test of dye based ink on $CaCO_3$ coating

The Y-axis dynamic gloss data are electronic signals. Those signals can be transfer back to volt unit by $\frac{Y-axis-reading}{4096}\cdot 10(volt)$. But after this transform the change of the

curve will become too small to be studied. So we just use these signals in our research. Right after printing, the gloss is high because the ink levels at the top of the coating and acts as a mirror-like surface. As ink settles down on the sample, the gloss decreases until the curve flattens and there is no more gloss change. The time at which the curve flattens, called heel time, characterizes the absorption rate. The shorter the heel time, the faster the absorption rate.

2.4 Other Experimental Devices/Methods

2.4.1 Rod Draw Down Coater

A 49733 Rod Draw Down Coater from RK Print-Coat Instruments Ltd. is used in this research. During coating, a wire-wound rod fixed on the rack distributes coating slurry onto paper. The rack is driven by a speed adjustable motor.

We prepare basic coating slurry to avoid involving other factor into our absorption rate study. For coating, we use three size plastic pigments, PPL (Large Plastic Pigment, Dow 723, Dow Chemical Co.), PPM (Middle Plastic Pigment, Dow 755, Dow Chemical Co.) and PPS (Small Plastic Pigment, Dow 788, Dow Chemical Co.). The same styrene butadiene latex (Dow 620NA, Dow Chemical Co.) has been used in all coatings. For all the three plastic pigment coatings, we use latex level at 20pph, and we use latex at 10pph and 30pph for PPM plastic pigment. We also use delaminated kaolin clay (Covergloss, Huber, Lot #HBR110155171) and $CaCO_3$ (Albaglos XL, precipitated calcium carbonate, Specialty Minerals Inc.) coating pigment at latex level 10pph. Different levels of latex

are marked after the coating when necessary. For an example, PPL 20pph indicates the large plastic pigment with 20pph latex in the coating. Three base sheets have been used: low absorbance paper (B1), high absorbance paper (B2) and plastic film (Mylar). In later part of the article, if not specified, B1 paper is the base paper for coating.

2.4.2 Mercury Porosity

A mercury porosimeter (PoreSizer 9320 from Micromeritics Instrument Corporation) is used in the mercury porosity tests. This porosimeter can test pore diameters ranging from approximately 360 to 0.006μm. The PoreSizer measures the volume distribution of pores in materials by mercury intrusion or extrusion. Mercury has a high surface tension and this property makes mercury, when in contact with a solid, assume the minimum surface area and largest radius of curvature at a given pressure. An increase in pressure on the mercury causes the radius of curvature of the mercury contacting the solid to become smaller. When the radius of curvature of the mercury is equal to that of the pore, mercury fills the volume of the pore. By monitoring how much mercury gets into the porous sample while the pressure changes, a pore distribution profile for the sample can be obtained. Figure 2.10 is a plot of mercury porosity of a large plastic pigment coating.

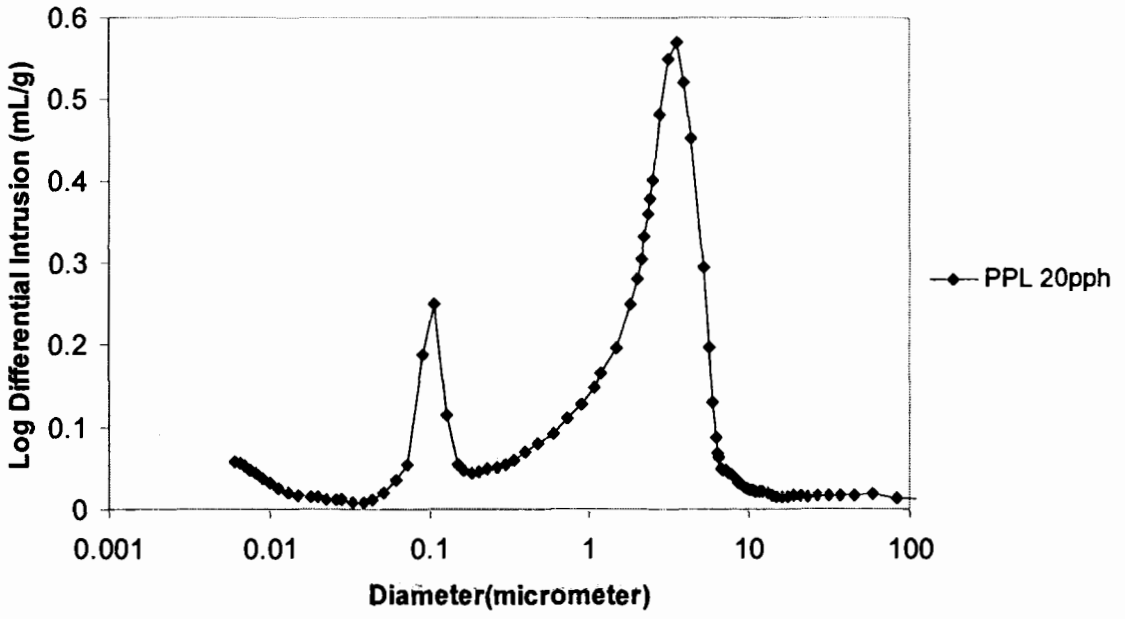

Figure 2.10: Mercury porosity test result of B1 paper based large plastic pigment coating.

There are two peaks in the plot: the smaller peak to the left is the pore distribution of the coating layer, and the higher peak to the right is the pore distribution of the base paper layer.

Based on the experimental data, we can calculate the volume void fraction of the coating layer:

$$\varepsilon = \frac{V_v}{V_v + V_s} \tag{2.4}$$

Where ε is volume void fraction, V_v is void volume of the coating and V_s is solid volume of the coating. V_v is calculated by the following:

$$V_v = (V_t - V_b) \cdot (W_p + W_c) \tag{2.5}$$

Where V_t is total intrusion volume of mercury per unit weight of the whole sample (ml/g), V_b is the intrusion volume of mercury in per unit weight of the base paper (ml/g), W_p is the base weight of the base paper (g/m^2) and W_c is the base weight of the coating (g/m^2). V_S is calculated by the following:

$$V_s = \frac{W_c}{\rho_c} \tag{2.6}$$

Where ρ_c is density of the coating.

2.4.3 Silicon Oil Void Test

The silicon oil void test is another method of obtaining the pore volume. To perform the test, the samples are first cut into sizes of approximately 5cm×5cm, and then the exact area is measured. The weight of the samples is also measured. The samples are then placed on oil-proof film, and silicon oil is applied to the samples. Fifteen minutes after the first application of silicon oil, more oil is applied to the samples to ensure that they are saturated with oil. The samples then sit for another thirty minutes. The oil is then completely wiped from the surfaces and the saturated sample weight is recorded.

The void is calculated from:

$$\text{Void} = (W_o - W_d)/\rho_o \cdot A \cdot L \tag{2.7}$$

Where W_o is the oil-saturated paper weight, W_d is the dry paper weight, ρ_o is the density of the silicon oil, A is the surface area of the sample, and L is the thickness of the sample. For the coated paper silicon oil test, we test how much silicon oil per unit area of base

paper may be absorbed, and then subtract this part from the coated paper. In actuality, however, part of the void of paper is occupied by coating pigment and is no longer available to absorb silicon oil in this test. Consequently, coating voids calculated from this method are lower than those obtained from mercury porosity tests.

2.4.4 Contact Angle

In contact angle test, a micro-liter scale syringe is used to get a 1 to 4 μL drop of liquid onto the sample. A camera records the size change of the diameter of the liquid drop on the substrate. Magnification is approximately 40x.

Setting the time the drop settles on the substrate to be zero, we measure the contact angle at 0.2 sec, 1 sec and 10 sec. Imagine the drop is part of a sphere, as shown in Figure 2.11.

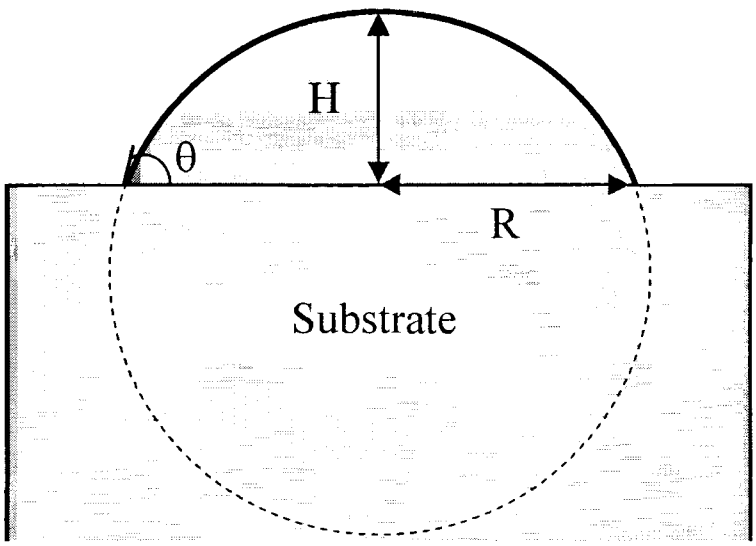

Figure 2.11: Contact angle measurement and calculation

According to geometric relationship, we can get an equation for the contact angle θ:

$$\sin\theta = \frac{2H \cdot R}{H^2 + R^2} \tag{2.8}$$

Or

$$\tan\left(\frac{\theta}{2}\right) = \frac{H}{R} \tag{2.9}$$

For sized paper, the external surface contact angle is different from the internal surface contact angle. Because that the outer surface of the paper has been sized. The internal contact angle of sized paper is measured by filing off the surface of the paper. The surface is first filed off by first using a medium roughness nail file and then a gloss nail file.

2.4.5 Air Permeability

A Sheffield-type Porosimeter is used to measure the air permeability of paper or coated paper samples. This device consists of an air flowmeter gauge, a test head, calibration orifices for standardization, and compressed air at around 45 psi.

To perform the test, the air flowmeter gauges are first calibrated. Then an appropriate pair of rubber orifice plates are chosen and put separately into the top and bottom holder. The sample is then inserted between the two rubber plates and the test head is closed tightly on the sample. The shut-off valve is opened, and using the correct flowmeter gauge the air flow rate passing the sample can be determined.

Air permeability data reflects the sample's porosity. In this research, it was also attempted to use this data as a path to get the Darcy Coefficient from the relation:

$$K = \frac{F}{A} \cdot \frac{\mu \cdot L}{\Delta P} \tag{2.10}$$

Where K is Darcy Coefficient, F is the flow rate of air passing through the paper sample, A is the area of the sample that the air passes through, μ is the viscosity of air, L is the thickness of the sample and ΔP is the pressure of the compressed air.

The test is run ten times for each sample.

2.4.6 Gloss

Gloss of substrates is tested at 20°, 60° and 75°. For testing gloss at 20° and 60°, a Micro-TRI-gloss Meter from BYK-Gardner USA is used. For testing gloss at 75°, a model D48, optical Hd gloss meter from Hunter Assoc. Lab, Inc. is used.

The test is run ten times for each sample.

2.4.7 Roughness

An alpha-step 200 Profilometer from Tencor Instruments is used to test surface roughness. This apparatus scans the sample's surface with a diamond tip stylus. For the scan range a 2mm distance, covered in 40 sec is chosen. The device gives out average roughness after each scan.

The test is run eighteen times for each sample.

CHAPTER 3: EXPERIMENTAL RESULTS AND ANALYSIS

The results of the experiments described in Chapter 2 are analyzed and compared. The key parameters that determine absorption rates are discussed. Uncoated paper absorption rate is discussed in terms of single layer media absorption. Coated paper absorption is discussed in terms of two layer media absorption. A correlation is found between absorption rates and both micro-tack and gloss evolution.

3.1 Codes of Inks, Papers and Coatings:

For convenience and commercial confidentiality, codes are used for inks and medias involved in the research. Table 3.1 is the codes for papers, inks and coatings used in the research. The inks are typical inkjet water based inks. The commercial coatings are typical coated grades for offset printing.

Table 3.1: Codes used in the research

Paper		Ink	
B1	80g Hansol woodfree paper	ID1	dye base ink
B2	85g LWC base paper	ID2	dye base ink
B3	20# Great White	IP1	pigment base ink
B4	24# Hammermill Fore MP	EG	ethylene glycol
B5	28# Hammermill Color Copy Paper		
B6	24# Weyerhauser First Choice Multiuse		
B7	60# Wausau Exact Color Copy Cover		
Coating			
PPL	Dow 723, large plastic pigment (0.45 micro diameter)		
PPM	Dow 755, middle plastic pigment (0.23 micro diameter)		
PPS	Dow 788, small plastic pigment (0.1 micro diameter)		
C1	commercial coating		
C2	commercial coating		
C3	commercial coating		

Tables 3.2, 3.3 and 3.4 are the properties of papers, inks and coatings respectively. In Table 3.2, the pore size of B3, B4, B5, B6 and B7 are estimated data, base on other sample similar in nature. In Table 3.3, properties of inks are from the manufacturer, and properties of water and ethylene glycol are from *McGraw Hill Chemical Properties*.

Table 3.2: Properties of seven papers

	Air permeability	Gloss			Roughness	Thickness	void fraction		Dominate pore size
							silicon oil	mercury	(diameter)
	(mm/s)	20°	60°	75°	um	um			um
B1	32.3	1.4	4	4.7	3.48	99	0.3482	0.3185	3.2884
B2	86.7	1.4	3.5	4.1	3.65	114	0.4477	0.4355	3.4781
B3	49.2	1.9	3.8	4.8	3.54	101	0.4029		3
B4	60.9	1.9	3.9	5.5	4.11	119	0.4134		3
B5	50.2	2.1	4.7	9.2	2.26	120	0.4461		3
B6	61.9	2	4.4	7.1	2.72	111	0.481		3
B7	40.2	2.1	5.2	9.3	2.73	189	0.4419		3

Table 3.3: Properties of five fluids

	viscosity	surface tension
	mPa*s	N/m
water	0.89	0.072
ethylene glycol	17.65	0.048
ID1	4.65	0.028
ID2	3.65	0.029
IP1	2.11	0.030

Table 3.4: Properties of coatings on B1 paper base.

	Air Permeability flow velocity	Gloss			Roughness	Coating Thickness	Void fraction		Dominate Pore size diameter
	(mm/s)	20°	60°	75°	(um)	(um)	silicon oil	mercury	(um)
PPL 20pph	2.1	1.5	10.8	44.0	2.2	27	0.309	0.321	0.13
PPM 10pph	3.5	2.0	18.0	55.7	2.0	29		0.361	0.08
PPM 20pph	1.9	1.9	16.2	55.0	1.8	26	0.321	0.344	0.08
PPM 30pph	0.7	1.5	11.8	48.3	1.9	26		0.195	0.08
PPS 20pph	5.6	2.2	16.4	51.5	1.7	26	0.311	0.354	0.05
Clay	1.1	1.6	10.9	43.6	1.6	14	0.263	0.233	0.1

3.2 Single Layer Substrate Absorption Rate

3.2.1 Influence of Void Volume on Absorption

According to the Lucas-Washburn equation, Eq. (1.6), as the void volume of the substrate increases, the absorption rate increases. However, our experimental data did not show this tendency for paper absorption in all case. Figure 3.1 is the absorption volume of water and ID1 ink on seven papers as a function of paper void fraction. The reason for this result could be that besides the void volume, paper fibers involve in absorption. Also, the contact angles of some of the sample are high as shown in Table 3.5. This suggests that they are sized which affects their absorption behavior.

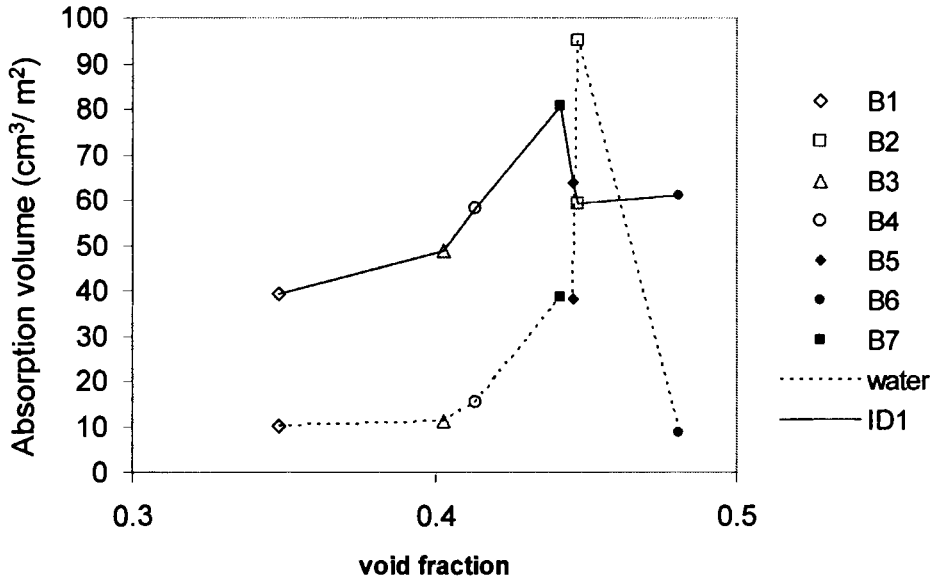

Figure 3.1: Absorption volume at 1.5 contact time of water and ID1 ink on seven papers verse paper void fraction.

3.2.2 Influence of Contact Angle on Absorption

Paper absorption is complicated because both the pore volume and the wood fibers are involved. How the fluid contacts and wets the fiber affect both volume and fiber absorption. Contact angle is generally used to characterize the surface chemistry of paper.

Figure 3.2 shows the absorption volume of the uncoated papers as a function of contact angle with ID1 ink and ethylene glycol. In the plot, it is absorption volume of ID1 ink at 0.3 sec absorbing time versus contact angle of ID1 ink on six papers at 0.2 sec, and absorption volume of ethylene glycol ink at 1.5 sec absorbing time versus contact angle on six papers at 1 sec. Because ID1 ink drop balances at around 0.2 sec, and ethylene glycol drop at 1 sec, different times have been chosen for the two fluids.

According to the Laplace equation, Eq. (1.1), smaller contact angle leads to higher capillary pressure, the drawing force in capillary absorption. Our experimental results showed the expected tendency in Figure 3.2. As contact angle increases, rate of absorption decreases.

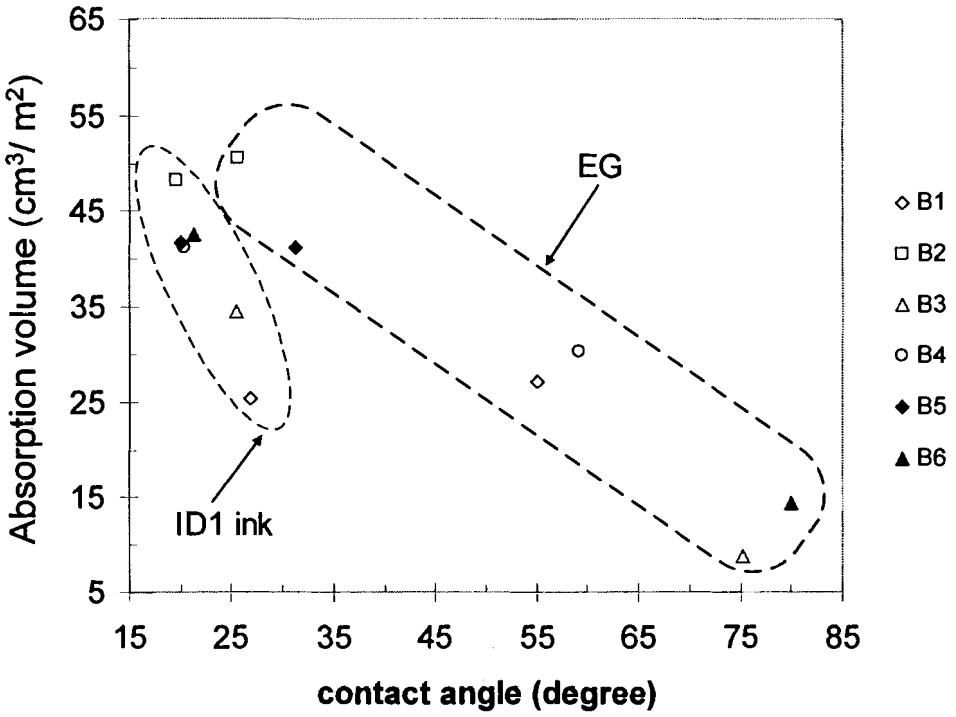

Figure 3.2: Effect of contact angle on one layer media absorption rate with ID1 and ethylene glycol.

A similar relationship between the absorption rate and contact angle is seen with water on the same papers shown in Figures 3.3 and 3.4. For water-paper contact angle, the contact angle of the external surface as well as the internal surface has been measured.

In the Figures 3.3 and 3.4, it is absorption volume of water at 1.5 sec absorbing time versus contact angle at 1 sec on external surface and on internal surface of six papers, respectively.

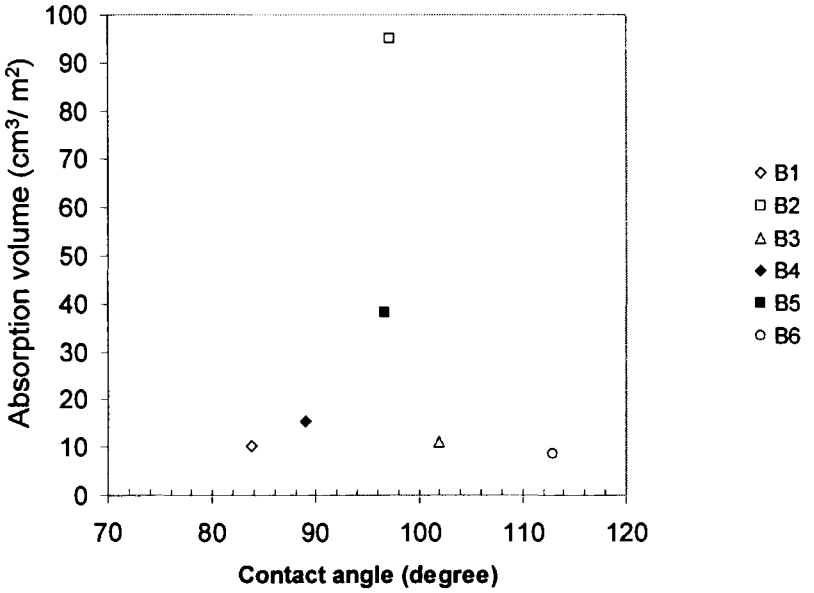

Figure 3.3: Absorption volume versus external contact angle of water on papers.

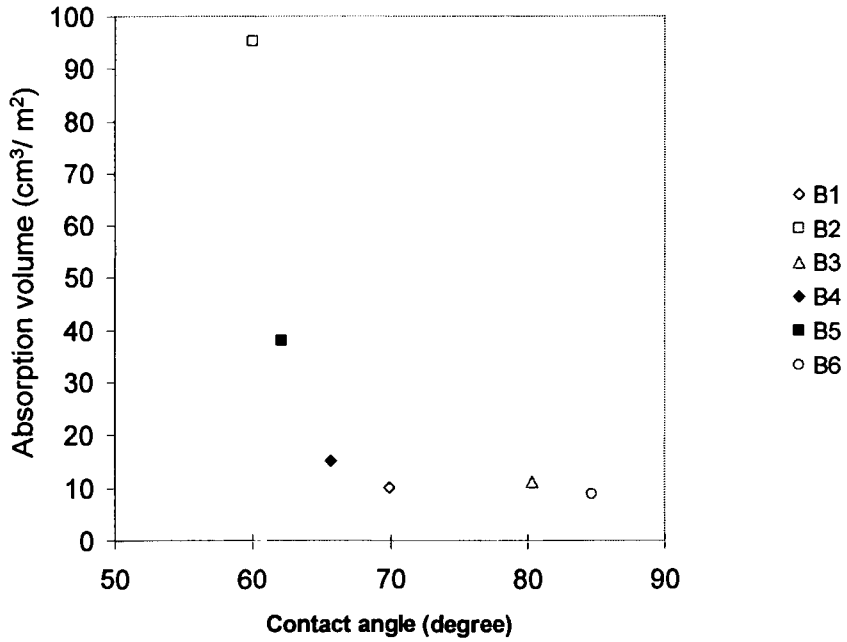

Figure 3.4: Absorption volume versus internal contact angle of water on papers.

Since the papers used here are all commercial samples, all of them have been sized to increase resistance to penetration of aqueous liquid. Filing the surface off of the paper sheet helps clear the effect of some of sizing agent, thus filed paper surface (internal surface) contact angle may represent contact angle of paper fiber and liquid. This could explain why internal surface contact angles are lower than external surface contact angle as shown in Tables 3.3 and 3.4. Though both Figures 3.3 and 3.4 have the similar tendency shown in Figure 3.2, the internal surface contact angles are better related to water-paper absorption volume than the external surface contact angles. Therefore, the internal contact angle is better related to absorption rate. The raw data for absorption volumes is in Appendix B. The measured contact angle of water, ethylene glycol and ID1 ink on seven papers is shown in Table 3.5. Contact angle of EG and ID1 is external contact angle. N/A in the table indicates samples in which contact angle could not be measured.

Table 3.5: Contact angle results at different contacting time of three fluids: water, ethylene glycol (EG) and ink ID1 on seven papers.

	water contact angle						EG contact angle			ID1 contact angle		
	external surface			internal surface								
time	0.2s	1s	10s	0.2s	1s	10s	0.2s	1s	10s	0.2s	1s	10s
B1	85.9	83.71	75.23	72.1	69.9	49.3	75.1	55.1	33.4	26.8	12.6	5.8
B2	106.6	97.2	48.7	80.7	60.0	N/A	82.7	50.5	18.4	19.6	9.5	N/A
B3	103.4	101.9	101.3	87.7	80.3	61.6	90.3	75.2	58.4	25.5	11.7	N/A
B4	90.8	88.9	86.7	68.3	65.7	56.9	81.6	59.2	33.2	20.4	9.5	N/A
B5	98.8	96.6	91.1	66.9	62.1	35.7	59.4	31.2	24.4	20.1	10.5	N/A
B6	115.7	112.9	112.0	87.4	84.8	75.5	96.7	80.0	54.7	21.3	10.9	N/A
B7	89.4	86.7	84.6	64.0	61.8	51.2	58.9	34.2	23.7	23.0	10.8	N/A

3.2.3 Influence of Fluid Properties on Absorption

The absorption rate is known to depend on contact angle, substrate void fraction, fluid viscosity and surface tension as in the Lucas-Washburn equation ,Eq. (1.4). For the same paper at the same absorption time, all the substrate properties are fixed. Therefore according to the Lucas-Washburn equation, absorbed volume should be linearly proportional to $(\gamma\cos(\theta)/\mu)^{0.5}$. Figure 3.5 show the result of 3 sec contact time absorption volume of three fluids versus $(\gamma\cos(\theta)/\mu)^{0.5}$ for the seven papers. For each paper, three fluids (ethylene glycol, ID1 ink and water) have been used. All data points for the same paper are connected with dotted lines. The left points in the dotted line are data from ethylene glycol, the middle points in the dotted line are data from ink ID1, and the right points in the dotted line are data from water.

Figure 3.5 shows that fluid absorption rate is not linearly related to $(\gamma\cos(\theta)/\mu)^{0.5}$. This is different from one layer absorption rate described by the Lucas-Washburn equation, Eq. (1.5).

The reason that our plot showed different tendency from the popularly accepted one-layer absorption Lucas-Washburn model on relationship of Absorption volume and $(\gamma^*\cos(\theta)/\mu)^{0.5}$ is not clear . One explanation could be that in addition to capillary absorption, the paper fibers are involved in the absorption, so Lucas-Washburn's model does not apply here.

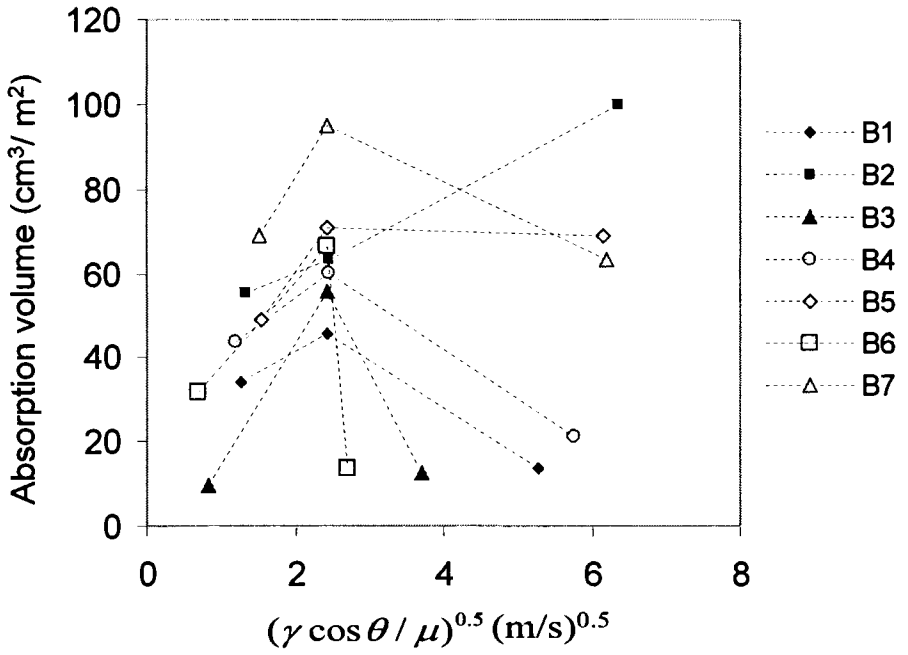

Figure 3.5: Fluid absorption volume versus $(\gamma\cos(\theta)/\mu)^{0.5}$on seven papers.

3.3 Two Layer Substrate Absorption Rate:

3.3.1 Influence of Base Paper Absorbance

Generally, coating layers are around 10~40 μm thick with a void fraction around 0.3. Therefore the available volume per unit area is 3~12cm^3/m^2. For a coated sample with an absorption volume in ordinary range (~15 μm), about half of the fluid is absorbed by the base paper.

The base paper's absorbance influences the whole coated paper's absorption rate as seen in Figure 3.6. The B2 paper has higher absorbance than B1. Figure 3.6 compares absorption rates for medium size plastic pigment coating at 20pph latex content on two different absorbance level papers. The coating layer slows the absorption rate on the high absorbance paper B2. However, for the low absorbance paper B1, it increases the rate at short contact times. For the coated high absorbance paper, the results are expected and can be explained as an added resistance from coating layer to absorption. For the coated low absorbance paper, the coating layer is more absorbent than the low absorbance paper, and thus helps increasing the absorption rate of coated paper until the coating layer is full.

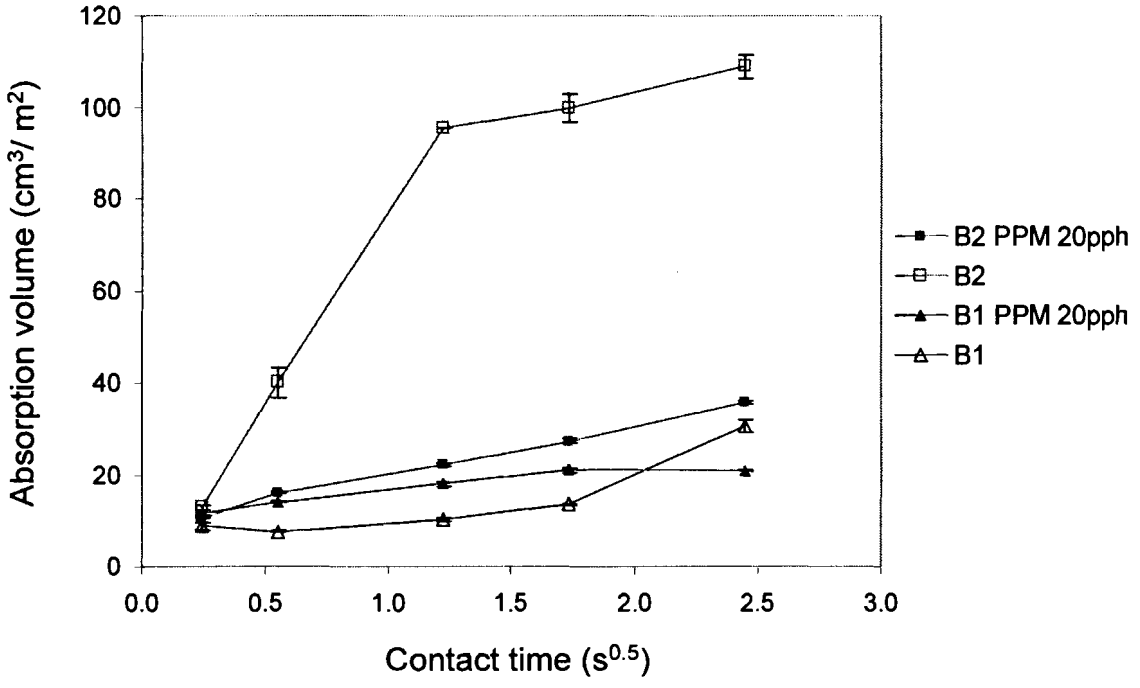

Figure 3.6: Water absorption volume on coated and uncoated low and high absorbance papers.

Figure 3.7 compares three other coatings on the same two base papers. The more absorbent paper based coating gives higher absorption rates in all cases. For the high absorbance paper base (B2) coated with $CaCO_3$, the absorption volume increases and exceeds that of middle plastic pigment and clay coatings. The explanation could be that $CaCO_3$'s loose structure results in less resistance to fluid penetration through the coating layer than with other coating layers. At short contact time, fluid is mainly absorbed by the coating layer and the $CaCO_3$ coating has a low driving force for absorption. But at long contact time, the base paper's absorbance starts to show more influence on the whole coated paper's absorption rate.

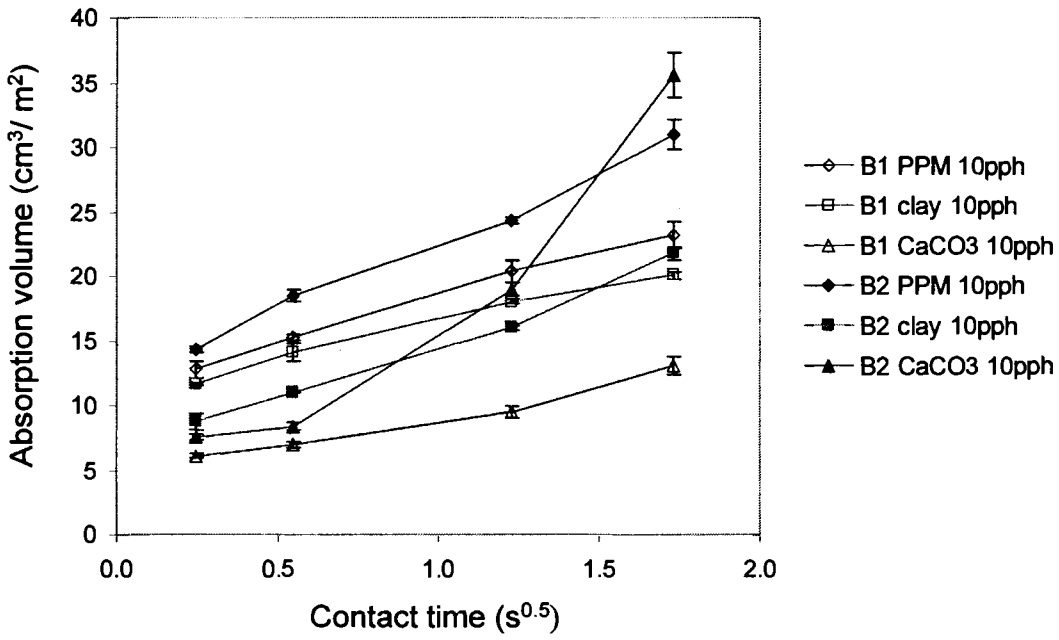

Figure 3.7: Water absorption volume on PPM 10pph, clay and $CaCO_3$ coatings with B1 and B2 base paper separately.

3.3.2 Influence of Substrate Pore Size

The Lucas-Washburn equation, Eq. (1.5), predicts that the depth of fluid penetrating into the substrate is proportional to the square root of the substrate's pore radius.

Figures 3.8 and 3.9 show the pore size influence on absorption rate. Contrary to the Lucas-Washburn equation, as pore size increases, absorption volume decreases. This result is hard to explain. It could be that upon drying, the latex is easier to block the connections between the large pores than the small pores. However, other factors like contact angle and void fraction are also involved. Further study is needed in this respect.

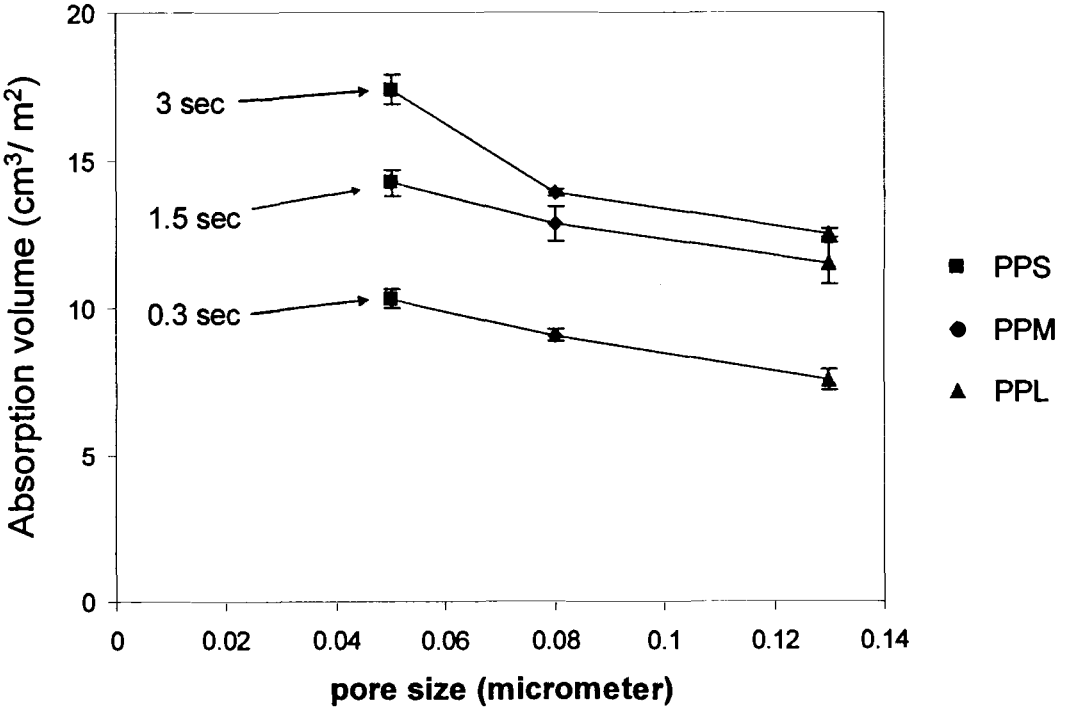

Figure 3.8: Ethylene glycol absorption volume at 3, 1.5 and 0.3 sec contact times for three plastic pigment coatings at 20pph latex level on B1 paper base.

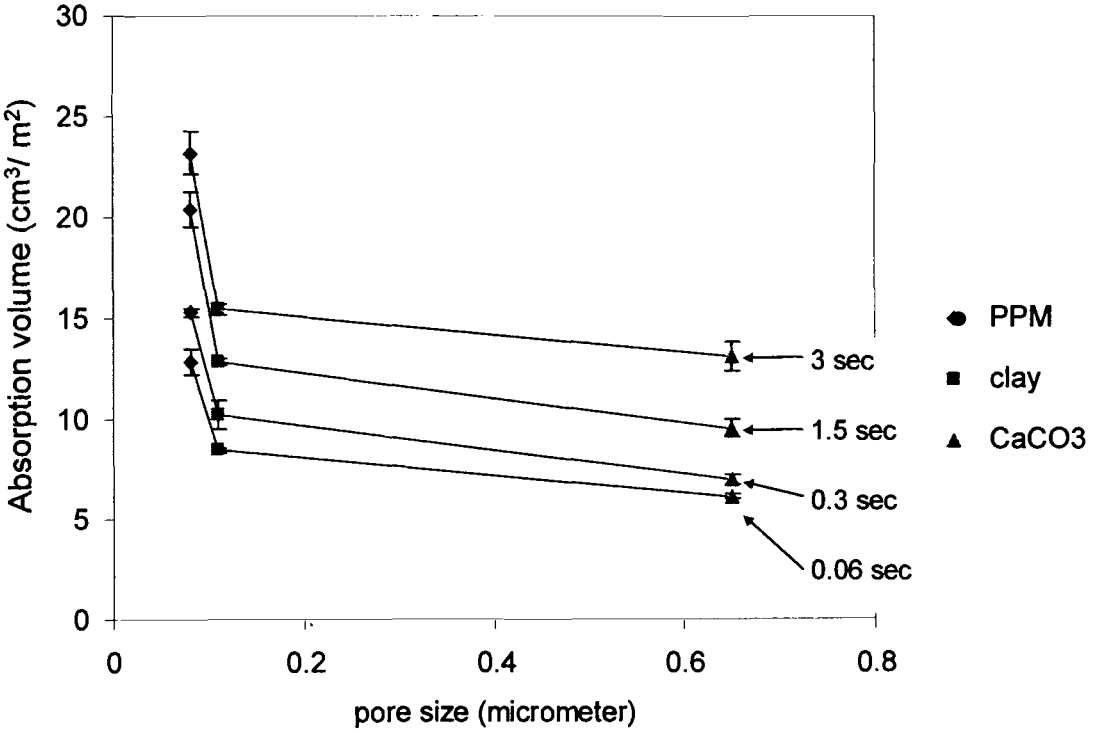

Figure 3.9: Water absorption volume at 3, 1.5 and 0.3 sec contact times for PPM, clay and $CaCO_3$ coatings at 10pph latex level on B1 paper base.

3.3.3 Influence of Binder Level

Figure 3.10 shows the effect of coating binder level on absorption rate. The absorption rate decreases as the latex level increases. Increasing binder level changes the structure of the coating by changing the distribution of pores, reducing pore volume and connecting large voids with small channels.

The influence of binder level on absorption rate can be plotted in terms of coating void fraction as in Figure 3.11. These trends duplicate the expected trends from the Lucas-Washburn equation. As the binder level increases, the coating void fraction becomes smaller. Therefore the absorption rate is slower.

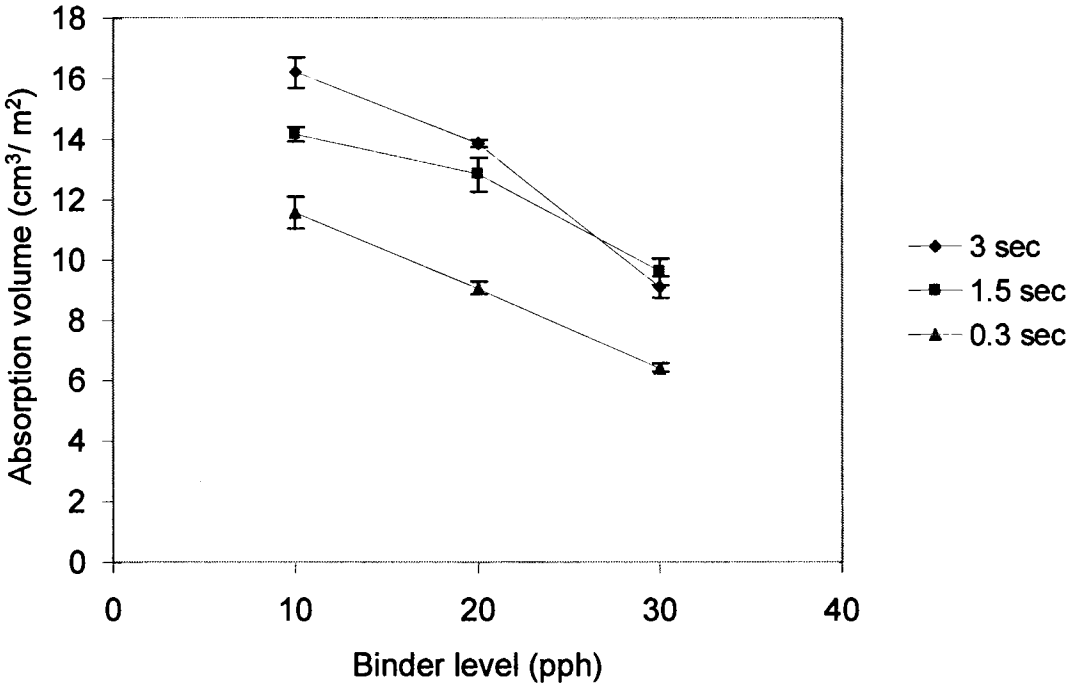

Figure 3.10: Ethylene glycol absorption volume on B1 paper based PPM coating with latex at 10pph, 20pph and 30pph separately.

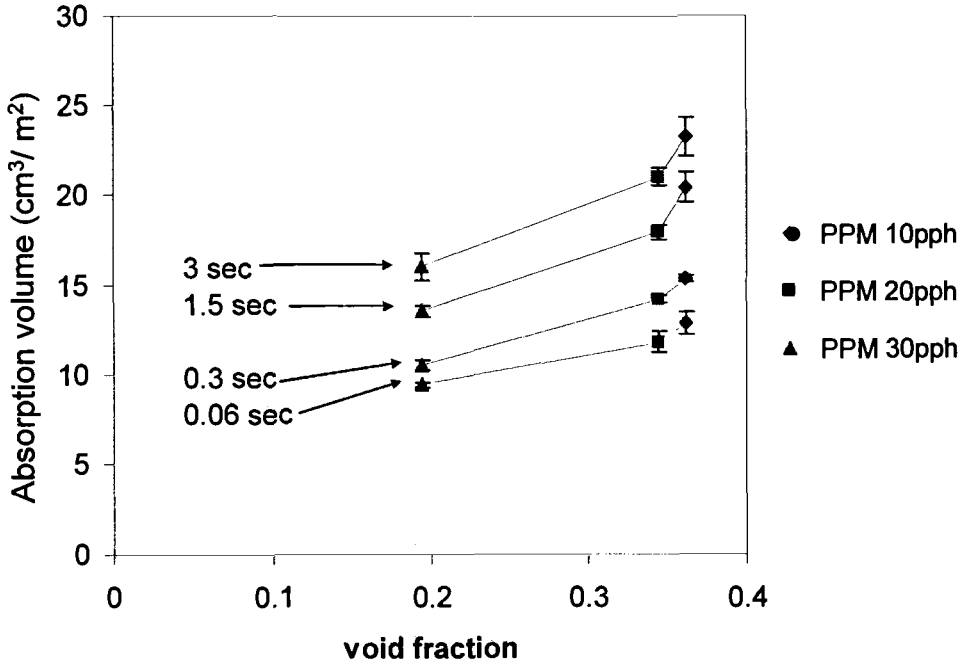

Figure 3.11: Water absorption volume on B1 paper based PPM coating at 10pph, 20pph and 30pph latex level versus void fraction of the coatings.

3.3.4 Influence of Fluid-Substrate Surface Contact Angle

The absorption rate is plotted as a function of cosine contact angle as given in Figure 3.12. Results for uncoated samples show that smaller contact angle led to faster absorption. However, this tendency is not clear in the Figure 3.12, because of the absorption rate is influenced by a number of other parameters. Table 3.6 shows the measured contact angle of water and ethylene glycol on B1 paper based coatings.

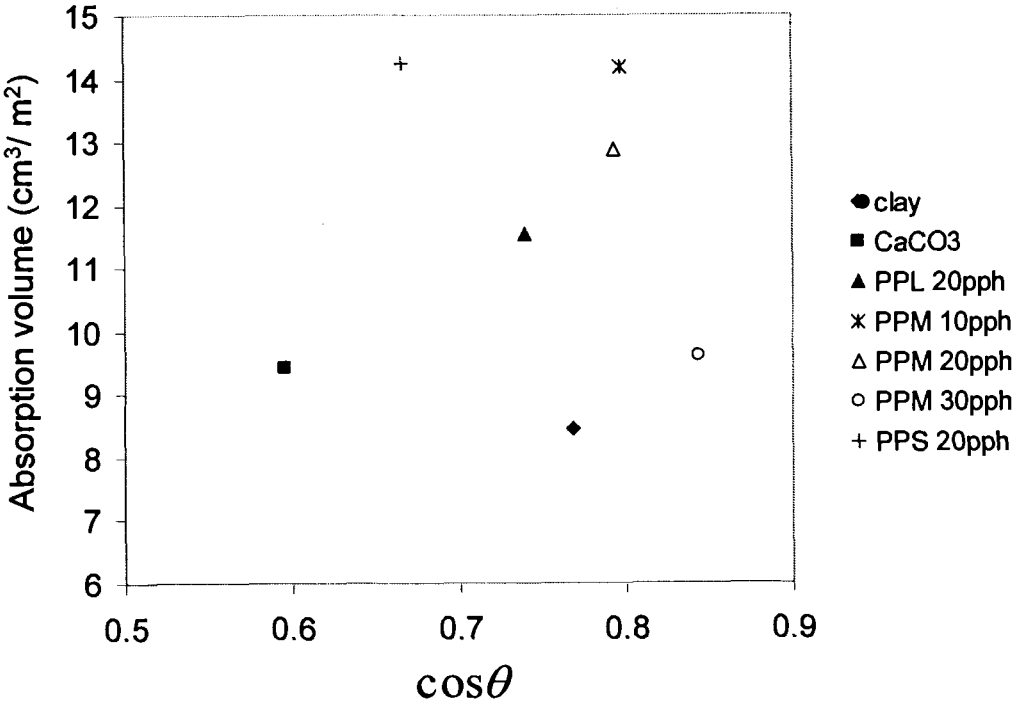

Figure 3.12: Ethylene glycol absorption volume at 1.5 sec contact time versus cosine contact angle at 1 sec for B1 paper based coatings.

Table 3.6: Water and ethylene glycol contact angle of coatings on B1 paper base.

	Water			EG		
contact time	0.2 s	1 s	10s	0.2 s	1 s	10s
clay	64.0	53.0	48.3	56.4	39.8	32.7
$CaCO_3$	76.7	59.1	51.6	69.0	53.5	39.7
PPL 20pph	79.8	65.2	61.7	70.1	42.3	35.4
PPM 10pph	61.2	50.1	42.6	54.6	37.1	23.7
PPM 20pph	75.6	66.4	64.3	54.3	37.5	28.3
PPM 30pph	69.8	64.4	60.5	54.9	32.5	30.6
PPS 20pph	75.6	62.4	54.5	85.6	48.3	31.8

3.3.5 Influence of Fluid Properties

A plot of absorption volume against $(\gamma\cos(\theta)/\mu)^{0.5}$ as shown in Figure 3.13 has been developed to find out the combined influence of fluid properties on absorption rate. All data points for the same coating are connected with dotted lines. The left points in the dotted line are data from ethylene glycol, the middle points are data from ink ID1, and the right points are data from water.

The results should be linear lines if the Lucas-Washburn equation holds. The results show this trend except some deviation. This is because more parameters such as base paper absorbance involved in the absorption.

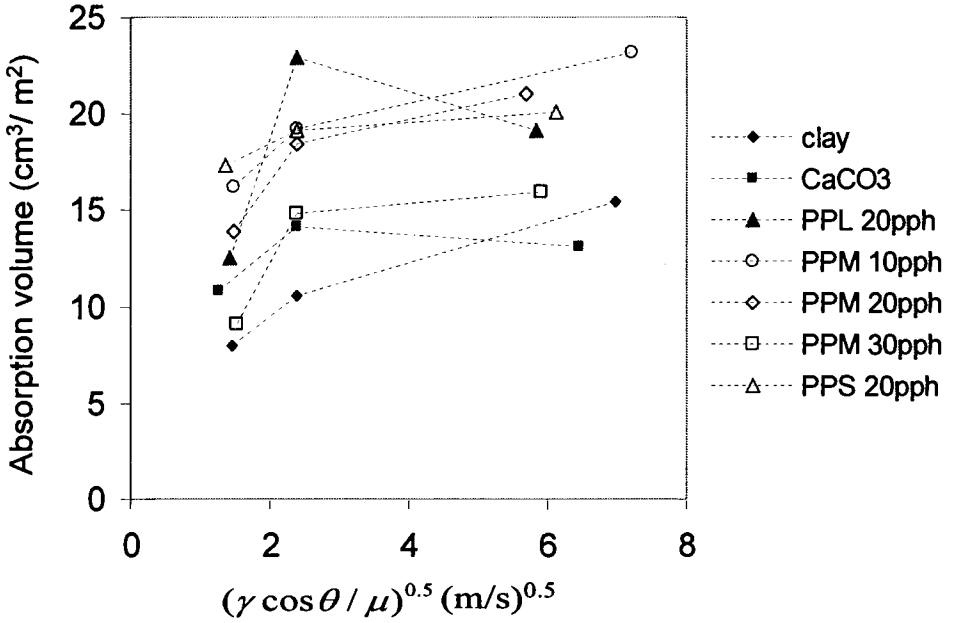

Figure 3.13: Fluid absorption volume at 3 sec contact time versus $(\gamma\cos(\theta)/\mu)^{0.5}$ on B1 paper based seven coatings.

3.4 An Observation from the Absorption Test:

According to the Lucas-Washburn equation, Eq. (1.5), the depth of the fluid penetrating into the substrate is proportional to penetration time:

$$L = k \cdot t^a \tag{3.1}$$

Where L is penetration depth into the substrate per unit area, k is the equation coefficient, t is time, and a is the power coefficient.

The coefficient a is equal to 0.5 in the Lucas-Washburn equation. To compare our experimental data with the Lucas-Washburn equation, a histogram of the values of a from our experiment was generated and is shown in Figure 3.14. In the Figure, absorption tests for five kinds of fluid (water, ethylene glycol, ID1, ID2 and IP1) on 23 different kinds of coated and uncoated papers are included. In all, 81 series of absorption test results are studied. As we described in Chapter 2, roughness of the substrate is involved in TLV in the Bristow absorption test. Therefore, we use Eq. 3.2 to calculate a:

$$TLV = k \cdot t^a + R_u \tag{3.2}$$

Where TLV is equivalent to L the penetration depth, Ru is roughness of the substrate.

Figure 3.14 shows that the value of a is mostly around 0.2 . This result is close to that found by Danino and Marmur (1994) instead of the Lucas-Washburn equation. Danino and Marmur attributed this deviation from the Lucas-Washburn model to the limited liquid reservoir, because their unlimited liquid reservoir experiment results agreed with the Lucas-Washburn model. They said that in amount-limited liquid absorption, the liquid tended to redistribute by flowing from the large pores into the small ones. Thus

leaves parts of substrate unsaturated. And since penetration into small capillaries is slower than penetration into large ones, the penetration from a finite reservoir is slower than the penetration from an unlimited reservoir.

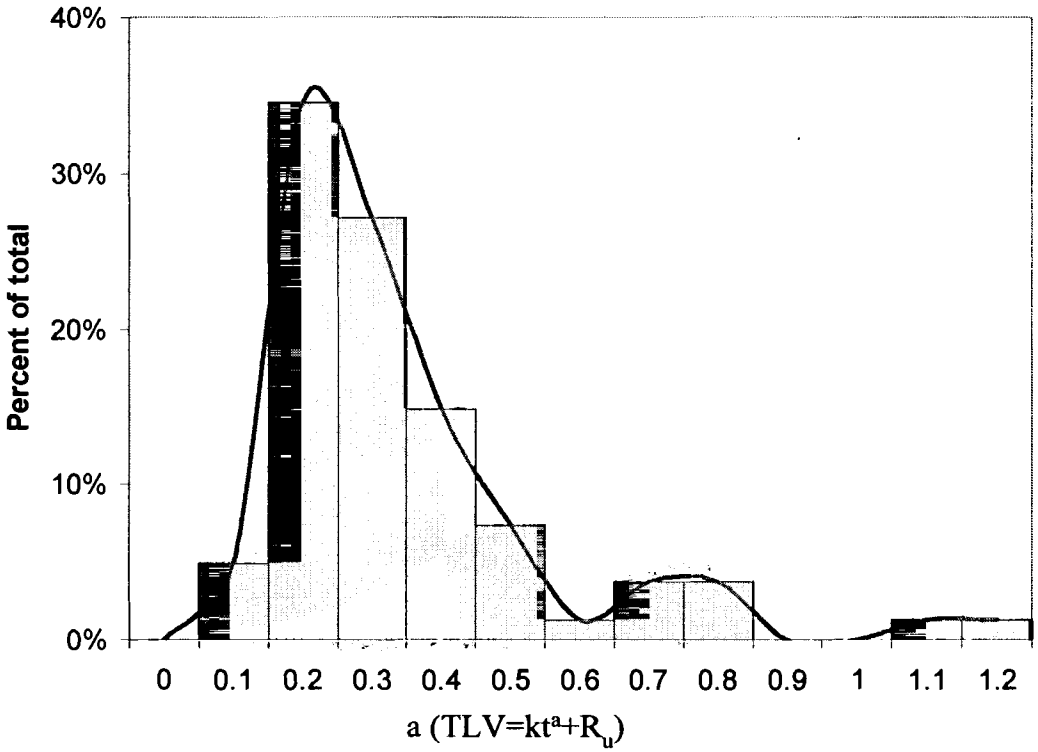

Figure 3.14: Distribution of the power coefficient *a*

Another reason could be that during the liquid flow inside the network of pores in the porous medium, some disconnections appear in the flow stream. The penetration is no longer continuous capillary flow in this case and is slower than the Lucas-Washburn continuous penetration.

3.5 Micro-Tack Test Results

For some of the tack tests, the tack force data curve is flat at the beginning. This flat tack force curve happens for fast absorption coatings and most papers. However, a flat curve does not necessarily mean a fast absorption rate. For some papers, even if their rate of absorption is low, their rough surface makes it impossible for a large fluid bridge to form between the tack head and the substrates. Therefore the tack force is low and the curve is similar to that of the fast absorption substrates.

Figure 3.15 shows tack test curves of IP1 ink on five papers. The tack force curve remains low and flat right after the first touch. No obvious peak is shown in these tests. From the absorption data in the Appendix B, we know these papers are very absorbent for the ink IP1. Among these papers, the absorption volume for B7 is almost twice as much as that of B3 papers. However, curves of B3 and B7 flatten at about the same time.

Figure 3.16 shows tack test result of two dye inks (ID1 and ID2) and one pigment ink (IP1) on non-absorbing plastic film (Mylar). As time passes during the tack tests, volatile components in the ink evaporate and the ink becomes thicker. Therefore the tack force becomes larger. After all the volatile components evaporate, the remaining components of the ink remain the same for an extended period. The tack force is expected to stay around the same value and the curve of tack force stays flat. Note that the tack force of IP1 is the highest among the three inks, ID2 is second, and ID1 has the lowest tack force. The same sequence can be observed on other coated samples to be discussed.

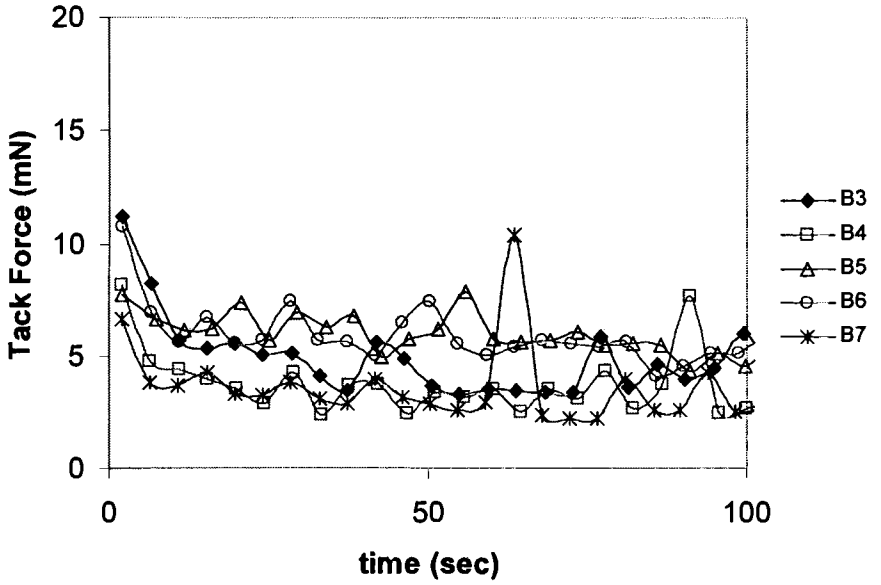

Figure 3.15: Tack test of pigment ink IP1 on five papers.

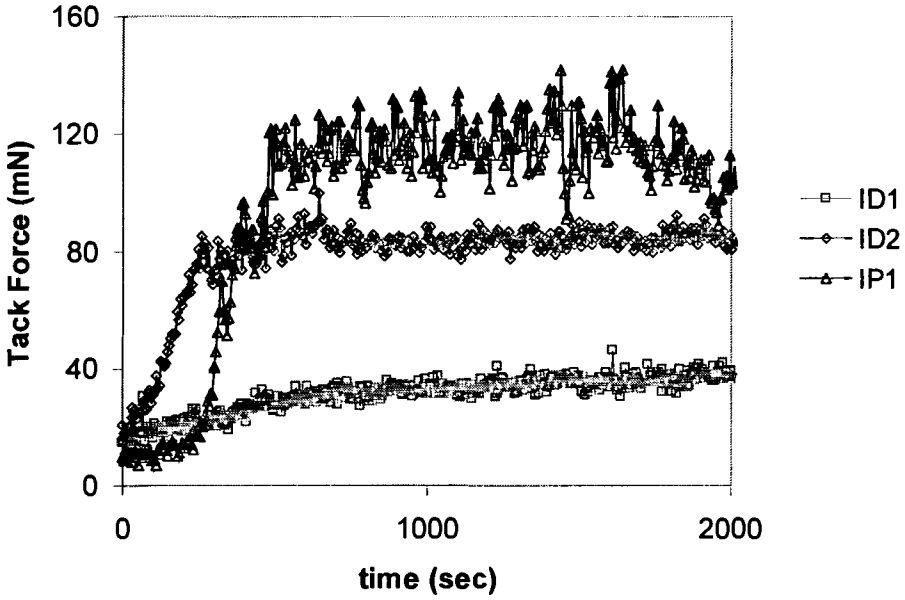

Figure 3.16: Tack test of ID1, ID2 and IP1 inks on Mylar plastic film.

Figure 3.17 is the tack test of IP1 ink on coatings with B1 and B1 base paper separately as well as three commercial coated papers. The time where the tack force reaches its highest point is called tack peak time. The tack peak time may reflect the absorption rate of substrates. Shorter tack peak time means faster absorption rate.

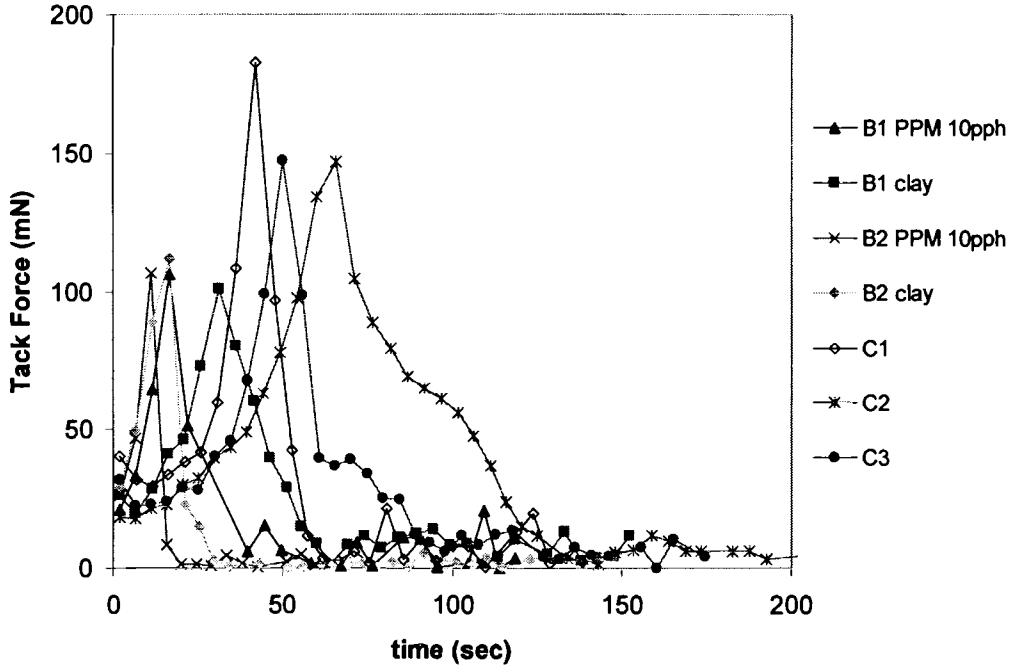

Figure 3.17: Tack test of pigment ink IP1 on PPM 10pph and clay coatings on B1 and B2 base paper, and on three commercial coated papers C1, C2 and C3.

A good correlation is found as shown in Figure 3.18, between the time to reach the peak tack value and the absorption volume of the sample. Therefore, the dynamics seen in the tack curve must be related to absorption rate.

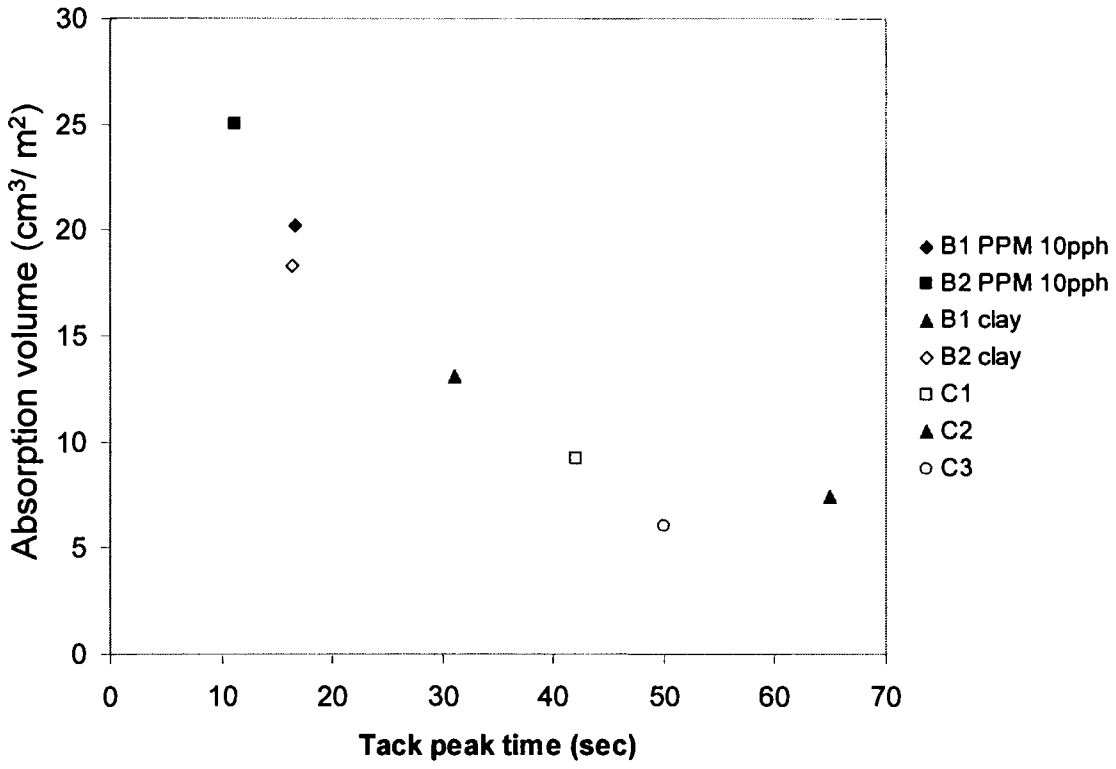

Figure 3.18: Three second absorption volume versus tack peak time for IP1 ink.

Figure 3.19 shows tack test of ID1 ink on coatings. Since the highest tack force with ID1 ink is low, the curves are more scattered than IP1 ink tack curves. After an initial climb, the tack force tends to decrease as a function of time. Again, the plot of absorption volume versus tack peak time gives a good relation as shown in Figure 3.20.

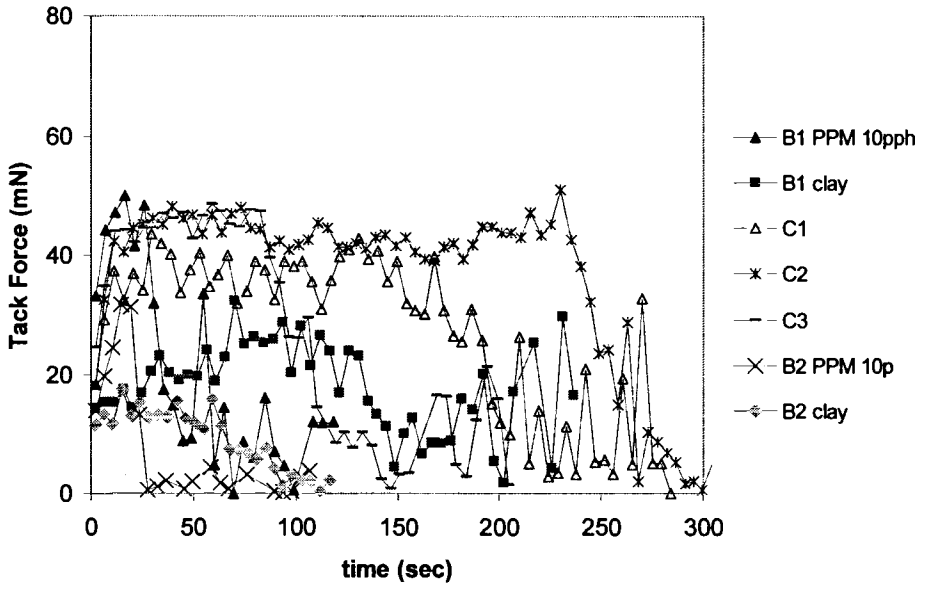

Figure 3.19: Tack test of dye ink ID1 on PPM 10pph and clay coatings on B1 and B2 base paper, as well as on three commercial coated papers C1, C2 and C3.

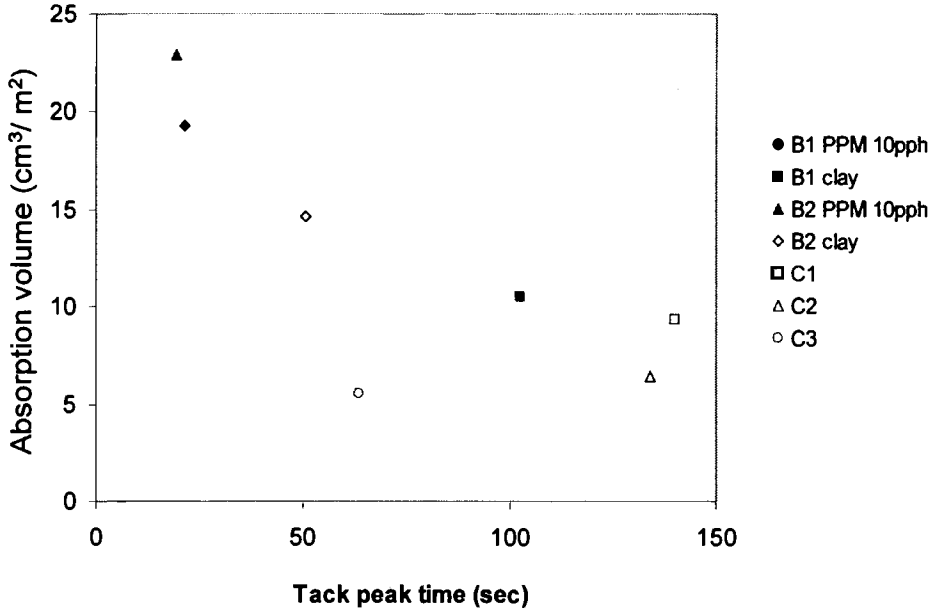

Figure 3.20: Absorption volume of ID1 ink at 3 sec contact time versus tack peak time.

Figure 3.21 shows tack test of ID2 ink on coatings. In the tack test of ID2, even though every curve reaches its tack peak, four coatings (B1 based clay, C1, C2 and C3) did not decrease as low as the three other coatings. According to absorption experiment results, these four coatings are the four least absorbent coatings among the seven. The reason for the different tack force curves could be that some ingredients in the ink react with the coating. Therefore some component of the ink gets trapped at the coating surface and keeps the tack force staying high for a long time. A good relation of TLV versus tack peak time had been gained for ID2 ink as shown in Figure 3.22.

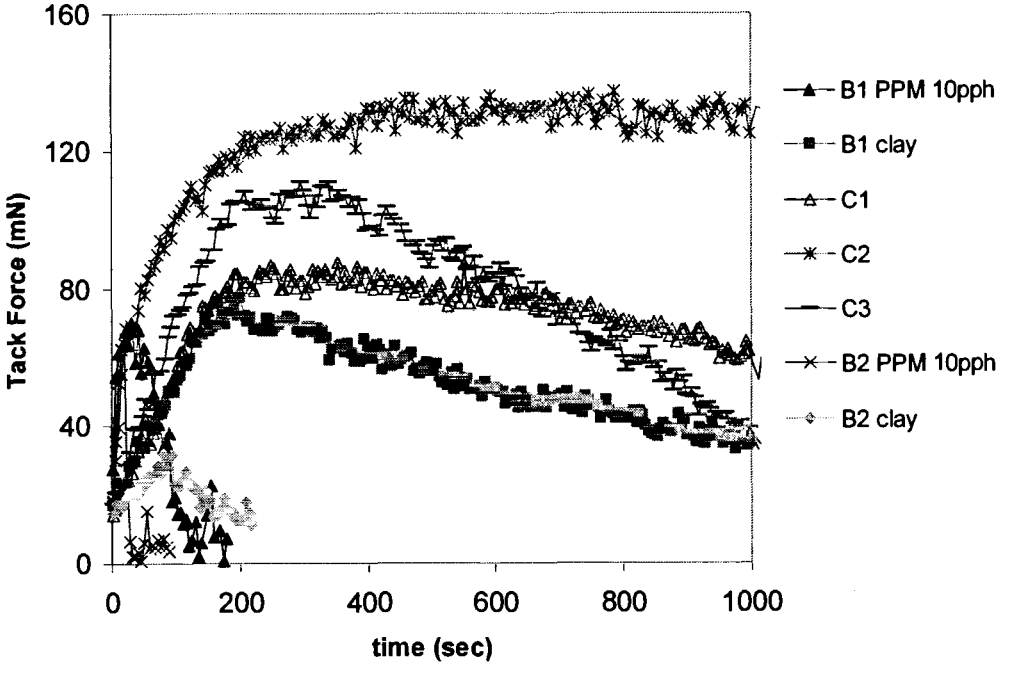

Figure 3.21: Dye ink ID2 tack test on coatings.

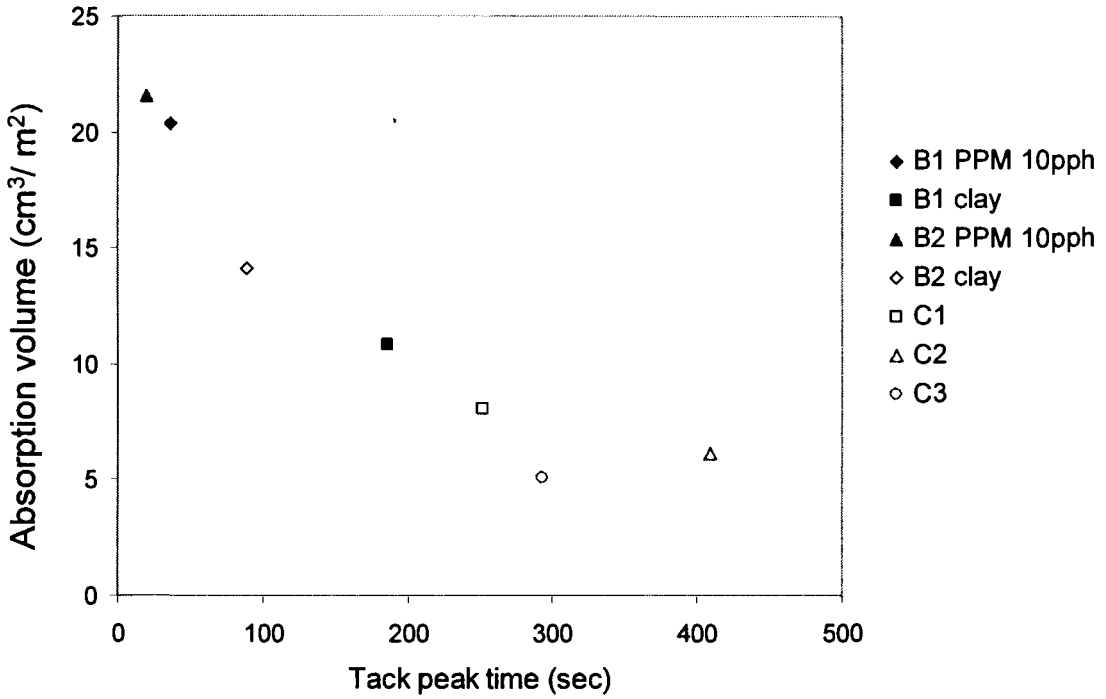

Figure 3.22: Absorption volume of ID2 ink at 3 sec contact time versus tack peak time.

Figure 3.23 shows that absorption volume is indirectly related to tack peak time when comparing different inks on the same coating as well as when comparing the same ink on different coatings as is shown in Figure 3.17 to Figure 3.22. The absorption volume of the three inks on the same coating did not show too much difference, but in tack test, the tact peak time data differ significantly for the three inks on the same coating. The reason could be that some components in the two dye inks (ID1 & ID2) remain sticky much longer than water.

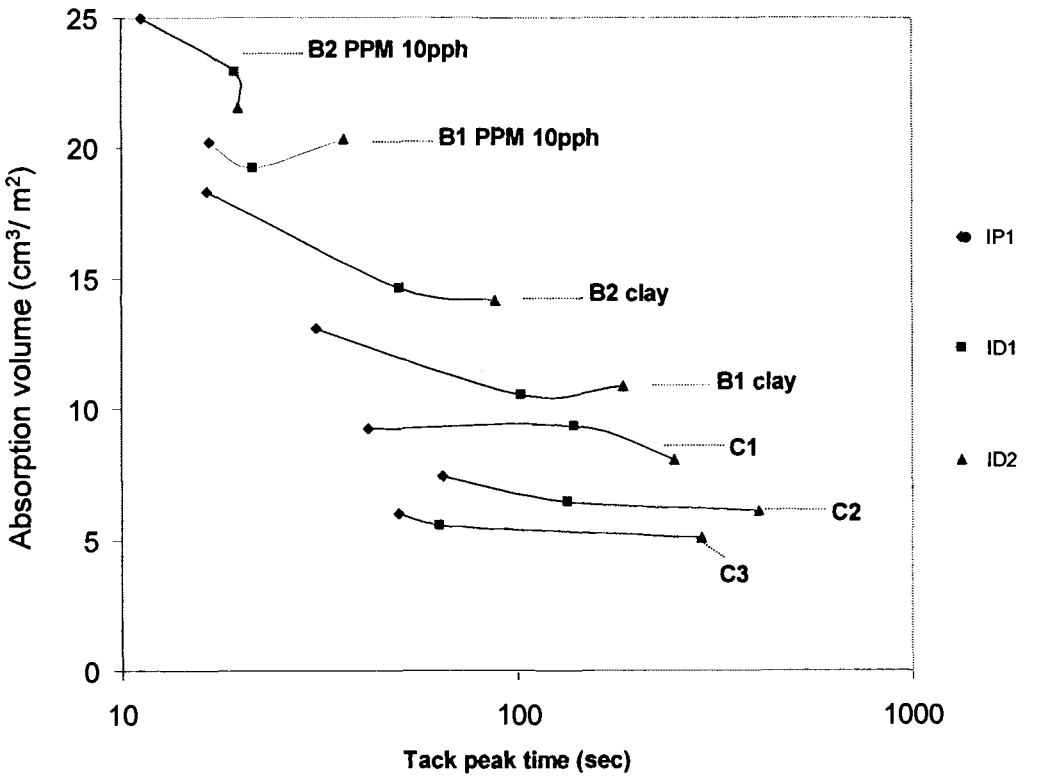

Figure 3.23: Absorption volume at 3 sec contact time verse tack peak time of three inks on seven coatings. Each line is comparison of the test results on one coating with three inks.

Since tack peak time results correspond well to absorption volume, and the range of tack peak time of ID2 is much wider than the other two inks, a regression equation for ID2 ink on tack test as shown in Figure3.24. Each point in the plot corresponds to the test results of one ink on one substrate.

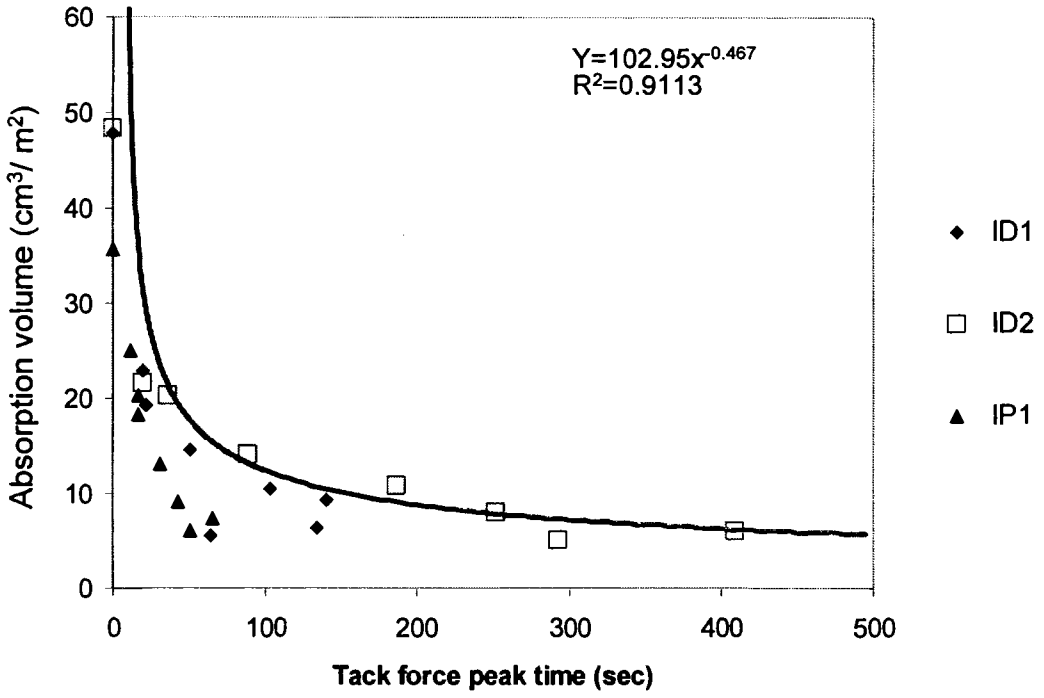

Figure 3.24: The regression Curve for 3 sec absorption volume versus tack peak time for ID2 ink.

In the regression shown in Figure 3.24, the absorption volume is proportional to tack peak time at almost minus half power. There is no obvious physical reason why this power should come up. A better understanding between fluid volume and tack force is needed.

3.6 Dynamic Gloss Test Results

Figure 3.25 shows a typical result for ink ID2 on the B1 paper based $CaCO_3$ coating. The gloss increases at short times, due to the leveling of the ink drops to form a mirror

surface. The gloss drops due to absorption as menisci are formed at the top of the ink surface. The heel time is defined as the time the gloss drops and stops changing as shown in Figure 3.25.

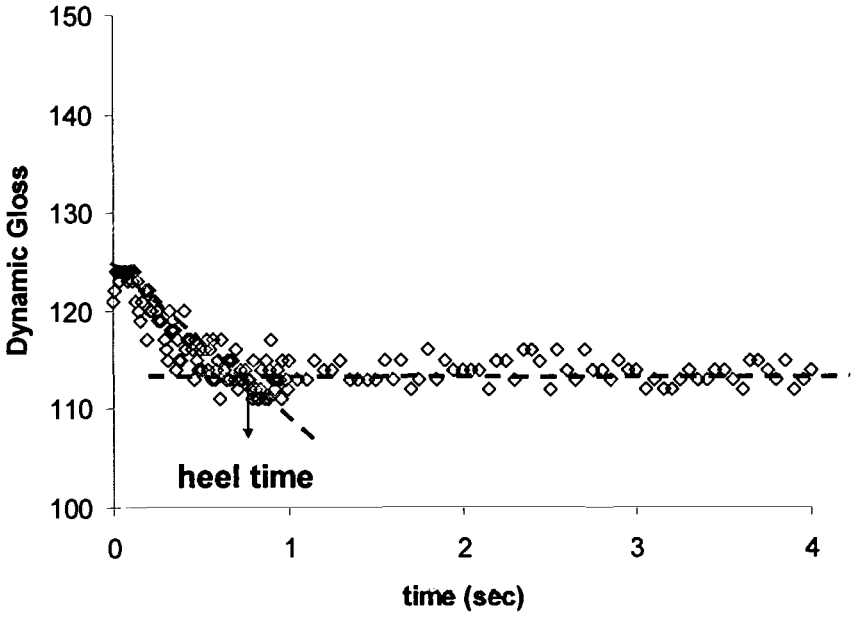

Figure 3.25: Heel Time definition in Dynamic Gloss test for ID2 ink on B1 paper based $CaCO_3$ coating.

Figure 3.26 shows dynamic gloss changes on $CaCO_3$ coating after it is printed with ID1 and ID2 ink separately. From Figure 3.26 we can see that the heel time of curve of ID1 ink is shorter than that of ID2 ink, which suggests that this $CaCO_3$ coating absorbs ID1 ink quicker than ID2 ink. This result agrees with what we get from absorption test shown in Appendix B.

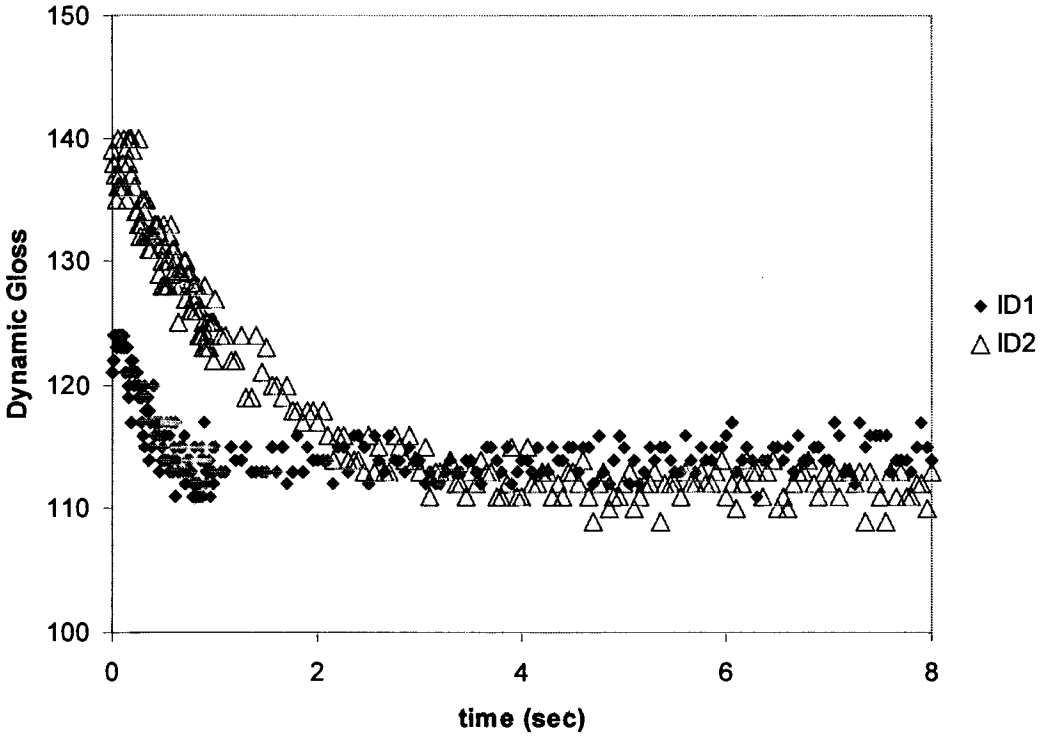

Figure 3.26: Dynamic gloss test of ID1 and ID2 inks on B1 paper based $CaCO_3$ coating.

Figure3.27 is another plot of dynamic gloss test result. In this figure, heel time for middle plastic pigment coating is the shortest among the three, and that for clay coating is the longest one. These results agree with absorption tests results shown in Appendix B.

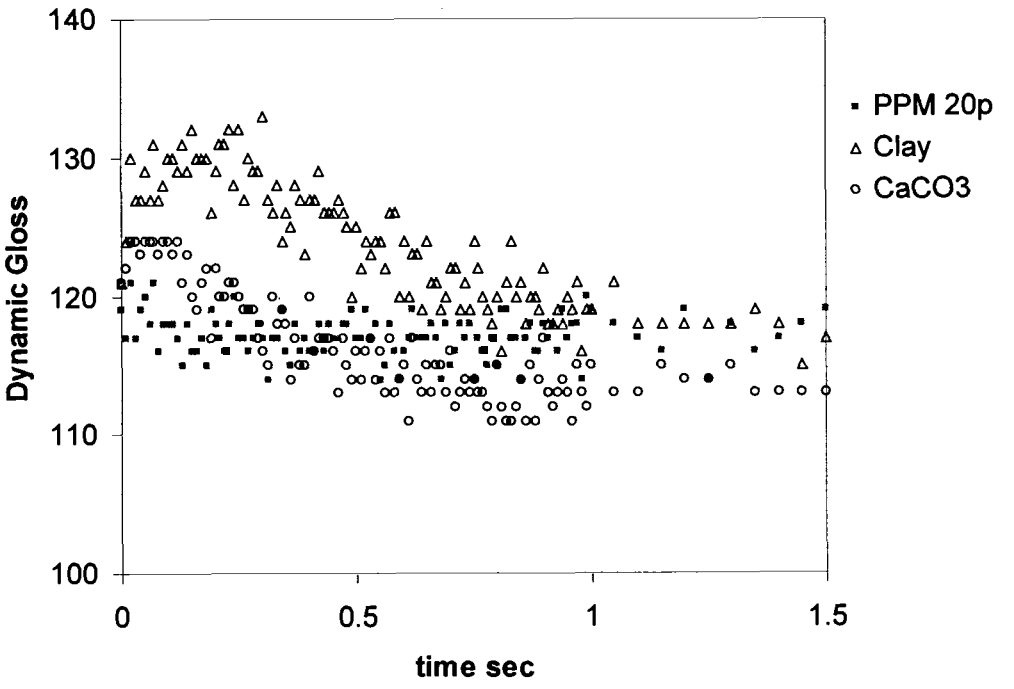

Figure 3.27: Dynamic Gloss test of ID1 ink on clay, $CaCO_3$ and PPM 20pph coating with B1 base paper.

By comparing dynamic gloss curve and absorption curves, we can say that dynamic gloss curve heel time correlates with the ink-substrate absorption rate, for different inks on the same coating or for the same ink on different coatings.

Figure 3.28 relates dynamic gloss heel time to three second absorption volume for two kinds of inks on six different coating substrates. For those curves whose gloss change ends before the device starts recording, their heel time are counted as 0 sec. As expected, the figure shows that substrates' absorption rate decreases with dynamic heel time

increases. Due to limited range of experiment data we collect, the correlation coefficient value of the trend line is low.

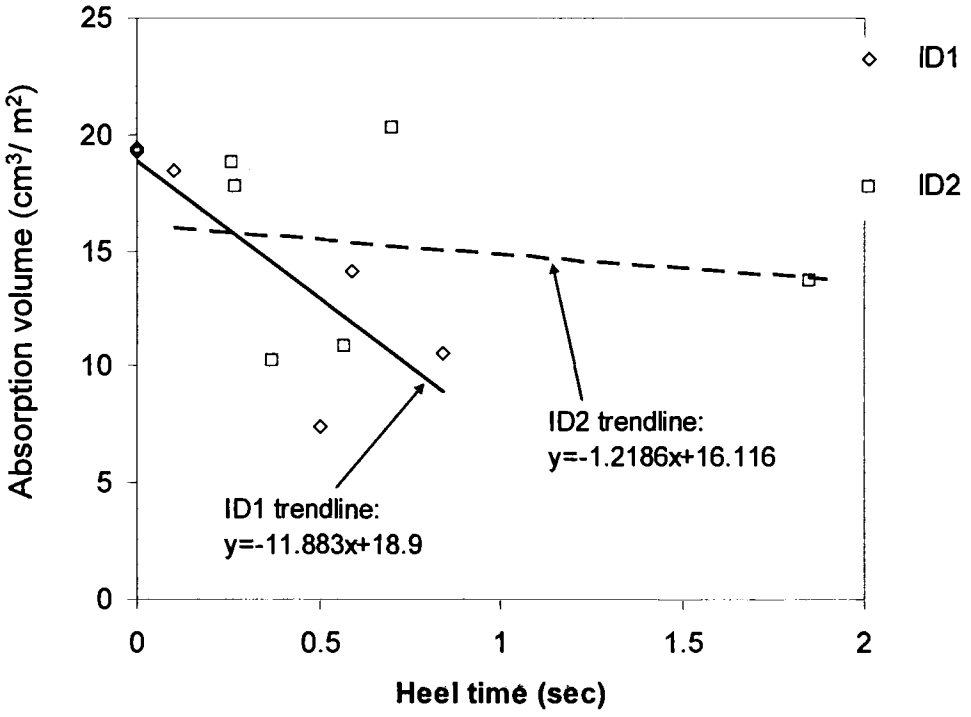

Figure 3.28: Absorption volume versus dynamic heel time for two inks on substrates.

3.7 Summary

For absorption on single layer paper, the rate of fluid absorption is found to be affected by fluid-substrate surface chemistry and fluid properties. Contact angle had been used to characterize the fluid-substrate surface chemistry. Low contact angle leads to high absorption rate. Combined influence of fluid viscosity, surface tension and contact angle on absorption rate has been studied. The relation between them is not linear as described

by the Lucas-Washburn model. Paper void fraction has not shown effect on the absorption rate.

For two layer porous media, i.e. coated paper, the rate of fluid absorption is found to be related with base paper absorbing ability, the substrate's pore size, binder level in the coating and fluid-substrate contact angle. When the base paper is highly absorbent, the absorption rate through a coating layer is high. The influence of base paper's absorbance is strongest at longer penetration times and more open coating structure. Small pore size of substrate and low fluid-substrate contact angle were found to be beneficial to penetration. Low binder level in coating helps fluid penetration. The combined influence of fluid viscosity, surface tension and contact angle affects the absorption rate. The absorption rate is directly proportional to $(\gamma\cos(\theta)/\mu)^{0.5}$ as the Lucas-Washburn equation predicts.

The micro-tack test was used with water based ink on substrate to measure the ink setting time. In some case, the tack force does not decay to zero even though all the ink should be absorbed. A good relation between the absorption volume and tack peak time has been obtained.

The dynamic gloss test has been used to measure the ink setting rate. The dynamic gloss heel time has been correlated with absorption rate.

CHAPTER 4: ABSORPTION RATE MODELING

In this chapter, several absorption rate models are used and compared to predict absorption rate. The major driving force in these absorption models is capillary pressure. The resistance is flow through porous media. By characterizing the properties of the pores and those factors involved in capillary pressure, the depth of fluid penetrating into the substrate is predicted as a function of time. Those predictions are compared with experimental data to check the accuracy of the prediction.

There are two types of substrate in the modeling: single layer substrate and two layer substrates. We use seven kinds of papers including some commercial papers in single layer substrate modeling. One model is discussed in single layer modeling. For two layer substrates, we used six kinds of coatings. Six models are discussed in two layer modeling, and the best model is identified.

4.1 Single Layer Porous Substrate Absorption Model

Flow in porous media has been shown to follow the Carmon-Kozeny Equation (Carman, 1937, 1938, 1956; Kozeny, 1927):

$$\upsilon = \varepsilon \frac{dL}{dt} = -\frac{\Delta P}{L} \cdot \frac{\varepsilon^3}{k_1 \cdot \mu \cdot (1-\varepsilon)^2 \cdot S_o^2} \tag{4.1}$$

where υ is the speed of the fluid passing through the media, ε is void volume fraction of media, L is the depth that the fluid penetrates into the media during time t, ΔP is the pressure exerted on the media, k_1 is a coefficient with a value of 4.1, μ is viscosity of fluid and S_o is the specific particle areas per particle volume, for a sphere $S_o = \frac{3}{r}$ where r is particle's radius.

The Darcy coefficient

$$K = -\frac{\varepsilon^3}{k_1 \cdot (1-\varepsilon)^2 \cdot S_o^2} \tag{4.2}$$

Plug Eq. (4.2) into Eq. (4.1), gives:

$$\frac{dL}{dt} = \frac{\Delta P \cdot K}{L \cdot \varepsilon \cdot \mu} \tag{4.3}$$

By integrating Eq. (4.3), we get:

$$TLV = \varepsilon \cdot L = \sqrt{\frac{2\Delta P \cdot K \cdot \varepsilon \cdot t}{\mu}} \tag{4.4}$$

In our modeling process we compare L the penetration depth with experimental Bristow absorption volume TLV. For coefficient K, we get the value from Darcy's Law through air permeability experiments as:

$$K = \frac{\upsilon_a \cdot \mu_a \cdot L_s}{\Delta P_a} \tag{4.5}$$

Where υ_a is velocity that air passes through the sample in the Sheffield air permeability apparatus, μ_a is the viscosity of air, L_s is the thickness of the sample, and ΔP_a is the pressure of air exerted on the sample.

For ΔP in the Eq. (4.4), Eq. (1.1) can be used. By plugging in Eq. (1.1) into Eq. (4.4), we get:

$$TLV = \sqrt{\frac{4K \cdot \varepsilon \cdot t \cos\theta \cdot \gamma}{\mu \cdot R}} \tag{4.6}$$

In the Lucas-Washburn equation Eq. (1.6), absorption volume TLV is proportional to $R^{0.5}$. In our model TLV is proportional to $R^{-0.5}$. However, the Darcy coefficient will depend on R probably to the square power according to Eq. (4.2).

In measuring contact angle of one-layer substrate papers, we found that some sized paper's surface contact angle with water is greater than 90°. This makes the result of capillary pressure negative, which means water will not penetrate into the substrate. But the penetration did happen for those sized papers. Internal water-paper contact angles have been measured as well as the external contact angles. The results are shown in Chapter 3, Table 3.5.

Figures 4.1 and 4.2 show the predictions of Eq. (4.6), using one second internal and external contact angle separately. This external surface contact angle prediction is better than the internal surface contact angle prediction, except four samples, which would predict no absorption. In fact, when considering how a high external surface contact angle slows down the wetting process and that the contact time (ranging from 0.3 sec to 3 sec) in this calculation is not long enough to neglect this affect, the adoption of external surface contact angle in the calculation sounds more reasonable.

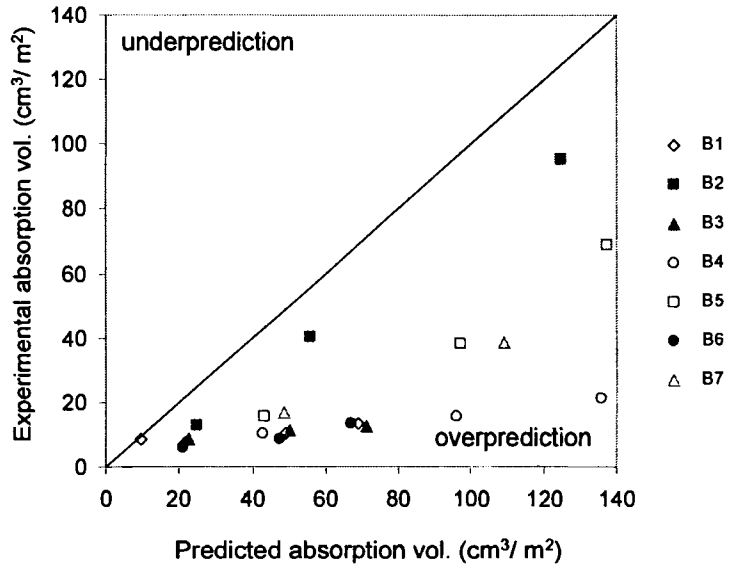

Figure 4.1: Water absorption prediction with Eq. (4.6) on seven kinds of papers calculated with internal contact angle.

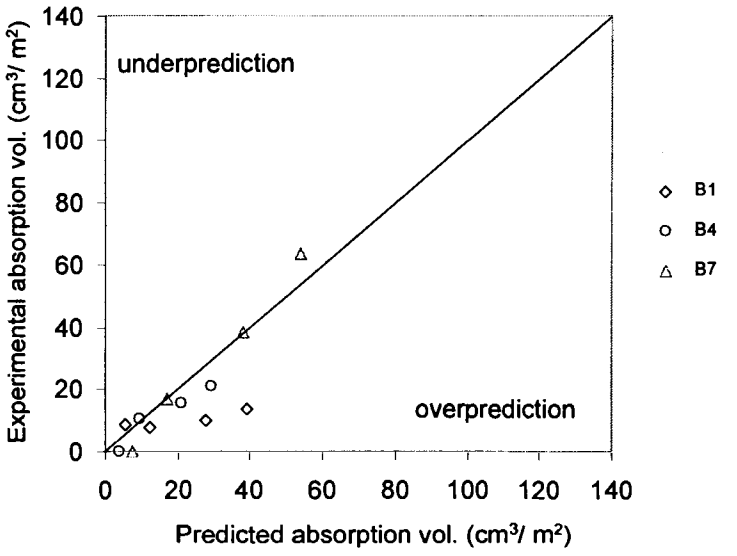

Figure 4.2 Prediction of water absorption with Eq. (4.6) on three kind of paper calculated with external contact angle

For those highly sized papers whose contact angle is higher than 90°, we could have been able to get an empirical equivalent contact angle by mathematically combining external surface contact angle and internal surface contact angle together. For instance, using a ratio of 0.4 external surface contact angle to 0.6 internal surface contact angle for paper B3 and B5. However, this will definitely increase the complexity of prediction and subsequently hurt its usability. Further study is needed on how internal and external contact angle combined can be used to predict absorption of highly sized papers.

Figure 4.3 shows the result of prediction of ethylene glycol absorption with Model 1 on seven kinds of papers. Since ethylene glycol's surface tension is much lower than that of water, the contact angle values on these papers are all below 90°. The result is reported in Chapter 3 Table 3.6.

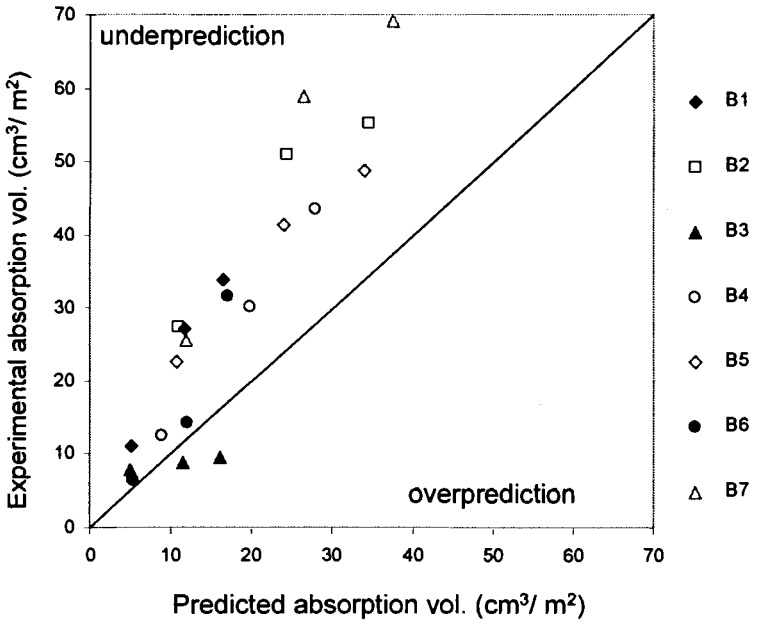

Figure 4.3: Prediction of ethylene glycol absorption with Eq. (4.6) on seven kinds of paper with external contact angle.

Figure 4.4 shows the predictions of dye based ink ID1 absorption with Eq. (4.6) on seven kinds of paper. The reason that we under predict absorption with ethylene glycol and dye ink could be we have not included the affect of paper fiber's absorption of liquid. The over-prediction of water absorption on those papers could be because the paper fibers swell during the water absorption process. Pores are thus blocked and further absorption is prevented. The degree of fiber-swelling blocking might not be that large in ethylene glycol and ID1 ink absorption because generally both absorption rates are high, and most of the absorption may have happened before the blocking seriously affected the absorption process.

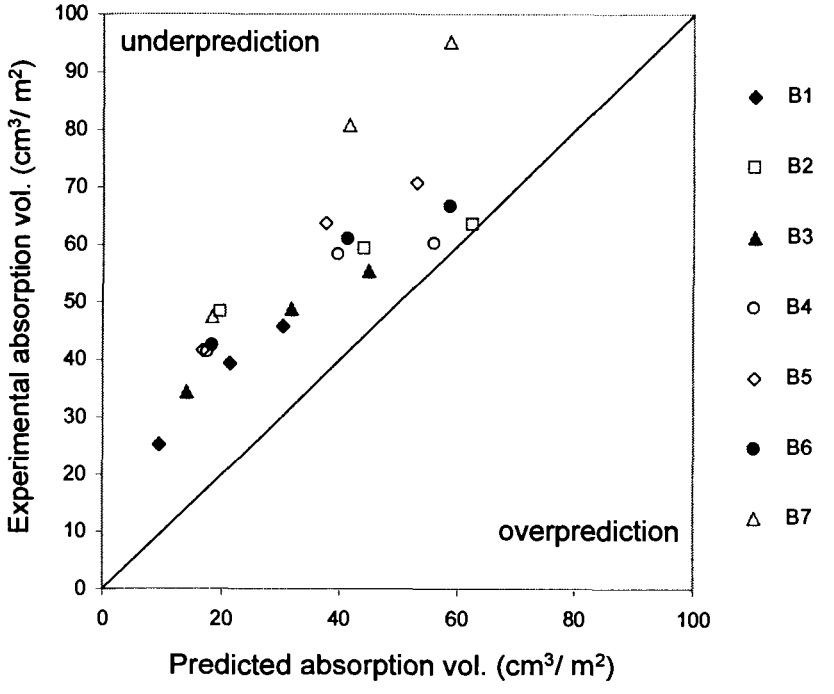

Figure 4.4: Prediction of ink ID1 absorption with Eq. (4.6) on seven kinds of paper with external contact angle.

Figures 4.5 shows predictions of absorption volume of water, ethylene glycol and ID1 on seven papers calculated from the Lucas-Washburn equation Eq. (1.7). The Lucas-Washburn equation over predicts the absorption volume by a factor of approximately 20. According to Olivar (1995), the tortuosity of fine-grained sand is around 5. Therefore the Lucas-Washburn equation in terms of tortuosity (τ) factor, Eq. (1.10), might be able to predict better. More information about tortuosity of papers is needed to do further comparison.

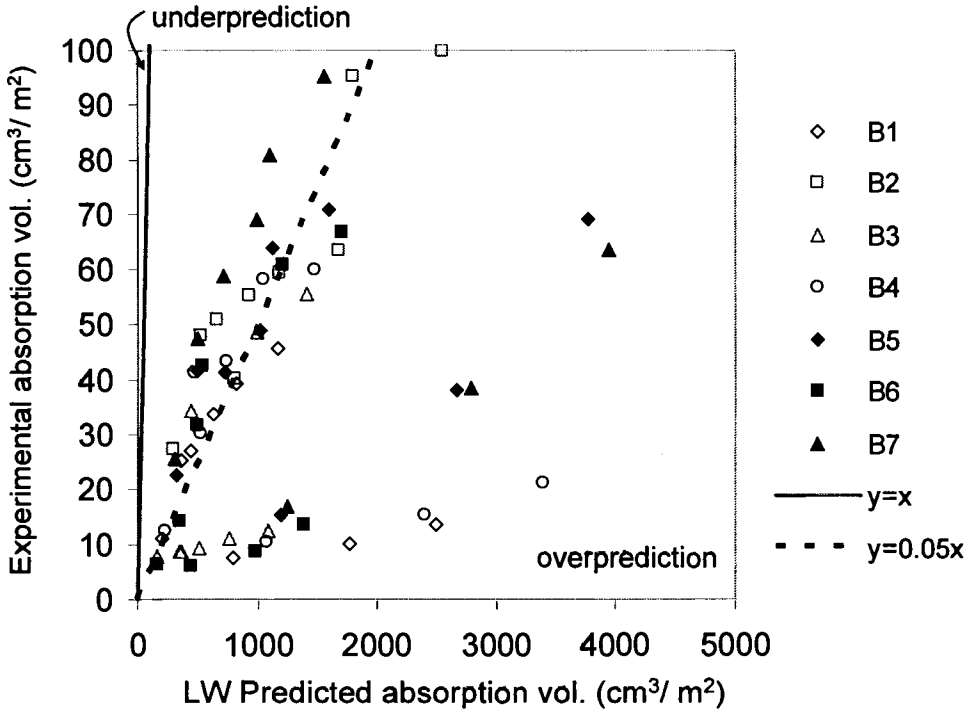

Figure 4.5: Absorption volume prediction from the Lucas-Washburn equation on water, ethylene glycol and ID1 with seven papers.

4.2 Two Layer Porous Substrate Absorption Model

In the two-layer porous substrate absorption predictions, four models (Model 1,2,3 and 4) are compared to characterize the substrate as a one-layer porous substrate. Model 5 is developed to calculate ink penetrating into two layers -- coating and base paper. Based on Models 2 or 4, Model 6 uses Darcy Coefficients getting from the Bristow absorption tests to do the prediction.

Model 1:

This model is the same as the one we use in fluid-paper penetration prediction, using the Eq. (4.6). Notice that here θ is the contact angle between the fluid and the coating. And the Darcy coefficient is calculated from air permeability but using coating thickness instead of the whole media thickness. With the realization that the coating layer is much thicker than the base paper, the resistance will come mainly from the coating layer.

Most of the predictions using Model 1 are over-predicted except for the runs with ethylene glycol and ID1 ink. Figure 4.6 shows the result of prediction of ethylene glycol absorption with Model 1 on several coatings on B1 base paper:

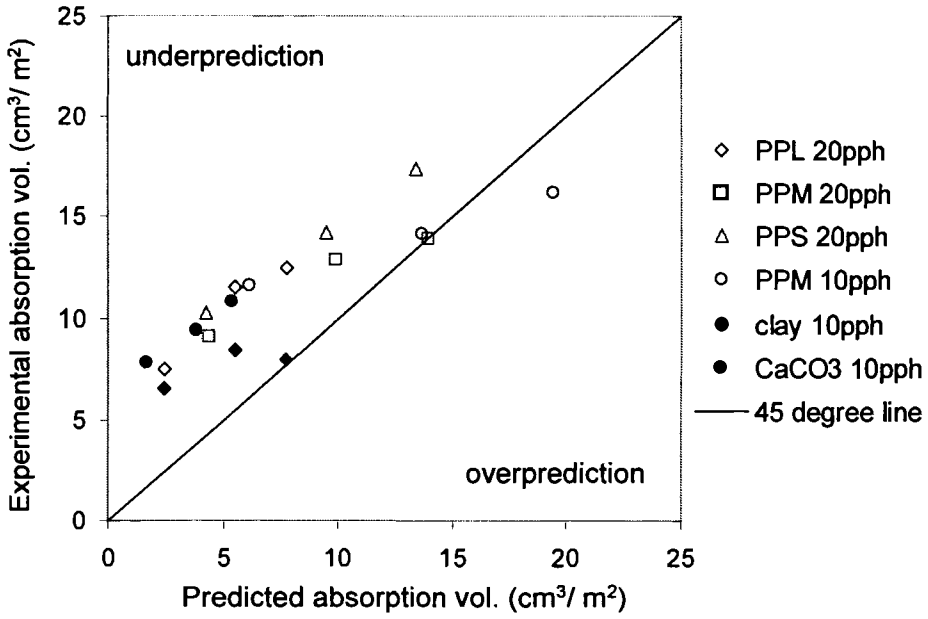

Figure 4.6: Prediction of ethylene glycol absorption with Model 1 on plastic pigment, clay, and CaCO3 coatings on B1 paper base.

Model 2:

Model 2 also use Eq. (4.5) to do the predictions. But in Model 2, we use fluid-base paper contact angle instead of fluid-coating contact angle. The fluid quickly fills the coating layer and spends most of its time filling the paper. Therefore the base paper's absorbance does change absorption rate to a high degree.

Figure 4.7 and Figure 4.8 show predictions with Model 2 on water and ID1 ink. By using fluid-base paper contact angle instead of fluid-coating contact angle, predictions from Model 2 are closer to experimental data than those from Model 1. The prediction of ID1 ink with Model 2 is like the predictions of water with Model 2. Most prediction data are

close to experimental data except for small plastic pigment coating, which are always over-predicted. As this pigment size is small, even this coating is formed at the same latex concentration as large and middle plastic pigment, there could be more throats and dead ends formed in this coating than with the other two coatings. Even though the void of small plastic pigment is larger and its coating pore size is smaller than that of large and middle plastic pigment, which makes the absorption prediction higher, the practical occupied volume is much lower than the volume used in the prediction. This might partially explain why our prediction about the small plastic pigment is always higher than experimental values.

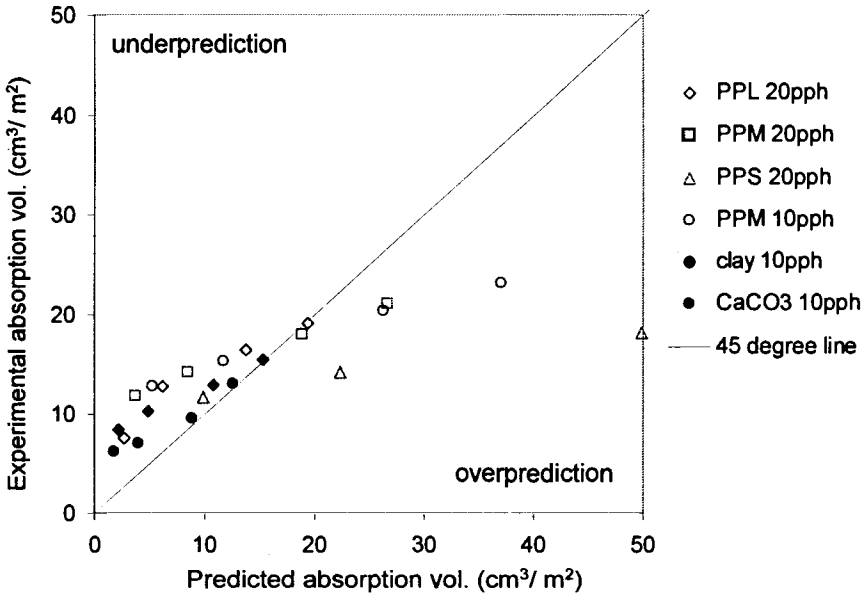

Figure 4.7: Prediction of water absorption with Model 2 on B1 paper based coatings.

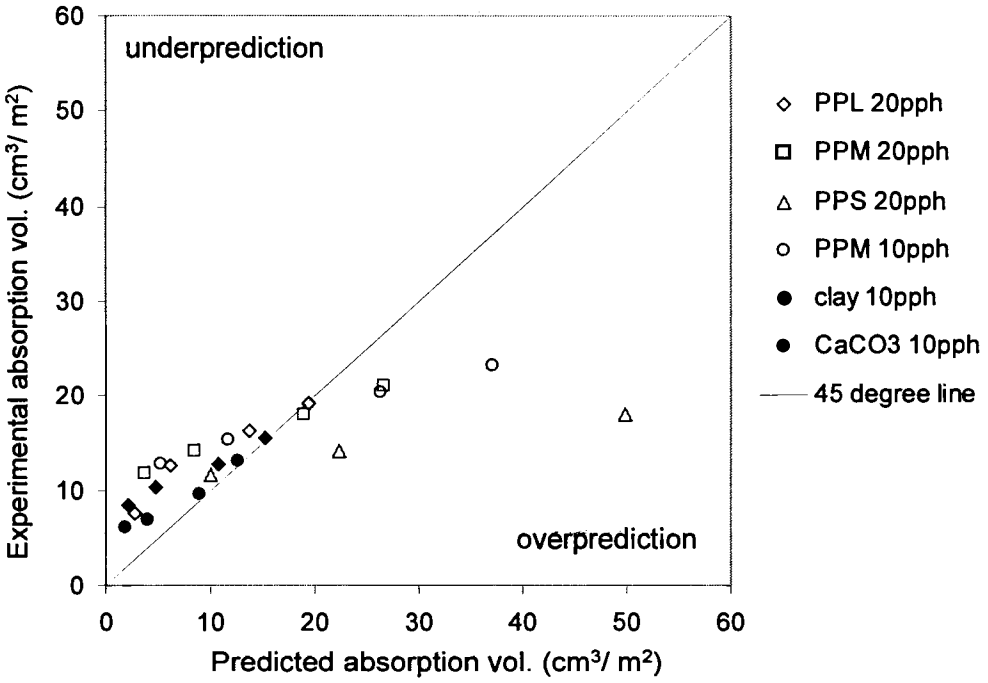

Figure 4.8: Prediction of ID1 ink absorption with Model 2 on coatings on B1 base paper.

Model 3:

In both Model 1 and Model 2, the calculated capillary pressure is usually higher than atmospheric pressure, sometime reaching 10^6 Pa. This pressure diving force is more than can actually exist, because this is suction type pressure. Therefore we assume in the Model 3 that when the capillary pressure is equal to or higher than atmospheric pressure, the balance is obtained and the capillary pressure ΔP stays at 10^5 Pa. We also assume that in Eq. (4.3), the penetrated length dL is independent of substrate thickness L. This gives the Eq. (4.7):

$$TLV = \frac{K \cdot \Delta P \cdot t}{L \cdot \varepsilon \cdot \mu} \tag{4.7}$$

Figure 4.9 is the prediction of water absorption with Model 3 on coatings. Most of the predictions are under predicted.

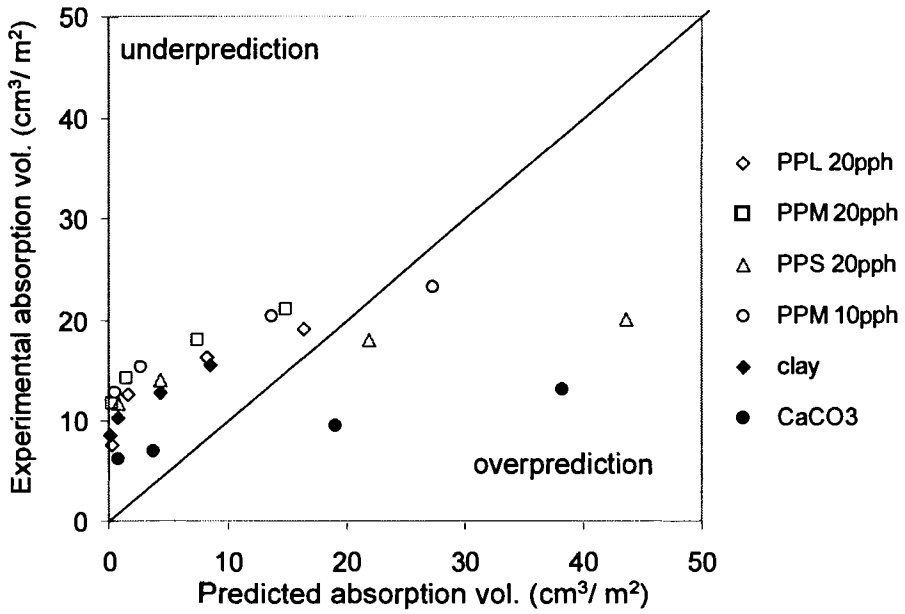

Figure 4.9: Prediction of water absorption with Model 3 on coatings on B1 base paper.

Model 4:

In Model 4 the absorption process is considered as two parts: fluid absorbed by the coating layer and by the base paper layer. When fluid penetrates the coating layer, the capillary pressure of coating layer ΔP_c is:

$$\Delta P_c = \frac{2 \cdot \cos\theta_c \cdot \gamma}{R_c} \tag{4.8}$$

Where θ_c is contact angle between fluid and coating, and R_c is the dominate pore radius of the coating layer.

From Eq. (4.4), we can obtain t_c, the time required for the fluid to fill up the coating layer:

$$t_c = \frac{TLV_c^2 \cdot \mu}{2 \cdot \Delta P_c \cdot \varepsilon_c \cdot K} \tag{4.9}$$

where ε_c is the void volume fraction of the coating layer, and TLV_c is the absorbed fluid volume by the coating layer part, given as:

$$TLV_c = L_c \cdot \varepsilon_c \tag{4.10}$$

Where L_c is the thickness of the coating layer.

As fluid penetrates the base paper layer, the base paper capillary pressure ΔP_p is:

$$\Delta P_p = \frac{2 \cdot \cos\theta_p \cdot \gamma}{R_p} \tag{4.11}$$

Where θ_p is contact angle between fluid and base paper, and R_p is the dominate pore radius of the paper layer.

The total liquid volume in the paper TLV_p is a linear function of time, because the resistance to flow into the paper comes from flow through the coating layer:

$$TLV_p = \frac{2 \cdot K \cdot \cos\theta_p \cdot \gamma \cdot (t - t_c)}{\mu \cdot L_c \cdot R_p} \tag{4.12}$$

Where t is the total penetration time.

The total absorption volume TLV for Model 4 is:

$$TLV = TLV_c + TLV_p + R_u \tag{4.13}$$

where R_u is the roughness of the coated sample.

It is a new idea to calculate the total TLV separately in coating layer and base paper layer. Also, adding the roughness helps in predicting short contact time absorption. However, predictions of Model 4 are under predicted compared with the experimental data as shown in Figure 4.10. The reason could be that paper fiber absorption volume is not included.

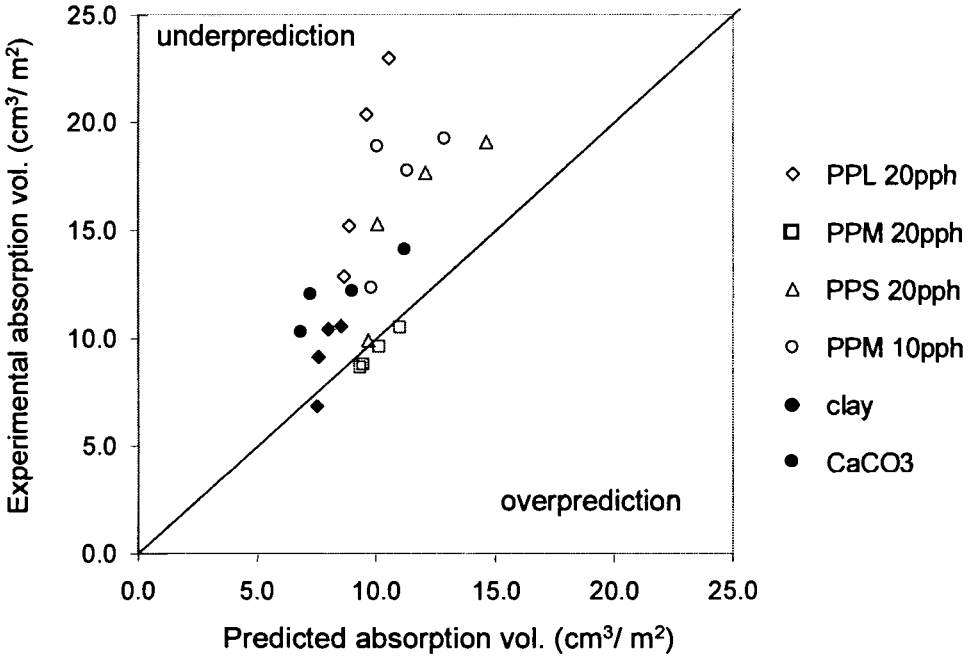

Figure 4.10: Prediction of ID1 absorption with Model 4 on coatings on B1 base paper.

Model 5:

Basically Model 5 is the same as Model 4, except the Darcy coefficient K is from ethylene glycol retentions test instead of air permeability. Also in the Model 5, contact angle is considered as 0 in the Bristow absorption test the ink container spreads ink flatly on the tested substrates.

Results obtained from Model 5 are over predicted as shown in Figure 4.11. One reason is that the Darcy coefficient K obtained from the ethylene glycol retention test is much higher than that obtained from air permeability test. This could be because that under experimental pressure, cracks appear in wet coating layer. The tested flow rate is therefore higher than it should have been.

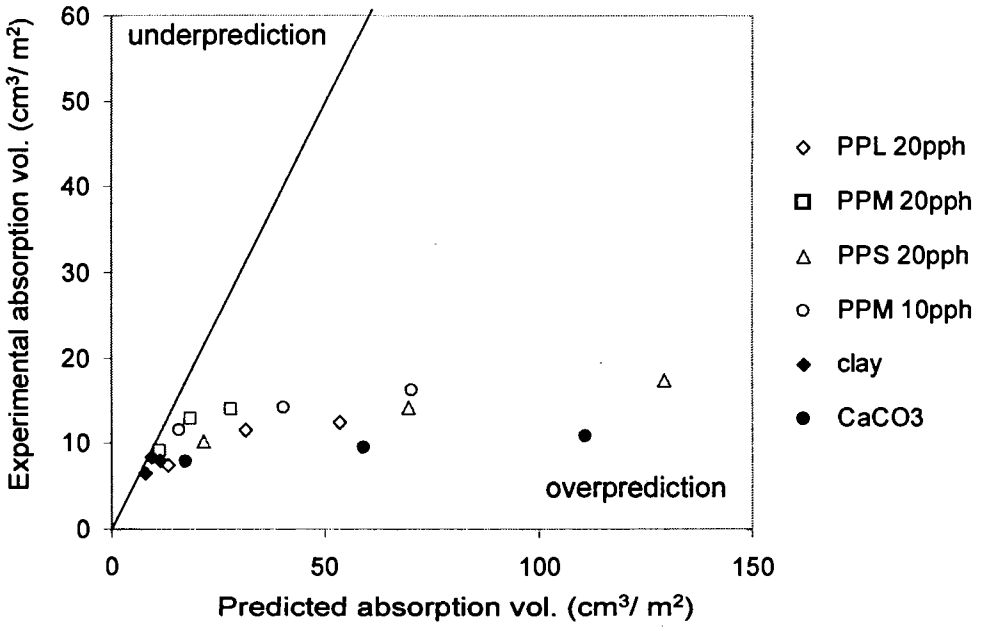

Figure 4.11: Prediction of ethylene glycol absorption with Model 5 on coatings on B1 base paper.

All of these models, to this point, tend to over predict or under predict the absorption rate. The key parameter is the Darcy coefficient. Either based on the sample thickness or the coating thickness, this parameter is obtained from the sample before the penetration starts. However, when paper is in contact with a polar fluid, the fibers may swell and change the structure of the paper or coating layer. The whole situation is more complex

than the starting point. The need, therefore, is to obtain a Darcy coefficient during the process of the penetration.

Model 6:

The key point of the Model 6 is calculating Darcy coefficient K from water Bristow absorption test, using the equations of Model 2 or Model 4 in reverse order. With the calculated K, Model 6-2 and 6-4 use equations from the Model 2 or Model 4, respectively, to predict the absorption rates of other fluids. The Model 6-4 works better than the Model 6-2.

Model 6-2:

For the Model 6-2, the water absorption volume TLV_w is used to calculated the Darcy coefficient K:

$$K = \frac{TLV_w^2 \cdot \varepsilon \cdot \mu_w \cdot R_c}{4\cos\theta_{w-p} \cdot \gamma_w \cdot t} \tag{4.14}$$

Where μ_w is the viscosity of water, R_c is the dominant pore radius of the coating layer, $\theta_{w\text{-}p}$ is the contact angle between water and the base paper, and γ_w is the surface tension of water.

This calculated Darcy coefficient is used with Eq. (4.15) to predict other fluid absorption volume TLV_f:

$$TLV_f = \sqrt{\frac{4\cos\theta_f \cdot \gamma_f \cdot K \cdot t}{\varepsilon \cdot \mu_f \cdot R_c}} \tag{4.15}$$

Where θ_f is the contact angle between the fluid and the base paper, γ_f is the surface tension of the fluid, and μ_f is the viscosity of the fluid.

Model 6-4:

$TLV_{w\text{-}p}$, the water absorbed by the paper, is:

$$TLV_{w-p} = TLV_w - L_c \cdot \varepsilon_c - R_u \tag{4.16}$$

$\Delta P_{w\text{-}c}$, the capillary pressure in the coating layer, is:

$$\Delta P_{w-c} = \frac{2\cos\theta_{w-c} \cdot \gamma_w}{R_c} \tag{4.17}$$

Where $\theta_{w\text{-}c}$ is the contact angle between water and the coating layer.

$\Delta P_{w\text{-}p}$, the capillary pressure in by the base paper layer, is:

$$\Delta P_{w-p} = \frac{2\cos\theta_{w-p} \cdot \gamma_w}{R_p} \tag{4.18}$$

Where $\theta_{w\text{-}c}$ is the contact angle between water and the coating layer.

With Eq. (4.16) ~ (4.18), the Darcy coefficient K can be obtained by Eq. (4.19):

$$K = \frac{TLV_{w-p} \cdot \mu_w \cdot L_c + \dfrac{\Delta P_{w-p} \cdot L_c^{\,2} \cdot \varepsilon_c \cdot \mu_w}{2\Delta P_{w-c}}}{\Delta P_{w-p} \cdot t} \tag{4.19}$$

With this calculated K, repeat the steps in the Model 4, the absorption volume of other fluid in the substrate can be gained.

Among all of the models, the Model 6 gives the closest prediction.

Figures 4.12 and 4.13 show the prediction results of several ink absorptions on middle and small plastic pigment coatings. The small size pigment coating causes prediction problems with the other models. However, the predictions of this coating with the Model 6 are good.

In Figures 4.12 and 4.13, for the same model 6-4 prediction, prediction of two dye ink is the best, pigment ink is second and ethylene glycol is the worst. Because the Darcy coefficient is from the water Bristow test, the prediction is better for the water based inkjet ink than ethylene glycol. Also, particle size in water based dye ink (~ 10nm) is much smaller than the particle size in water based pigment ink (~ 100 nm), which makes the dye ink behavior more close to that of water than the pigment ink.

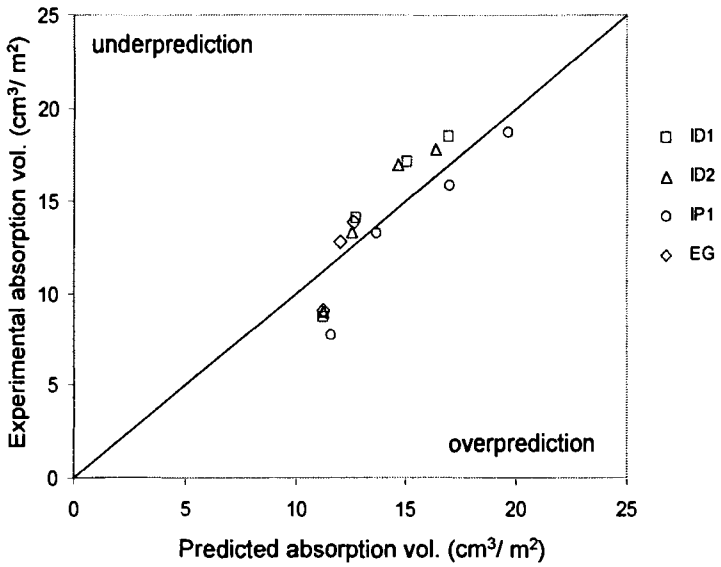

Figure 4.12: Prediction of absorption volume of four inks on B1 paper based PPM 20pph coating with Model 6-4.

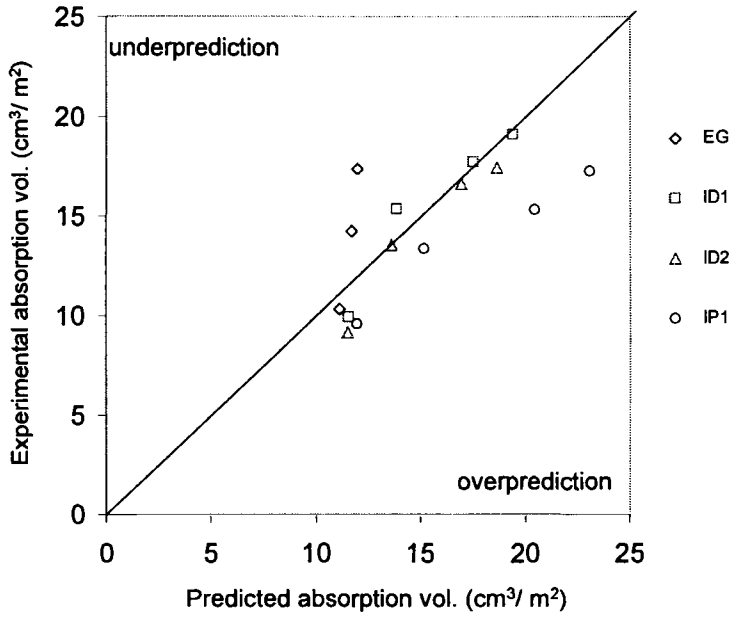

Figure 4.13: Prediction of absorption volume of four inks on B1 paper based PPS 20pph coating with Model 6-4.

Even though the Model 6-4 is the best predicting among the models we discussed, calculations of the Model 6-4 is also more complicated. When simple calculation is needed, the Model 6-2 could be taken as an alternative. Figures 4.14, 4.15, and 4.16 compare how Model 6-2 and Model 6-4 work in predicting absorption for different coatings. The code number after the ink code is the model number.

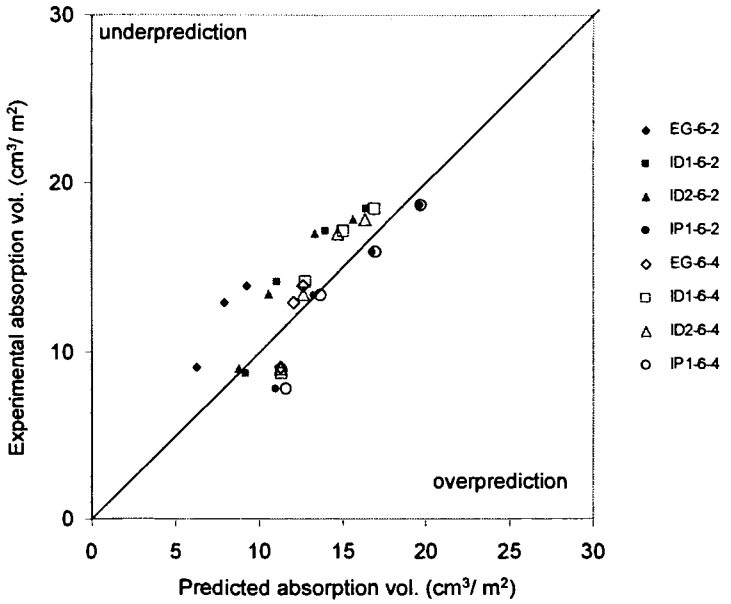

Figure 4.14: Comparison of using Models 6-2 and 6-4 in predicting Absorption volume on B1 paper based PPM 20pph coating.

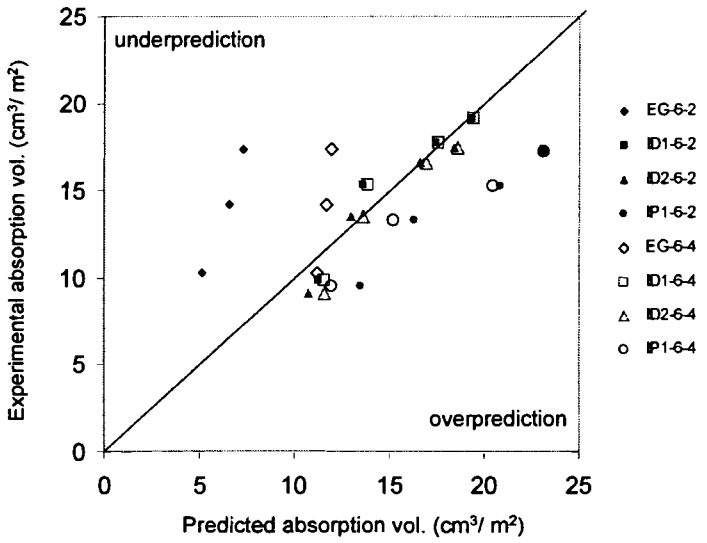

Figure 4.15: Comparison of Model 6-2 and Model 6-4 in predicting absorption volume on B1 paper based PPS 20pph.

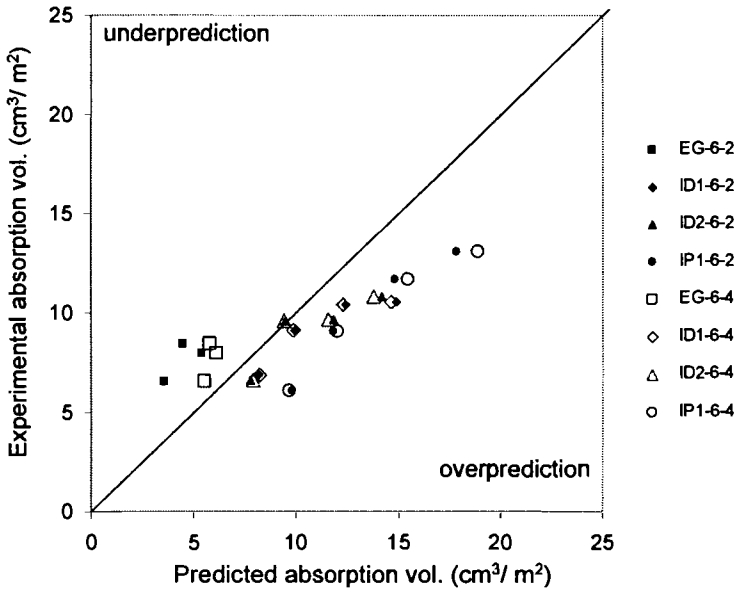

Figure 4.16: Comparison of Model 6-2 and Model 6-4 in predicting absorption volume on B1 paper based clay coating.

In calculation of the Models 6-2 and 6-4, it has been found that the Darcy coefficient K decreases as contact time increases, instead of being a constant. Using this changing series of K usually gives a better result than using an average K. However, it's more convenient to use average K in the calculations. Figures 4.17 and 4.18 show comparisons of using average K and series K in the estimation of middle plastic pigment coating on B1 base paper, with the Model 6-2 and the Model 6-4, separately.

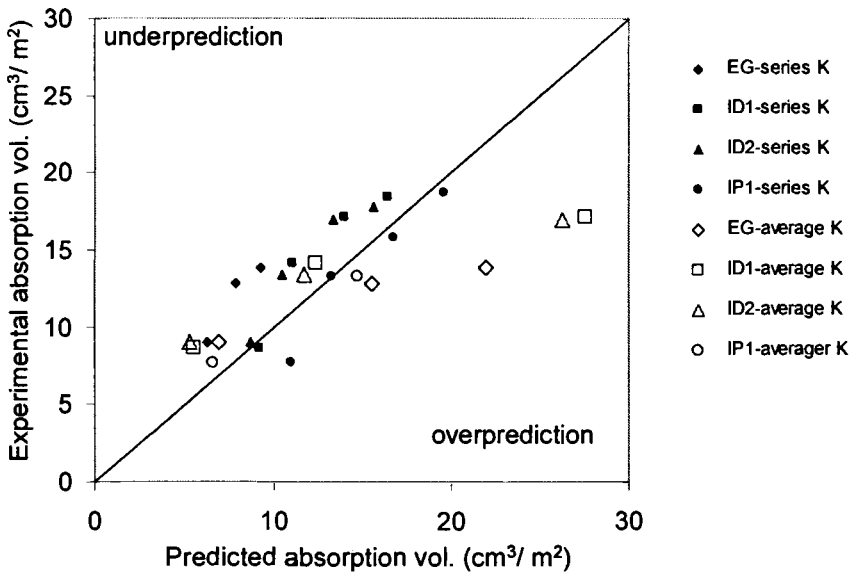

Figure 4.17: Comparison of using series Darcy Coefficient K and average Darcy Coefficient K in Model 6-2 prediction of PPM 20pph coating absorption volume.

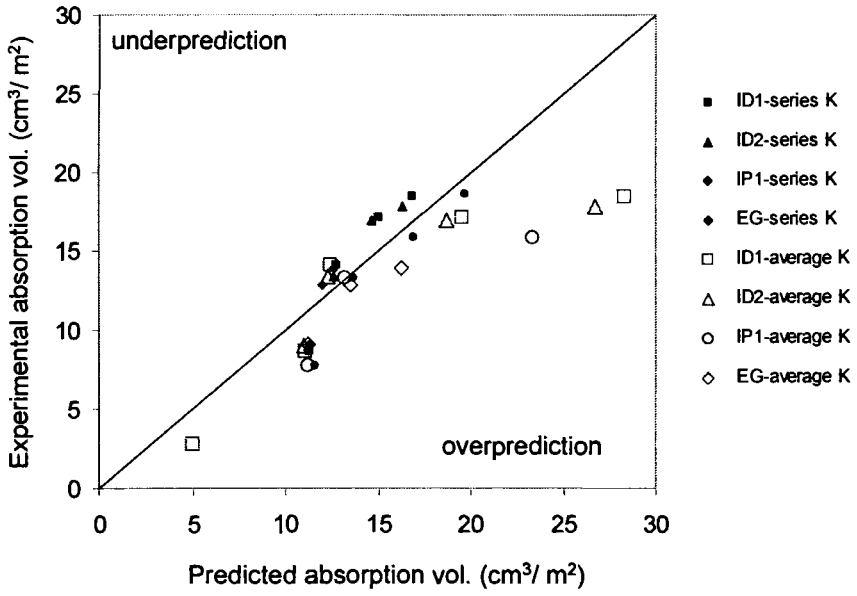

Figure 4.18: Comparison of using series Darcy Coefficient K and average Darcy Coefficient K in Model 6-4 prediction of PPM 20pph coating absorption volume.

In the series K prediction, the value of K is indirectly proportional to contact time t as shown in Figure 4.19:

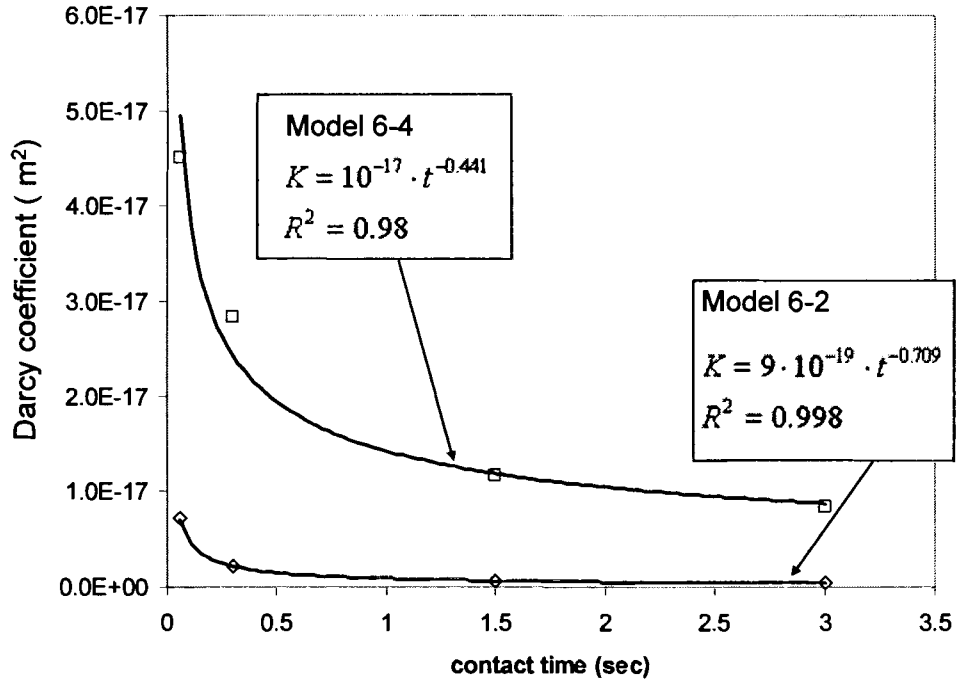

Figure 4.19: Darcy coefficient form Model 6 versus contact time for PPM 20pph coating on B1 base paper.

Remembering what was discussed in Chapter 3 about the experimental absorption volume TLV being more likely proportional to $t^{0.2}$ than $t^{0.5}$, we may understand why series K results in a better prediction. The reason could be that the structure of the coating or base paper change during the fluid absorption. Thus changes the penetration parameter, the Darcy coefficient.

Figures 4.20 are prediction results of absorption volume of water, ethylene glycol and ID1 on five coatings calculated from the Lucas-Washburn equation, Eq. (1.7). The Lucas-Washburn equation over predicts the absorption volume by a factor of approximately 20. Since the Lucas-Washburn equation describes the fluid penetration behavior in single layer porous substrate, we did not expect it works in coated paper. However, as we discussed with single layer absorption, the Lucas-Washburn equation in terms of tortuosity factor of the coated paper might help the prediction.

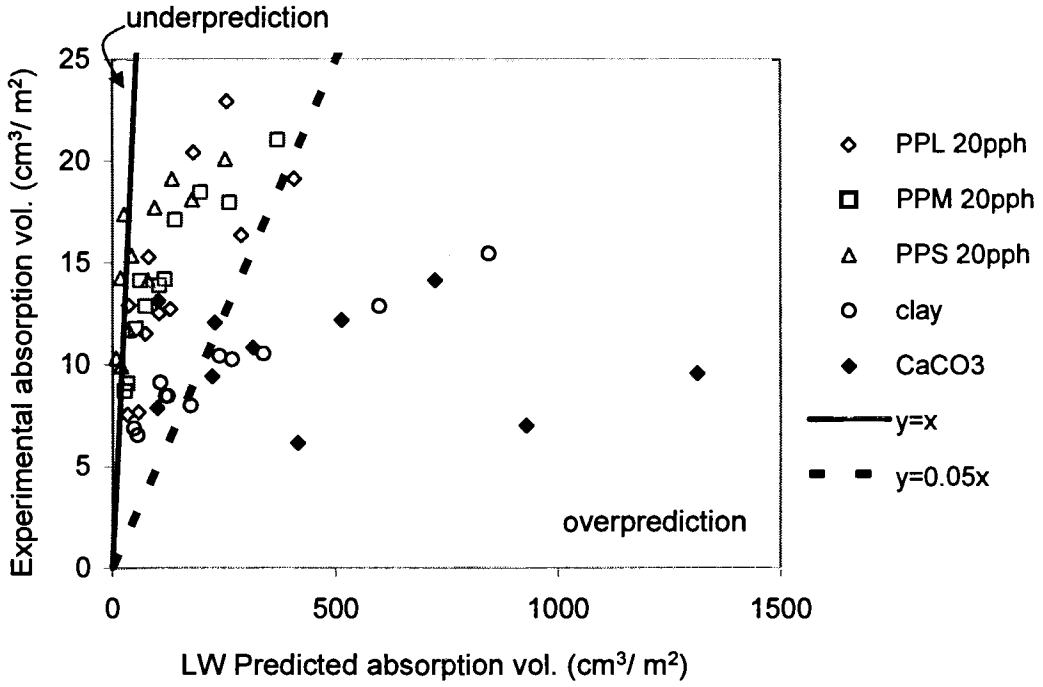

Figure 4.20: Absorption volume prediction from the Lucas-Washburn equation on water, ethylene glycol and ID1 with five coatings on B1 paper base.

4.3 Summary

One model has been used for single layer substrate absorption rate prediction. The prediction results of ethylene glycol and ID1 ink is good. The results of prediction of water absorption with out external surface contact angle are better than with the internal surface contact angle.

Six models have been used for two layer substrate absorption rate prediction. The Model 6 works best among all models because the Darcy coefficient in the Model 6 is from experiment water absorption data. The Darcy coefficient obtained from this method is not a constant but changes with the fluid penetration time. The change of the structure of the substrates may be a reason for this changing Darcy coefficient.

As a comparison, predictions of absorption of the same coated and uncoated papers from the Lucas-Washburn equation have been made. The Lucas-Washburn equation over predicts the results by a factor of approximately 20. Adding the tortuosity of the substrate to the Lucas-Washburn equation might help the prediction.

CHAPTER 5: CONCLUSIONS AND RECOMMENDATIONS

Key parameters that affect dilute fluid penetration in uncoated and coated paper have been studied.

For uncoated paper, the rate of fluid absorption is found to be related to fluid-substrate contact angle and fluid properties.

- ✓ Low contact angle leads to high absorption rate. Internal contact angles are better related to the absorption rates than the external ones.
- ✓ The combined influence of contact angle, fluid viscosity and surface tension on absorption rate has been studied. However, a single simple expression did not describe the results. The relationship between absorption volume and $(\gamma\cos\theta/\mu)^{0.5}$ is not linear as described by the Lucas-Washburn model.
- ✓ Paper void fraction is not well related to the absorption rate.

For coated paper, the rate of fluid absorption is found to be related to base paper absorbing ability, the substrate's pore size, binder level in the coating and fluid-substrate contact angle.

- ✓ The coating with high absorbance base paper has a higher absorption rate than that with a low absorbance base paper. The influence of base paper's absorbance is stronger at longer penetration times and on more open coating structure.

- ✓ Small pore size of substrate and low fluid-substrate contact angle were found to be beneficial to penetration.
- ✓ Low binder level in coating helps fluid penetration.
- ✓ The combined influence of viscosity and surface tension of fluid affects the absorption rate. The absorption volume is directly proportion to the value of $(\gamma\cos(\theta)/\mu)^{0.5}$ as the Lucas-Washburn equation predicts.

A new method, the micro-tack test has been used to measure the inkjet ink setting time. Some dye based inks have long tack peak time even though the ink absorption rate is not low. A good relationship between the absorption volume and tack peak time has been obtained.

The dynamic gloss test has been used to measure the inkjet ink setting rate. The gloss increases at short time then decreases until it reaches the dry gloss value. The dynamic gloss heel time has been correlated to absorption rate.

One model has been used for single layer substrate absorption rate prediction. The predictions of ethylene glycol and ID1 ink are good. The prediction of water absorption with external contact angle is better than with the internal contact angle.

Six models have been used for two layer substrate absorption rate prediction. The model with the changing Darcy coefficient works best among all models. The change of the structure of the substrates may be a reason for this result.

Predictions of absorption of the same samples from the Lucas-Washburn equation have been made. The Lucas-Washburn equation over predicts the results by a factor of approximately 20. The tortuosity factor of the substrate might help the prediction.

Recommendations

The internal contact angle seems better related to the absorption rate of uncoated paper than the external contact angle. But the internal contact angles in this work are obtained from filing the surface off of the sized papers, which could not assure the elimination of the effects of sizing. In further research, it would be beneficial to use unsized paper as a control and to size the paper to get different external contact angle to study the relation between the absorption rate and both internal and external contact angle.

In the study of coated papers absorption rate, the base paper's absorbance involvement prevented a clearer view of the absorption mechanism. Therefore, coatings on porous base substrates with no-absorbance-fabric would be a promising research subject in the next step. Also, as a need of industry, study of double layers and triple layers of coating will be helpful in understand how fluid penetrates from top coating to bottom coating.

As the absorption test results show that the absorption volume is proportional to $t^{0.2}$, it would be beneficial to see how this experimental relationship works in modeling.

BIBLIOGRAPHY

Asai A., Shioya M., Hirasawa S., and Okazaki T., "Impact of an ink drop on paper," IS&T's 7th Int. Con. On Adv. in Non-impact Print. Tech., Oct., (1991).

Aspler, J.S., Davis, S., and Lyne, M.B., "The surface chemistry of paper in relation to dynamic wetting and sorption of water and lithographic fountain solutions," *J. Pulp Paper Sci.*, 13(1):55, (1987).

Aspler, J.S., Maine, C., De Grace, J.H., Aang, Y.H., and Taylor, S., "Printing tack, part 1: influence of paper structure of ink 'tack' measured in a printing nip," *Adv. Printing Sci. and Technol.*, 22, 139, (1994).

Bosanquet, C.M., "On the flow of liquid into capillary tubes," *Phil. Mag.*, S6 45, 525, (1923).

Bouchon, M., "Drop spreading on porous surfaces ," M.S. Thesis, The University of Maine (2000).

Bristow, Paperi ja Puu 50(11); 639-646, (1968).

Carman, P.C., *Trans. Inst. Chem. Eng. London*, 15, 150 (1937).

Carman, P.C., *J. Soc. Chem. Ind.*, 57, 225 (1938).

Carman, P.C., "Flow of gases through porous media," Butterworths, London, (1956).

Danino D., and Marmur, A., "Radial capillary penetration into paper: limited and unlimited liquid reservoirs," *J. Colloid and Interface Sci.*, 166, 245-250, (1994).

Desjumaux, D., Bousfield, D.W, Glatter, T.P., Donigian, D.W., Ishley, J.N., and Wise, K.J., "Influence of pigment size on wet ink gloss development," *J. Pulp Paper Sci.,* 24(5):150-155, (1998).

Donigian, D., Ishley, J.N., and Wish, K.J., "Coating pore structure and offset printed gloss," *Tappi J.,* 80(5):163-172, (1997).

Eklund, D.E., and Salminen, P.J., "Water transport in the blade coating process," *Tappi J.* 69(9):116, (1986).

Holman, P.K., Uhland, S.A., Cima, M.J., and Sachs, E., "Surface adsorption effects in the inkjet printing of an aqueous polymer solution on a porous oxide ceramic substrate," *J. Colloid and Interface Sci.,* 247, 266-274 , (2002)

Hoogeveen, N.G., Stuart, M.A.C., and Fleer, G.J., "Polyelectrolyte adsorption on oxides. II. Reversibility and exchange," *J. Colloid an Interface Sci.* 182, 133, (1996).

Kozeny, J., Royal Academy of Science, Vienna, Proc. Class I, 136, 271,(1927).

Lepoutre, P., "Liquid absorption and coating porosity," *Paper Technol. Ind.*, 19, 298, (1978).

Marmur, A., "The radial capillary," *J. Colloid and Interface Sci.*, 124,301, (1988).

Matthews, G.P., and Spearing, M.C., "Modelling characteristic properties of sandstones," *Transp. Porous Media*, 6, 71, (1991).

Matthews, G.P., and Spearing, M.C., "Measurement and modelling of diffusion, porosity and other pore level characteristics of sandstones," *Mar. Pet. Geol.*, 9, 146, (1992).

Matthews, G.P., Moss, A.K., Spearing, M.C., and Voland, F., "Network calculation of mercury intrusion and absolute permeability in sandstone and other porous media," *Power Technology*, 76, 95-107, (1993).

Matthews, G.P., "Computer modeling of fluid permeation in porous coatings and paper- an overview," *Nordic Pulp and Paper Research J.*, 15, 5, 476-485, (2000).

Olivar, A. L. de Lima, "Water saturation and permeability from resistivity dielectric, and porosity logs," 60, 6, 1756-1764, (1995).

Peat, D.M.W., Matthews, G.P., Worsfold, P.J., and Jarvis, S.C., "Simulation of water retention and hydraulic conductivity by using a three-dimensional network," *European J. Soil Sci.*, 51, (2000).

Price, *Tappi J.,* 36(1):42-46, (1953).

Ridgway, C.J., Ridgway, K., and Matthews, G.P., "Modeling void space of tablets compacted over a range of pressure," *Pharmacy Pharmacology*, 49, 377, (1997).

Ruoff, A.l., Prince, D.L., Giddings, J.C., and Stewart, G.H., *Kolloid Aitschrift*, 166(2), 144, (1959).

Ruoff, A.l., Prince, D.L., Giddings, J.C., and Stewart, G.H., *Kolloid Aitschrift*, 173(1), 14, (1960).

Salminen, P.J., "Water transport into paper – the effect of some liquid and paper variables," *Tappi J.,* 9, 195-200, (1988).

Schoelkoph, J., Ridgway, C.J., Gane, P.A.C., Matthews, G.P., and Spielmann, D.C., "Measurement and network modeling of liquid permeation into compacted mineral blocks," *J. Colloid and Interface Sci.*, 227, 119, (2000).

Schoelkopf., J., Gane, P.A.C., Ridgway, C.J., and Matthews, G.P., "Influence of inertia on liquid absorption into paper coating structures," *Nordic Pulp and Paper Research J.* , 15(5), 422, (2000).

Tollenaar, D., "Capillary and wetting in paper structures: properties of porous systems," Surfaces and Coatings Related to Paper and Wood, by Marchessault and Skaar, Syracuse University Press, 195-219, (1967).

Xiang, Y., Bousfield, D.W., Hassler, J., Coleman, P., and Osgood, A., "Measurement of local variation of ink tack dynamics," *J. Pulp and Paper Sci.*, 25(9), 326, (1999).

Xiang, Y., and Bousfield, D.W., "Influence of Coating Structure on Ink Tack Dynamics," *J. Pulp and Paper Sci.*, 26(6), 221, (2000).

Xiang, Y., "Ink-Coating interactions," Paper Surface Science Program Meeting, University of Maine, (2002).

APPENDIX A: PROPERTIES OF FLUID AND MEDIA

Table A.1: Properties of seven papers

	Air permeability	Gloss			Roughness	Thickness	void fraction		Dominate pore size
							silicon oil	mercury	(diameter)
	(mm/s)	20°	60°	75°	um	um			um
B1	32.3	1.4	4	4.7	3.48	99	0.348	0.3185	3.288
B2	86.7	1.4	3.5	4.1	3.65	114	0.4478	0.4355	3.478
B3	49.2	1.9	3.8	4.8	3.54	101	0.403		3
B4	60.9	1.9	3.9	5.5	4.11	119	0.413		3
B5	50.2	2.1	4.7	9.2	2.26	120	0.446		3
B6	61.9	2	4.4	7.1	2.72	111	0.481		3
B7	40.2	2.1	5.2	9.3	2.73	189	0.442		3

Table A.2: Properties of five fluids

	viscosity	surface tension
	mPa*s	N/m
water	0.89	0.072
ethylene glycol	17.65	0.048
ID1	4.65	0.028
ID2	3.65	0.029
IP1	2.11	0.030

Table A.3: Properties of coatings on B1 paper base.

	Air Permeability	Gloss			Roughness	Coating Thickness	Void fraction		Dominate Pore size
	flow velocity						silicon	mercury	diameter
	(mm/s)	20°	60°	75°	(um)	(um)	oil		(um)
PPL 20pph	2.1	1.5	10.8	44.0	2.2	27	0.309	0.321	0.13
PPM 10pph	3.5	2.0	18.0	55.7	2.0	29		0.361	0.08
PPM 20pph	1.9	1.9	16.2	55.0	1.8	26	0.321	0.344	0.08
PPM 30pph	0.7	1.5	11.8	48.3	1.9	26		0.195	0.08
PPS 20pph	5.6	2.2	16.4	51.5	1.7	26	0.311	0.354	0.05
Clay	1.1	1.6	10.9	43.6	1.6	14	0.263	0.233	0.1

APPENDIX B: TABLES OF RESULTS

Table B.1: Contact angle results at different contacting time of three fluids: water, ethylene glycol (EG) and ink ID1 on seven papers.

	water contact angle						EG contact angle			ID1 contact angle		
	external surface			internal surface								
time	0.2s	1s	10s	0.2s	1s	10s	0.2s	1s	10s	0.2s	1s	10s
B1	85.9	83.7	75.2	72.1	69.9	49.3	75.1	55.1	33.4	26.8	12.6	5.8
B2	106.6	97.2	48.7	80.7	60.0	N/A	82.7	50.5	18.4	19.6	9.5	N/A
B3	103.4	101.9	101.3	87.7	80.3	61.6	90.3	75.2	58.4	25.5	11.7	N/A
B4	90.8	88.9	86.7	68.3	65.7	56.9	81.6	59.2	33.2	20.4	9.5	N/A
B5	98.8	96.6	91.1	66.9	62.1	35.7	59.4	31.2	24.4	20.1	10.5	N/A
B6	115.7	112.9	112.0	87.4	84.8	75.5	96.7	80.0	54.7	21.3	10.9	N/A
B7	89.4	86.7	84.6	64.0	61.8	51.2	58.9	34.2	23.7	23.0	10.8	N/A

Table B.2: Water and ethylene glycol contact angle of coatings on B1 paper base.

	Water			EG		
contact time	0.2 s	1 s	10s	0.2 s	1 s	10s
clay	64.0	53.0	48.3	56.4	39.8	32.7
$CaCO_3$	76.7	59.1	51.6	69.0	53.5	39.7
PPL 20pph	79.8	65.2	61.7	70.1	42.3	35.4
PPM 10pph	61.2	50.1	42.6	54.6	37.1	23.7
PPM 20pph	75.6	66.4	64.3	54.3	37.5	28.3
PPM 30pph	69.8	64.4	60.5	54.9	32.5	30.6
PPS 20pph	75.6	62.4	54.5	85.6	48.3	31.8

Table B.3: Water Bristow absorption rate on seven papers

Water Bristow Absorption				
contact time (s)	3	1.50	0.30	0.060
	TLV cm^3/m^2	TLV cm^3/m^2	TLV cm^3/m^2	TLV cm^3/m^2
B1	13.6	10.2	7.7	8.7
B2	99.9	95.2	40.3	12.9
B3	12.5	11.2	8.7	
B4	21.2	15.4	10.4	
B5	69.0	38.1	15.5	
B6	13.6	8.8	6.0	
B7	63.5	38.6	16.8	

Table B.4: Ethylene glycol Bristow absorption rate on seven papers

Ethylene Glycol Bristow Absorption					
Contact time (s)		6	3	1.5	0.3
B1	TLV (cm^3/m^2)	40.4	33.9	27.2	11.1
B2	TLV (cm^3/m^2)	54.1	55.3	51.0	27.4
B3	TLV (cm^3/m^2)		9.5	8.8	7.9
B4	TLV (cm^3/m^2)		43.6	30.3	12.6
B5	TLV (cm^3/m^2)		48.9	41.3	22.6
B6	TLV (cm^3/m^2)		31.8	14.3	6.6
B7	TLV (cm^3/m^2)		69.1	58.9	25.7

Table B.5: ID1 Bristow absorption rate on seven papers

ID1 Bristow Absorption				
contact time(s)		3	1.5	0.3
B1	TLV (cm^3/m^2)	45.8	39.4	25.4
B2	TLV (cm^3/m^2)	63.5	59.4	48.3
B3	TLV (cm^3/m^2)	55.6	48.8	34.5
B4	TLV (cm^3/m^2)	60.2	58.4	41.3
B5	TLV (cm^3/m^2)	70.9	64.0	41.7
B6	TLV (cm^3/m^2)	66.7	61.0	42.6
B7	TLV (cm^3/m^2)	95.2	80.7	47.6

Table B.6: Water Bristow absorption results of coatings on base of B1, B2 and Mylar.

Ink : Water							
	contact time	sec	6	3	1.5	0.3	0.06
B1 paper base	PPL 20pph	TLV (cm^3/m^2)		19.2	16.4	12.7	7.7
	PPM 10pph	TLV (cm^3/m^2)		23.2	20.4	15.3	12.8
	PPM 20pph	TLV (cm^3/m^2)	21.0	21.1	18.0	14.2	11.8
	PPM 30pph	TLV (cm^3/m^2)		16.0	13.5	10.5	9.4
	PPS 20pph	TLV (cm^3/m^2)		20.1	18.1	14.1	11.7
	clay	TLV (cm^3/m^2)		15.5	12.9	10.3	8.5
	$CaCO_3$	TLV (cm^3/m^2)		13.1	9.6	7.0	6.1
UK paper base	PPM 10pph	TLV (cm^3/m^2)		31.0	24.3	18.5	14.4
	PPM 20pph	TLV (cm^3/m^2)	35.8	27.5	22.3	16.2	10.6
	Cover Gloss	TLV (cm^3/m^2)		21.8	16.1	11.1	8.8
	$CaCO_3$	TLV (cm^3/m^2)		35.6	19.0	8.4	7.6
Mylar base	PPM 20pph	TLV (cm^3/m^2)		13.7	13.0	13.1	10.1

Table B.7: Ethylene glycol Bristow absorption results of coatings on base of B1, B2 and Mylar.

ink: Ethylene Glycol						
	Contact time	sec	6	3	1.5	0.3
B1 paper base	PPL 20pph	TLV (cm^3/m^2)		12.5	11.5	7.5
	PPM 10pph	TLV (cm^3/m^2)		16.2	14.2	11.6
	PPM 20pph	TLV (cm^3/m^2)	13.6	13.9	12.9	9.1
	PPM 30pph	TLV (cm^3/m^2)		9.1	9.6	6.4
	PPS 20pph	TLV (cm^3/m^2)		17.4	14.3	10.3
	clay	TLV (cm^3/m^2)		8.0	8.5	6.5
	$CaCO_3$	TLV (cm^3/m^2)		10.8	9.4	7.9
B2 paper base	PPM 10pph	TLV (cm^3/m^2)		21.4	17.9	12.5
	PPM 20pph	TLV (cm^3/m^2)	20.5	16.9	14.9	9.4
	clay	TLV (cm^3/m^2)		9.9	9.4	7.3
	$CaCO_3$	TLV (cm^3/m^2)		17.6	12.3	7.5
Mylar base	PPM 20pph	TLV (cm^3/m^2)		10.9	10.3	6.8

Table B.8: Bristow absorption rate of ink ID2 and IP1 on seven papers at 3 sec contact time.

ID2 Bristow Absorption			IP1 Bristow Absorption	
contact time(s)		3		3
B1	TLV (cm^3/m^2)	46.7		62.0
B2	TLV (cm^3/m^2)	66.2		95.2
B3	TLV (cm^3/m^2)	46.4		63.2
B4	TLV (cm^3/m^2)	58.5		84.1
B5	TLV (cm^3/m^2)	65.2		88.9
B6	TLV (cm^3/m^2)	65.6		84.4
B7	TLV (cm^3/m^2)	81.7		122.7

Table B.9: Bristow absorption result of IP1 ink on coatings

ink: IP1						
	contact time	sec	3	1.5	0.3	0.06
B1 paper base	clay	TLV (cm^3/m^2)	13.1	11.7	9.1	6.1
	$CaCO_3$	TLV (cm^3/m^2)	13.1	11.3	10.1	8.2
	PPL 20pph	TLV (cm^3/m^2)	16.7	14.1	8.3	5.5
	PPM 10pph	TLV (cm^3/m^2)	20.3	17.4	14.8	10.1
	PPM 20pph	TLV (cm^3/m^2)	18.7	15.9	13.3	7.7
	PPM 30pph	TLV (cm^3/m^2)	15.1	13.1	9.6	5.4
	PPS 20pph	TLV (cm^3/m^2)	17.3	15.3	13.3	9.6
B2 paper base	PPM 10pph	TLV (cm^3/m^2)	25.0	21.1	16.6	12.0
	clay	TLV (cm^3/m^2)	18.3	14.9	10.9	7.6
	$CaCO_3$	TLV (cm^3/m^2)	31.3	25.4	14.9	10.2
	C1	TLV (cm^3/m^2)	9.2	7.0	2.9	2.0
	C2	TLV (cm^3/m^2)	7.4	6.1	4.9	2.7
	C3	TLV (cm^3/m^2)	6.0	5.0	2.6	2.0

Table B.10: Bristow absorption result of ID1 ink on coatings

ink : ID1						
	Contact time	sec	3	1.5	0.3	0.06
B1 paper base	clay	TLV (cm^3/m^2)	10.6	10.4	9.1	6.9
	$CaCO_3$	TLV (cm^3/m^2)	14.1	12.2	12.1	10.2
	PPL 20pph	TLV (cm^3/m^2)	23.0	20.4	15.3	12.9
	PPM 10pph	TLV (cm^3/m^2)	19.3	17.8	18.9	12.4
	PPM 20pph	TLV (cm^3/m^2)	18.5	17.1	14.1	8.7
	PPM 30pph	TLV (cm^3/m^2)	14.9	14.2	10.1	6.4
	PPS 20pph	TLV (cm^3/m^2)	19.1	17.7	15.4	9.9
B2 paper base	PPM 10pph	TLV (cm^3/m^2)	23.0	20.2	15.8	11.7
	clay	TLV (cm^3/m^2)	14.7	12.0	10.0	6.9
	$CaCO_3$	TLV (cm^3/m^2)	30.1	23.1	13.6	11.9
	C1	TLV (cm^3/m^2)	9.3	6.7	3.9	3.1
	C2	TLV (cm^3/m^2)	6.4			
	C3	TLV (cm^3/m^2)	5.6	4.9	4.7	3.1

Table B.11: Bristow absorption result of ID2 ink on coatings

ink: ID2						
	Contact time	sec	3	1.5	0.3	0.06
B1 paper base	clay	TLV (cm^3/m^2)	10.8	9.7	9.6	6.6
	$CaCO_3$	TLV (cm^3/m^2)	13.7	11.4	10.2	8.6
	PPL 20pph	TLV (cm^3/m^2)	16.9	15.4	12.6	7.9
	PPM 10pph	TLV (cm^3/m^2)	20.4	17.6	15.0	9.8
	PPM 20pph	TLV (cm^3/m^2)	17.8	17.0	13.4	9.0
	PPM 30pph	TLV (cm^3/m^2)	18.1	16.2	10.2	6.6
	PPS 20pph	TLV (cm^3/m^2)	17.4	16.6	13.5	9.2
B2 paper base	PPM 10pph	TLV (cm^3/m^2)	21.6	19.6	16.1	11.5
	clay	TLV (cm^3/m^2)	14.1	12.5	9.9	7.3
	$CaCO_3$	TLV (cm^3/m^2)	27.1	21.4	15.0	11.9
	C1	TLV (cm^3/m^2)	8.1	7.1	3.7	2.5
	C2	TLV (cm^3/m^2)	6.1			
	C3	TLV (cm^3/m^2)	5.1	4.3	3.7	4.4

BIOGRAPHY OF THE AUTHOR

Ran Wei Rioux was born in Changsha, China on October 17th, 1972. She obtained the Bachelor degree in Chemical Engineering at The Beijing University of Chemical Technology, in July 1995. She worked as a supervisor in the Pulp Preparation and Acetone Recovery Dept. at the Zhuhai Cellulose Fiber Co., in Guangdong, China, from August 1995 to March 1997. She came to the University of Maine in August 2000 to obtain a Master of Science degree in Chemical Engineering. She joined the Paper Surface Science Program as a research assistant.

Ran is a candidate for the Master of Science degree in Chemical Engineering from The University of Maine in May, 2003.